REPORT DOCUMENTATION PAGE

Form Approved
OMB No. 0704-0188

1. REPORT DATE *(DD-MM-YYYY)*	2. REPORT TYPE	3. DATES COVERED *(From - To)*
31-3-2007	Final Technical	1-11-2003 - 31-12-2006

4. TITLE AND SUBTITLE

(U) EXPERIMENTAL AND DETAILED NUMERICAL STUDIES OF FUNDAMENTAL FLAME PROPERTIES OF GASEOUS AND LIQUID FUELS

5a. CONTRACT NUMBER

5b. GRANT NUMBER
FA9550-04-1-0006

5c. PROGRAM ELEMENT NUMBER
61102F

6. AUTHOR(S)

FOKION N. EGOLFOPOULOS

5d. PROJECT NUMBER
2308

5e. TASK NUMBER
BX

5f. WORK UNIT NUMBER

7. PERFORMING ORGANIZATION NAME(S) AND ADDRESS(ES)

University of Southern
California
Los Angeles, CA 90089

8. PERFORMING ORGANIZATION REPORT NUMBER

9. SPONSORING / MONITORING AGENCY NAME(S) AND ADDRESS(ES)

AFOSR/NA
875 Randolph Street
Suite 325, Room 3112
Arlington VA 22203
Dr Julian Tishkoff

10. SPONSOR/MONITOR'S ACRONYM(S)

11. SPONSOR/MONITOR'S REPORT NUMBER(S)

12. DISTRIBUTION / AVAILABILITY STATEMENT

Approved for public release; distribution is unlimited

AFRL-SR-AR-TR-07-0182

13. SUPPLEMENTARY NOTES

14. ABSTRACT

The dynamic behavior of laminar flames was studied for a wide range of conditions. The parameters considered included the fuel type, reactant composition, flame temperature, and combustion mode. Both gaseous and liquid fuels, including jet fuels and their surrogates, were considered. Flame ignition and extinction limits were determined experimentally and numerically for fuels and reaction conditions that have not been considered previously. For both low and high molecular weight fuels, it was determined that diffusion and kinetics can have similar effects on flames. Furthermore, it was found that kinetic mechanisms that predict laminar flame speeds, do not necessarily predict extinction limits, even though both propagation and extinction are high temperature phenomena. Finally, it was determined that the chain mechanisms that control near-limit flames may change notably as the reactant temperature and pressure increase well above their standard values. These results enhance current understanding of the combustion behavior of fuels that are of relevance to air-breathing propulsion. Furthermore, the derived experimental data constitute a basis for partially validating combustion kinetics as well as proposed surrogates of jet fuels.

15. SUBJECT TERMS

Air-Breathing Propulsion, Combustion Kinetics, Flames, Surrogate Jet Fuels

16. SECURITY CLASSIFICATION OF:			17. LIMITATION OF ABSTRACT	18. NUMBER OF PAGES	19a. NAME OF RESPONSIBLE PERSON
a. REPORT	b. ABSTRACT	c. THIS PAGE			Julian M. Tishkoff
Unclassified	Unclassified	Unclassified	Unlimited	120	19b. TELEPHONE NUMBER *(include area code)* (703)696-8478

Final Technical Report

EXPERIMENTAL AND DETAILED NUMERICAL STUDIES OF FUNDAMENTAL FLAME PROPERTIES OF GASEOUS AND LIQUID FUELS

(AFOSR Grant FA9550-04-1-0006)
(Period: 11/1/2003-12/31/2006)

FOKION N. EGOLFOPOULOS
Department of Aerospace & Mechanical Engineering
University of Southern California
Los Angeles, California 90089-1453

Summary/Overview

The dynamic behavior of laminar flames was studied for a wide range of conditions. The parameters considered included the fuel type, reactant composition, flame temperature, and combustion mode. Hydrogen, carbon monoxide, single-component gaseous and liquid hydrocarbons, alcohols, as well as jet fuels and their surrogates were studied experimentally in the counterflow configuration. The experiments were modeled through the use of detailed description of chemical kinetics and molecular transport. During the reporting period, progress was made in the following: (1) ignition of premixed and non-premixed flames of gaseous and liquid fuels, (2) extinction of premixed and non-premixed flames of gaseous and liquid fuels, (3) assessment of the effect of diffusion on the flame behavior, and (4) lean flammability limits under high temperature and high pressure conditions. For both low and high molecular weight fuels, it was determined that diffusion and kinetics can have similar effects on flames. Furthermore, it was found that kinetic mechanisms that predict laminar flame speeds, do not necessarily predict extinction limits, even though both propagation and extinction are high temperature phenomena. Finally, it was determined that the chain mechanisms that control near-limit flames may change notably as the reactant temperature and pressure increase well above their standard values. These results enhance current understanding of the combustion behavior of fuels that are of relevance to air-breathing propulsion. Furthermore, the derived experimental data constitute a basis for partially validating combustion kinetics as well as proposed surrogates of jet fuels.

Technical Discussion

1.0 Introduction

The accurate knowledge of the oxidation kinetics of hydrocarbon fuels is essential for the design of the next generation of air-breathing engines operating at speeds and altitudes that are notably greater than the ones currently achieved. State-of-the-art knowledge of hydrocarbon oxidation chemistry is limited to that of H_2 and CH_4. For example, the GRI-3.0 mechanism [1] closely predicts a wide range of flame properties for H_2 and CH_4 mixtures with air, especially at high temperatures; however, even for H_2 and CH_4, their oxidation kinetics at low temperatures have not been probed systematically in previous flame studies. The oxidation kinetics of higher carbon hydrocarbons are subjected to significant uncertainties even at the C_2-level [*e.g.*, 2]. Furthermore, systematic flame studies of liquid hydrocarbons are limited compared to gaseous studies.

This research was both experimental and numerical. The experimental measurements focused on the determination of global flame properties relevant to the phenomena of ignition and extinction. This was important, as these different flame phenomena are sensitive to different kinetics subsets at different temperatures. The high-temperature kinetics were validated against flame extinction data obtained for a wide range of fuels, such as H_2, CO, C_1-C_3 hydrocarbons, and liquid fuels such as C_7-C_8 hydrocarbons and alcohols. While laminar flame speeds cannot be determined directly, extinction strain rates (in counterflow configurations) can, and a methodology has been introduced to do so. Similar kinetics pathways control propagation and extinction in general for C_1-C_2 hydrocarbon flames [2], but this needs to be investigated further for fuels with higher carbon numbers. An alternative technique also was introduced for studying flame ignition in counterflow configurations by using vitiated air that was produced from the oxidation of ultra-lean H_2/air flames as the ignition source rather heated air. The ignition behavior of several fuels thus was tested.

2.0 Experimental and Numerical Methodologies

The experiments were performed in the opposed-jet configuration and through the use of a recently developed digital particle image velocimetry (DPIV) technique [3]. The use of DPIV allowed for the determination of the instantaneous velocity field so that the imposed strain rate, K, could be measured *directly*. The extinction strain rate, K_{ext}, was determined *directly* by establishing flames very close to extinction and by reducing (for fuel-lean conditions) the fuel flow rate [4,5,6] rather than increasing the strain rate. The latter procedure also requires extrapolations. The experiments were modeled using a quasi one-dimensional code with detailed descriptions of molecular transport, chemical kinetics, and thermal radiation [7]. The chemical kinetics schemes tested included:

- the H_2/O_2 mechanisms of Mueller *et al.* [8] and Davis *et al.* [9];
- the GRI30 mechanism [1] for H_2 and C_1-C_3 hydrocarbons;
- a mechanism developed by Wang and coworkers [10] for C_1-C_4 hydrocarbons;
- three mechanisms for CH_3OH and C_2H_5OH oxidation [11-13];
- two mechanisms describing C_7-C_8 hydrocarbon oxidation [14,15].

3.0 Results and Discussion

3.1 *Ignition of Premixed and Non-Premixed Flames of Gaseous and Liquid Fuels*

A new methodology was developed, allowing ignition studies in the counterflow configuration [16]. The methodology includes the use of ultra-lean H_2/air flames as the ignition source, which eliminates the need of using heated air. The hot excess air dominates the composition of the post-flame products, while minor amounts of H_2O are present. In order to achieve a wide range of "ignition temperatures" from as low as 1,000 K to as high as 1,400 K a platinum screen is used at the burner exit to support the H_2/air flames catalytically. The use of the platinum screen also eliminates complications arising from the flame location, if the flame were stabilized by velocity gradients complicating data interpretation. Ignition of H_2, CO, and various hydrocarbons was achieved, and data were found to be in close agreement with those determined in past studies by Law and co-workers [*e.g.*, 17], in which heated air was used as the ignition source.

This approach was used for H_2, CO, and C_1-C_{12} single component hydrocarbons. Additionally, the flame ignition of various petroleum-derived and synthetic jet fuels also was investigated, as well as representative surrogates. For fuels for which reliable kinetic mechanisms are available, numerical simulations also were performed.

Various combustion phenomena of mixtures of H_2 and CO with air and CO_2 were studied in collaboration with Professors Hai Wang of USC and Eric L. Petersen of University of Central Florida, and more details can be found in Ref. 18. The oxidation kinetics of H_2 and CO mixtures were examined experimentally and computationally for a wide range of mixture compositions and reaction conditions. Shock-tube ignition delay times were obtained for five CO/H_2/air mixtures (equivalence ratio $\phi = 0.5$) over the pressure range of 1 to 20 atm and temperatures from 950 to 1330 K. The influence of CO and H_2 composition variations on flame ignition and propagation also was examined. Two types of experiments were carried out for $H_2/CO/CO_2$ mixtures with air. Laminar flame speeds, S_u^o, were determined in the twin-flame counterflow configuration using DPIV [3]. Ignition temperatures, T_{ign}, were determined by counterflowing a vitiated air jet against a premixed fuel/air jet [16]. Computationally, detailed modeling of the experiments was performed using a recently developed $H_2/CO/O_2$ reaction model [9]. Numerical simulations showed generally good agreement with the experimental data.

Flame ignition studies also were performed for C_1-C_4 hydrocarbons and notable differences between experimental and computed T_{ign}'s were identified. The ignition limits of *n*-C_7H_{16} and *iso*-C_8H_{18} flames were not simulated, as the mechanisms that were tested [14,15] were reduced and validated against data derived in vigorously burning flames.

The ignition characteristics of jet fuels and their surrogates also were investigated. The goal of this investigation was dual: first, to compare the performance of jet fuels with that of single-component hydrocarbons, and second, to assess the validity of proposed surrogates, which have been derived typically based on matching physical properties [*e.g.*, 19,20]. The liquid feed system was upgraded to vaporize practical jet fuels. The wall temperature of the evaporation chamber was controlled carefully to make sure that it was high enough to avoid condensation but low enough to avoid thermal cracking. T_{ign}'s of heated non-premixed fuel/N_2 mixtures of eight pure fuels from C_5 to C_{12}, ten practical fuels, and four JP8 surrogates were obtained by counterflowing them against cold oxygen. T_{ign}'s of mixtures of the same 20 fuels with nitrogen were obtained by counterflowing them against hot oxygen. The fuels studied were:

Pure fuels:	*n*-C_5H_{12}, *n*-C_6H_{14}, *n*-C_7H_{16}, *n*-C_8H_{16}, *iso*-C_8H_{16}, *n*-C_9H_{20}, *n*-$C_{10}H_{22}$, *n*-$C_{12}H_{26}$.
Practical fuels:	JP7-3347, JP8-3773, JP10-3942, RP1a-3642, RP1b-4572, JetAa-3602, JetAb-3638, JetAc-4658, Coal-Derived-4765, Fisher-Tropsch-4734
Surrogates:	S2 – Two-Component Surrogate [21]
	S3 – Three-Component Surrogate [22]
	S6 – Six-Component Surrogate [19]
	S12 – Twelve-Component Surrogate [20]

The compositions of the various jet fuels tested are shown in Table 1. JP10 is a single component jet fuel, i.e. *exo*-tetrahydrodicyclopentadiene. The compositions of the four surrogates tested are shown in Table 2. The compositions of the S6 and S12 surrogates were taken from the literature, and the compositions of the S2 and S3 surrogates were determined based on personal communications. More specifically the S2 composition is that used in Europe [21], while that of S3 was determined as part of the deliberations of the US surrogate fuels group [22].

	4658 Jet A composite blend	3327 JP-7	4734 F-T Jet	4572 RP-1	4765 Coal-based jet fuel DCL	3773 JP-8	World survey Jet A, Jet A-1, JP-8, JP-5, TS-1
Paraffins (*n*- + *i*-)	55.2	67.9	99.7	57.6	0.6	57.2	58.8
Cycloparaffins	17.2	21.2	<0.2	24.8	46.4	17.4	10.9
Dicycloparaffins	7.8	9.4	0.3	12.4	47.0	6.1	9.3
Tricycloparaffins	0.6	0.6	<0.2	1.9	4.6	0.6	1.1
Alkylbenzenes	12.7	0.7	<0.2	2.1	0.3	13.5	13.4
Indans/Tetralins	4.9	<0.2	<0.2	0.3	1.1	3.4	4.9
Indenes	<0.2	<0.2	<0.2	<0.2	<0.2	<0.2	<0.2
Naphthalene	<0.2	<0.2	<0.2	<0.2	<0.2	<0.2	0.13
Naphthalenes	1.3	<0.2	<0.2	0.3	<0.2	1.7	1.55
Acenaphthenes	<0.2	<0.2	<0.2	<0.2	<0.2	<0.2	<0.2
Acenaphthylenes	<0.2	<0.2	<0.2	0.4	<0.2	<0.2	<0.2
Tricyclic Aromatics	<0.2	<0.2	<0.2	<0.2	<0.2	<0.2	<0.2

	3638 Jet A	3602 Jet A	3642 RP-1
Aromatics (ASTM D1319)	12	24	2.9

Table 1. Composition of jet fuels tested.

Notation	Compound	% by Volume
S6	*m*-Xylene	15
	iso-Octane	10
	Methycyclohexane	20
	n-Dodecane	30
	n-Tetradecane	20
	Tetralin	5
S3	*n*-Decane	50
	n-Butylcyclohexane	25
	n-Butylbenzene	25

Notation	Compound	% by Mass
S12	*m*-Xylene	5
	iso-Octane	5
	Methylcyclohexane	5
	n-Dodecane	20
	n-Tetradecane	15
	Tetralin	5
	cyclo-Octane	5
	n-Decane	15
	Butylbenzene	5
	Tetramethylbenzene	5
	Methylnapthalene	5
	n-Hexadecane	10
S2	*n*-Decane	70
	n-Propylbenzene	30

Table 2. Composition of JP8 surrogates tested.

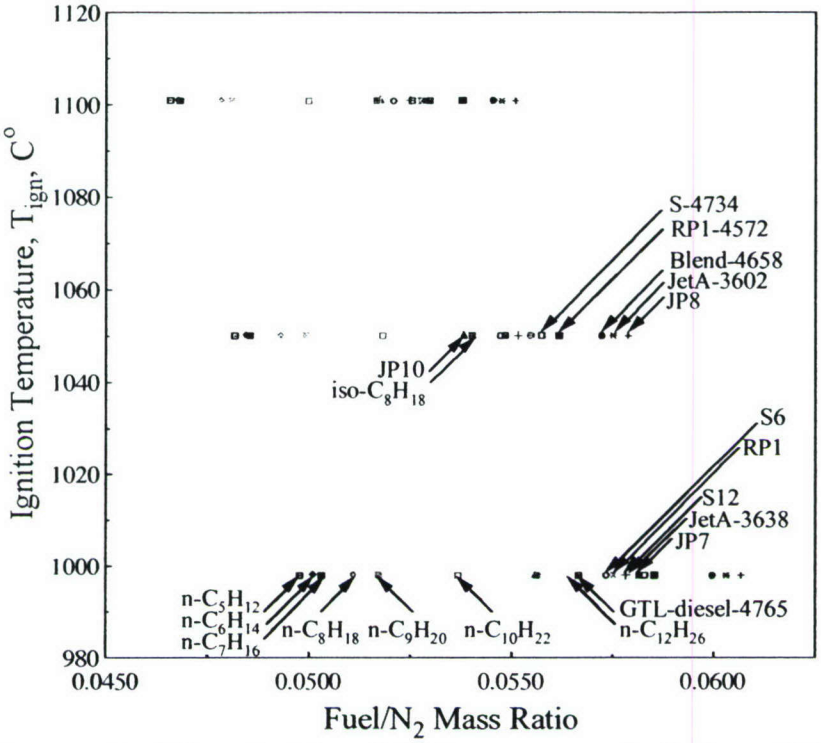

Figure 1. Non-premixed flame ignition of single-component, jet fuels, and JP8 surrogates.

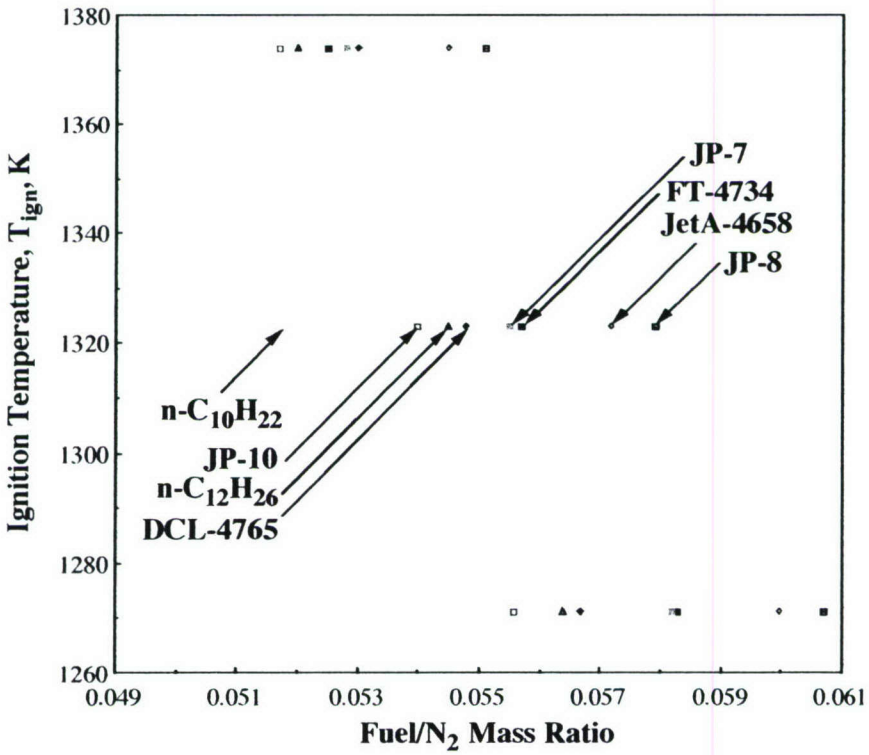

Figure 2. Non-premixed flame ignition of jet fuels.

In Fig. 1, for single-component fuels, lower carbon numbers result in greater ignition propensities. Among practical fuels, JP8 is the hardest, while the JP10 is the easiest to ignite. In Fig. 2 the ignition limits of all jet fuels are shown. In Fig. 3 the ignition response of JP8 and its four surrogates is compared. All surrogates exhibit similar ignition behavior; however, their ignition propensity is notably higher compared to JP8.

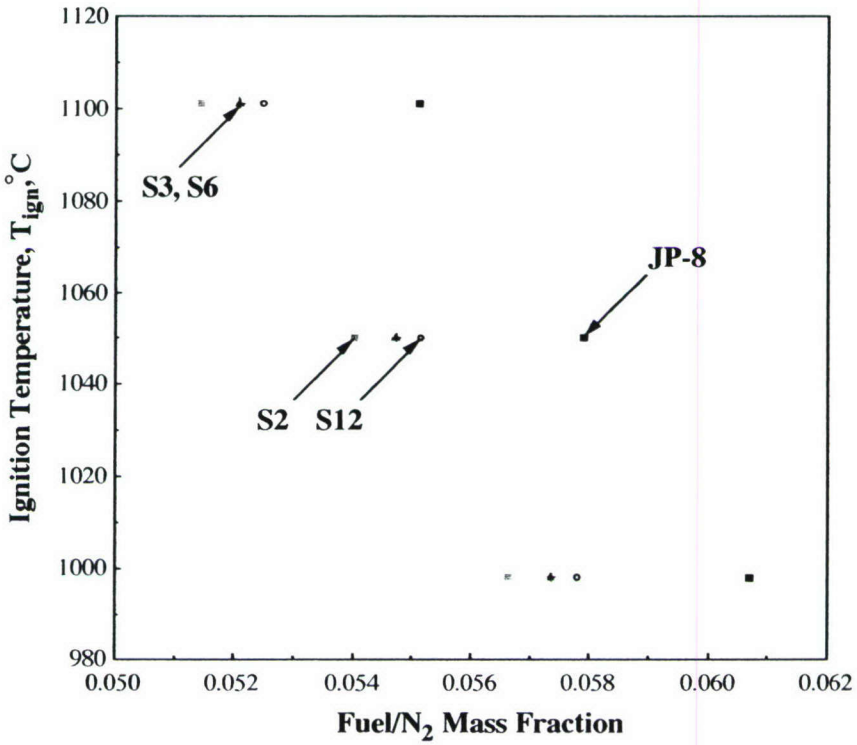

Figure 3. Non-premixed flame ignition of JP8 and its surrogates.

3.2 *Extinction of Premixed and Non-Premixed Flames of Gaseous and Liquid Fuels*

K_{ext}'s were determined in the opposed-jet configuration both experimentally and numerically for a number of fuels [*e.g.*, 5,6]. This work was performed for three reasons: First, to assess the validity of the thesis that propagation and extinction are controlled by similar kinetics, for fuels other than C_1-C_2 hydrocarbons. In other words, to test the thesis that a mechanism that predicts S_u^o's also should predict K_{ext}'s. Second, the experimental determination of K_{ext} is direct, as opposed to that of S_u^o, which requires either extrapolations or notable data processing. Thus, the comparison with the numerical predictions is more reliable. Finally, since S_u^o is the most common fundamental flame property that has been measured for a variety of fuels, it is important that similar data on extinction become available. Extinction studies allow for the assessment of the resistance of fuels to blow-off as function of kinetics, molecular transport, and fluid mechanics. Additionally, the sensitivity of extinction to kinetics is notably larger compared to that of propagation [*e.g.*, 5,6]. The extinction studies included a large number of fuels similar to the ignition studies described in Section 3.1, and details can be found in Refs. 4-6.

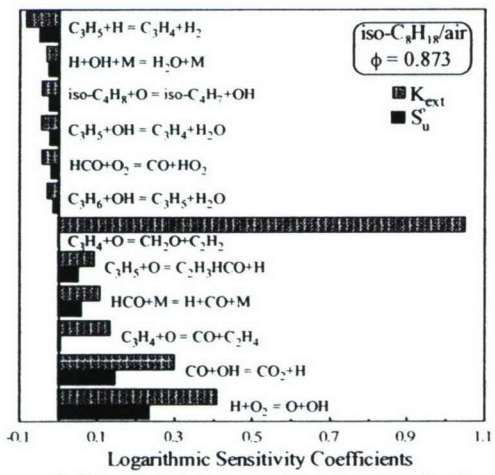

Figure 4. Sensitivities for iso-C_8H_{18}/air flames.

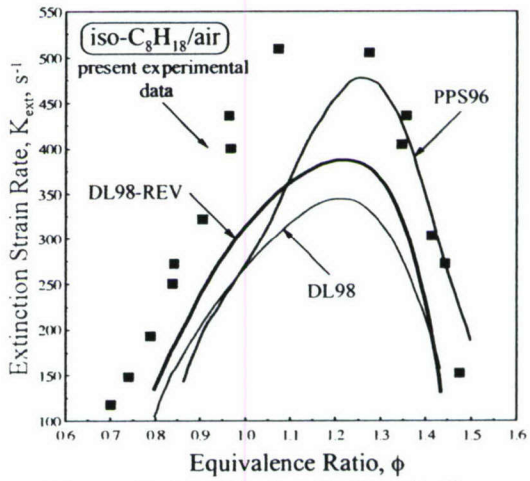

Figure 5. K_{ext} for iso-C_8H_{18}/air flames.

The current understanding of extinction phenomena was enhanced through the advancement of a numerical technique that allows the detailed determination of the sensitivities of K_{ext} on the kinetics. The approach is similar to that taken for S_u^o. Logarithmic sensitivity coefficients are shown in Fig. 4 for an iso-octane/air flame, and distinct differences of the effect of kinetics on propagation and extinction can be seen. A logarithmic sensitivity coefficient is defined as $[\partial \ln K_{ext}/\partial \ln A]$, where A is the pre-exponential factor. The physical mechanisms behind the observed differences were explained by a detailed reaction path analysis [5]. The flame extinction studies showed that for both H_2 and liquid fuels, while existing kinetic mechanisms predict S_u^o's they fail to predict experimentally determined K_{ext}'s. The rigorous sensitivity results allowed the reduction of such discrepancies. For example, the Davis & Law [14] (DL98) mechanism that closely predicts S_u^o's but not K_{ext}'s, was revised by adding the CH_2CHO species and its 22 subsequent reactions from Wang [10]. This minor revision (DL98-revised) improved prediction of K_{ext} by 15%, as seen in Fig. 5. This mechanism revision was found to

affect the prediction of K_{ext} twice as much as that of S_u^o. In Fig. 5 predictions are shown using the Pitsch *et al.* [15] (PPS96) mechanism. Both DL98 and PPS96 were validated against S_u^o data.

The extinction of flames of jet fuels and their surrogates also was investigated and compared with that of single-component liquid hydrocarbons. Figures 6 and 7 depict, for single-component fuels, greater extinction propensities with increasing carbon numbers. Among the practical fuels, JP7, JP8, JP10, and RP1a are less resistant to extinction compared to the other fuels tested. In Fig. 8 the surrogates of JP8 exhibit similar extinction behavior, but they are more resistant to extinction than JP8.

The results of Figs. 1, 2, 6, and 7 clearly illustrate that in terms of ignition and extinction, the practical fuels tested behave similarly to single-component hydrocarbons that are heavier than *n*-decane, an anticipated result based on their compositions.

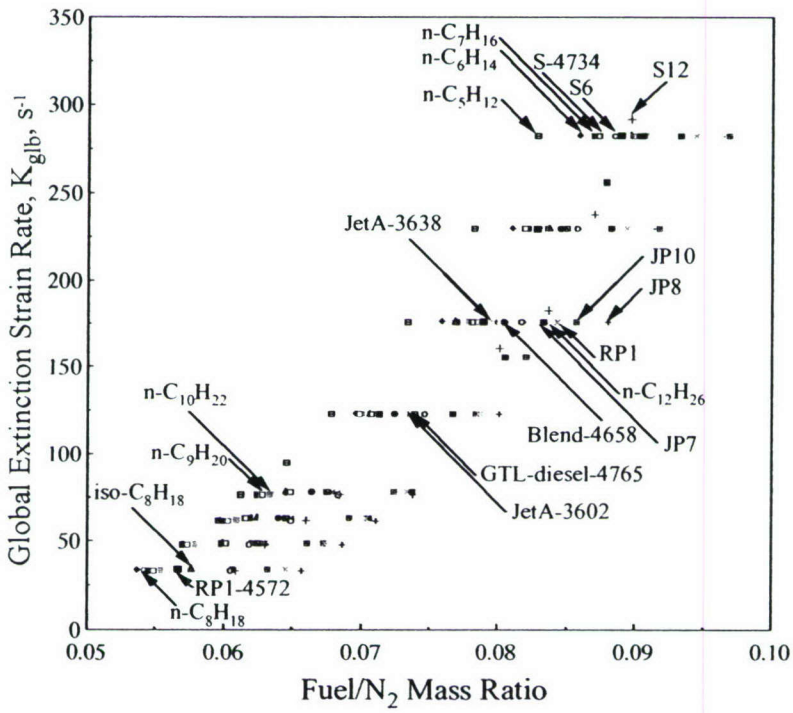

Figure 6. Non-premixed flame extinction of single-component, jet fuels, and JP8 surrogates.

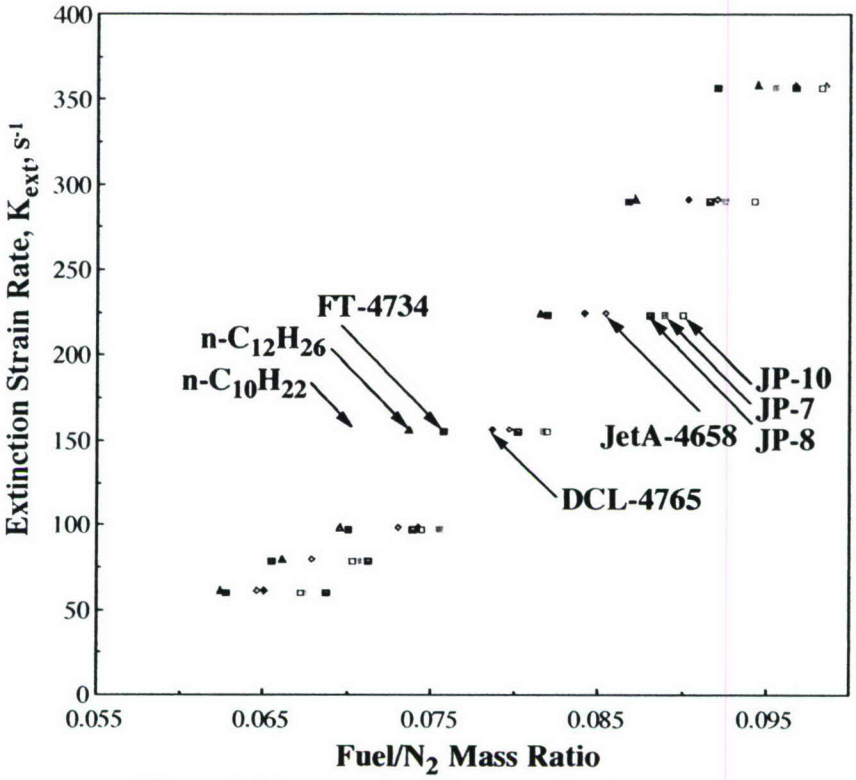

Figure 7. Non-premixed flame extinction of jet fuels.

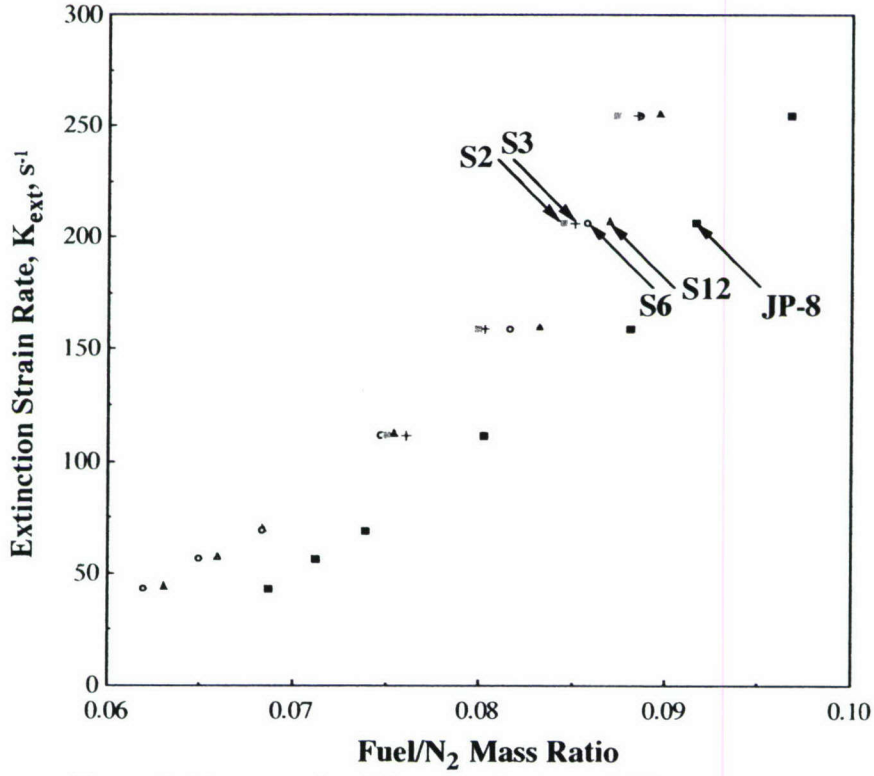

Figure 8. Non-premixed flame extinction of JP8 and its surrogates.

3.3 Assessment of the Effect of Diffusion on the Flame Behavior

Studies of flame extinction of ultra-lean H_2/air flames have revealed that K_{ext} is rather sensitive to the diffusion coefficients, and, in many cases, these sensitivities are of the same order as or higher than those of S_u^o [4]. This finding suggests that optimizing chemical kinetics against flame data without considering the effect of diffusion potentially could falsify rate constants. Based on this observation, studies on the extinction of additional fuels were conducted, and it was shown that under most conditions the effect of diffusion is of the same order of that of kinetics [5]. Table 3 depicts logarithmic sensitivity coefficients for both kinetics and diffusion for S_u^o and K_{ext} of CH_3OH/air, C_2H_5OH/air, *n*-C_7H_{16}/air, and *iso*-C_8H_{18}/air flames; the effect of kinetics is represented by the main branching reaction $H+O_2 \rightarrow OH+O$ (R1). For both lean *n*-C_7H_{16}/air and *iso*-C_8H_{18}/air flames, S_u^o exhibits a small negative sensitivity to diffusion, with values that are an order of magnitude less than the sensitivity to R1. On the other hand, the effect of diffusion on K_{ext} appears to be notably greater and of the same order as that of R1. Similar results were shown for lean C_2H_5OH/air flames, with the exception that the sensitivity of S_u^o to diffusion is rather similar in magnitude to R1. For lean CH_3OH/air flames the magnitudes of the sensitivities of S_u^o to diffusion and R1 are very close, while that of K_{ext} to R1 is an order of magnitude greater compared to diffusion.

Fuel	Mechanism		ϕ	Sensitivity to R1	Sensitivity to Fuel Diffusion
iso-octane	DL98	S_u^o	0.873	0.320	-0.017
		K_{ext}	0.873	0.409	0.186
n-heptane	DL98	S_u^o	0.800	0.308	-0.056
		K_{ext}	0.808	0.397	0.185
ethanol	FDC00	S_u^o	0.682	0.455	-0.137
		K_{ext}	0.682	0.794	0.422
methanol	FDC00	S_u^o	0.769	0.347	-0.316
		K_{ext}	0.769	0.581	0.032

Table 3. Logarithmic sensitivity coefficients of S_u^o and K_{ext} to the rate of the main branching reaction $H+O_2 \rightarrow OH+O$ (R1) and to the fuel diffusivity for CH_3OH/air, C_2H_5OH/air, *n*-C_7H_{16}/air, and *iso*-C_8H_{18}/air mixtures.

The relative importance of diffusion and chemical kinetics was investigated further by quantifying their effects on flame ignition, and the details can be found in Ref. 23. The study was conducted in stagnation flows for atmospheric, laminar, premixed and non-premixed H_2, *n*-C_7H_{16}, and *iso*-C_8H_{18} flames.

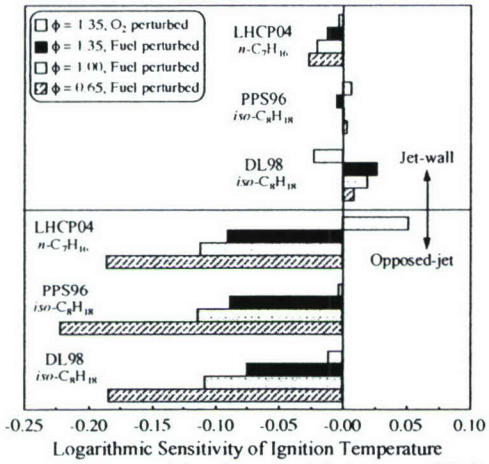

Figure. 9. Logarithmic sensitivity coefficients of ignition temperature of *iso*-C_8H_{18}/air and *n*-C_7H_{16}/air flames on diffusion.

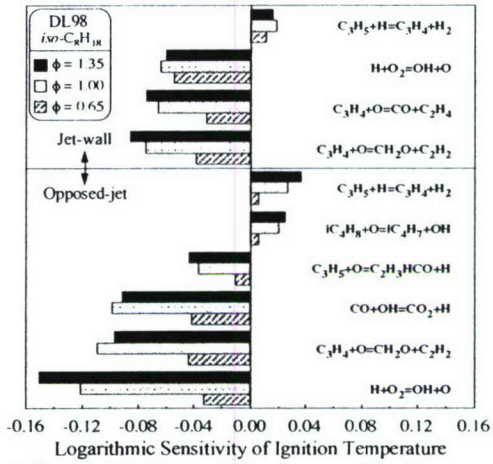

Figure 10. Logarithmic sensitivity coefficients of ignition temperature of *iso*-C_8H_{18}/air on kinetics.

Ignition of premixed flames was studied by: (1) increasing the temperature of a N_2 jet counterflowing against a fuel/air jet, and (2) increasing the temperature of a solid wall against which a fuel/air jet was injected. Ignition of non-premixed flames was studied by increasing the temperature of an air jet counterflowing against a fuel-containing jet. The simulations were performed along the stagnation streamline and included detailed descriptions of chemical kinetics, molecular transport, and radiative heat transfer. Sensitivity analyses of the ignition temperatures to the diffusion coefficients of the reactants, as well as to the kinetics, were performed. Results revealed that premixed flame ignition is rather sensitive to the fuel diffusivity in the opposed-jet configuration and notably less sensitive in the jet-wall. In the opposed-jet configuration, diffusive transport conveys the reactants towards the ignition kernel. In the jet-wall configuration, the reactants are transported towards the ignition kernel largely by convection and, as a result, ignition is not diffusion-limited. The two configurations resulted in similar T_{ign}'s only for fuel-rich cases, and T_{ign}'s tended to be lower as the equivalence ratio increased in the opposed-jet configuration. However, T_{ign}'s were found to depend mildly on the equivalence ratio in the jet-wall configuration. The sensitivity of ignition to diffusion in non-premixed systems was found also to be notable, especially for cases in which the fuel was diluted highly by an inert. For both premixed and non-premixed flames, the sensitivity of ignition to diffusion coefficients was of the same order or larger than that of kinetics, and representative results are shown in Figs. 9 and 10. Thus, uncertainties associated with transport coefficients need to be accounted for, when flame ignition data are used to validate kinetics. Otherwise, rate constants potentially could be falsified.

3.4 Lean Flammability Limits under High Temperature and High Pressure Conditions

This investigation was performed in collaboration with Professor Chung K. Law of Princeton University, and more details can be found in Ref. 24. The lean flammability limits of CH_4/air and C_3H_8/air mixtures were determined numerically for a wide range of pressures and unburned mixture temperatures in order to assess the near-limit flame behavior under conditions of relevance to air-breathing propulsion devices. The study included the simulation of freely propagating flames with the inclusion of detailed descriptions of chemical kinetics and molecular transport, radiative loss, and a one-point continuation method to solve around singular points as the flammability limit is approached. Results revealed that both pressure and unburned mixture temperature have significant effects on the lean flammability limit as well as the attendant limit flame temperature. Specifically, the lean limit was found first to increase and then decrease with pressure, while the limit temperature decreased with pressure in general, and could be reduced to values as low as 900 K at the highest values of unburned mixture temperatures and pressures that were considered. Sensitivity and species consumption path analyses showed that the chain mechanisms that control the near-limit flame response critically depend on the thermodynamic state of the mixture. Thus, mechanisms that are identified as important at near-atmospheric conditions may not be relevant at higher unburned mixture temperatures and pressures. The response of near-limit flames was found to resemble the homogeneous explosion limits of hydrogen/oxygen mixtures. While, at low pressures, the main branching and termination reactions are, respectively, $H + O_2 \rightarrow OH + O$ and $H + O_2 + M \rightarrow HO_2 + M$, at high pressures, the system branching is controlled by the HO_2-H_2O_2 kinetics. Potential avenues for extending the lean operation limits of engines were suggested based on the understanding gained from this analysis.

References

1. Smith, G.P., Golden, D.M., Frenklach, M., Moriarty, N.W., Eiteneer, B., Goldenberg, M., Bowman, C.T., Hanson, R.K., Song, S., Gardiner, Jr. W.C., Lissianski, V., Qin, Z., GRI-Mech 3.0, http://www.me.berkeley.edu/gri_mech/ (2000).
2. Egolfopoulos, F.N., Dimotakis, P.E., *Combust. Sci. Tech.* **162**, pp. 19-36 (2001).
3. Dong, Y., Vagelopoulos, C.M., Spedding, G.R., Egolfopoulos, F.N., *Proc. Combust. Inst.* **29**: 1419-1426 (2002).
4. Dong, Y., Holley, A.T., Andac, M.G., Egolfopoulos, F.N., Davis, S.G., Middha, P., Wang, H., *Combust. Flame* **142**, pp. 374-387 (2005).
5. Holley, A.T., Dong, Y., Andac, M.G., Egolfopoulos, F.N., *Combust. Flame* **144**, pp. 448-460 (2006).
6. Holley, A.T., Dong, Y., Andac, M.G., Egolfopoulos, F.N., Edwards, T., *Proc. Combust. Inst.* **31:** 1205-1213 (2007).
7. Egolfopoulos, F.N., Campbell, C.S., *J. Fluid Mech.* **318**, pp. 1-29 (1996).
8. Mueller, M.A., Kim, T.J., Yetter, R.A., Dryer, F.L., *Int. J. Chem. Kin.* **31**, pp. 113-119 (1999).
9. Davis, S.G., Joshi, A.V., Wang, H., Egolfopoulos, F.N. *Proc. Combust. Inst.* **30**: 1283-1292 (2005).
10. Wang, H., Personal Communications (2003).
11. Held, T.I., Dryer, F.L., *Int. J. Chem. Kin.* **30(11)**, pp. 805-830 (1998).
12. Fischer, S.L., Dryer, F.L., Curran, H.J., *Int. J. Chem. Kin.* **32(12)**, pp. 713-740 (2000).
13. Marinov, N.M., *Int. J. Chem. Kin.* **31(3)**, pp. 183-220 (1999).
14. Davis, S.G., Law, C.K., *Proc. Combust. Inst.* **27:** 521-527 (1998).

15. Pitsch, H., Peters, N., Seshadri, K., *Proc. Combust. Inst.* **26:** 763-771 (1996).
16. Langille, J.A., Dong, Y., Andac, M.G., Egolfopoulos, F.N., Tsotsis, T.T., *Combust. Sci. Tech.* **178(4)**, pp. 635-653 (2006).
17. Fotache, C.G., Kreutz, T.G., Zhu, D.L., Law, C.K., *Combust. Sci. Tech.* **109**, pp. 373-393 (1995).
18. Dong, Y., You, X., Sheen, D.A., Wang, H., Holley, A.T., Andac, M.G., Egolfopoulos, F.N., Kalitan, D.M., Petersen, E.L., "Flame and Ignition Kinetics of Dry Synthesis Gas-Like Mixtures," in preparation.
19. Violi, A., Fan, S., Eddings, E.G., Sarofim, A.F., Granata, S., Faravelli, T., Ranzi, E. *Comb. Sci. Tech.* **174,** pp. 399-417 (2002).
20. Schulz, W.D., *J. Prop. Power* **9**, pp. 5-9 (1993).
21. Lindstedt, R.P., Personal Communications (2006).
22. US Jet Fuels Group, Recommendation (2006).
23. Andac, M.G., Egolfopoulos, F.N., *Proc. Combust. Inst.* **31:** 1165-1172 (2007).
24. Egolfopoulos, F.N., Holley, A.T., Law, C.K., *Proc. Combust. Inst.* **31:** 3015-3022 (2007).

Personnel

This research was performed by the PI, two Research Associates (Dr. Yufei Dong and Dr. Gurhan Andac), and two graduate students (Jeff Langille and Adam Holley).

Publications

1. "An Optimized Kinetic Model of H_2/CO Combustion," by S.G. Davis, A.V. Joshi, H. Wang, and F.N. Egolfopoulos, *Proceedings of the Combustion Institute* **30**: 1283-1292 (2005).
2. "Extinction of Premixed H_2/Air Flames: Chemical Kinetics and Molecular Diffusion Effects," by Y. Dong, A.T. Holley, M.G. Andac, F.N. Egolfopoulos, S.G. Davis, P. Middha, and H. Wang, *Combustion and Flame*, Vol. **142**, pp. 374-387 (2005).
3. "Extinction of Premixed Flames of Practical Liquid Fuels: Experiments and Simulations," by A.T. Holley, Y. Dong, M.G. Andac, and F.N. Egolfopoulos, *Combustion and Flame*, Vol. **144**, pp. 448-460 (2006).
4. "Non-Premixed Ignition by Vitiated Air in Counterflow Configurations," by J.A. Langille, Y. Dong, M.G. Andac, F.N. Egolfopoulos, and T.T. Tsotsis, *Combustion Science and Technology*, Vol. **178(4)**, pp. 635-653 (2006).
5. "Diffusion and Kinetics Effects on the Ignition of Premixed and Non-Premixed Flames," by M.G. Andac and F.N. Egolfopoulos, *Proceedings of the Combustion Institute* **31**: 1165-1172 (2007).
6. "Ignition and Extinction of Non-Premixed Flames of Single-Component Liquid Hydrocarbons, Jet Fuels, and their Surrogates," by A.T. Holley, Y. Dong, M.G. Andac, F.N. Egolfopoulos, and T. Edwards, *Proceedings of the Combustion Institute* **31**: 1205-1213 (2007).
7. "An Assessment of the Lean Flammability Limits of CH_4/Air and C_3H_8/Air Mixtures at Engine-Like Conditions," by F.N. Egolfopoulos, A.T. Holley, and C.K. Law, *Proceedings of the Combustion Institute* **31**: 3015-3022 (2007).
8. "Flame and Ignition Kinetics of Dry Synthesis Gas-Like Mixtures," by Y. Dong, X. You, D.A. Sheen, H. Wang, R. Kinslow, M. Call, A.T. Holley, M.G. Andac, F.N. Egolfopoulos, D.M. Kalitan, and E.L. Petersen, in preparation.

Interactions/Transitions

Presentations at Meetings and Conferences

1. "Premixed Flame Extinction of Practical Liquid Fuels," by A. Holley, A. Balteria, Y. Dong, M.G. Andac, Y. Fan, and F.N. Egolfopoulos, paper No. 03F-25, Fall Technical Meeting, *Western States Section/Combustion* Institute, University of California Los Angeles, Los Angeles, CA, October 20-21, 2003.

2. "Ignition of H_2 and CO by Vitiated Air in Counterflow Configurations," by J. Langille, J. Pasale, Y. Dong, M.G. Andac, T. T. Tsotsis, and F.N. Egolfopoulos, paper No. 03F-33, Fall Technical Meeting, *Western States Section/Combustion* Institute, University of California Los Angeles, Los Angeles, CA, October 20-21, 2003.

3. "Experimental and Numerical Studies of Flame Extinction: Validation of Chemical Kinetics," by Y. Dong, A. Holley, M.G. Andac, and F.N. Egolfopoulos, S.G. Davis, and H. Wang, paper No. 03F-89, Fall Technical Meeting, *Western States Section/Combustion* Institute, University of California Los Angeles, Los Angeles, CA, October 20-21, 2003.

4. "Ignition of H_2 and CO by Vitiated Air in Counterflow Configurations," by J. Langille, J. Pasale, Y. Dong, M.G. Andac, T. T. Tsotsis, and F.N. Egolfopoulos, paper No. 04S-6, Spring Technical Meeting, *Western States Section/Combustion* Institute, University of California at Davis, Davis, CA, March 29-30, 2004.

5. "Experimental and Numerical Studies of Extinction of Premixed Lean H_2/Air Flames," by Y. Dong, A. Holley, M.G. Andac, and F.N. Egolfopoulos, S.G. Davis, and H. Wang, paper No. 04S-19, Spring Technical Meeting, *Western States Section/Combustion* Institute, University of California at Davis, Davis, CA, March 29-30, 2004.

6. "Premixed Flame Extinction of Practical Liquid Fuels," by A. Holley, A. Balteria, Y. Dong, M.G. Andac, Y. Fan, and F.N. Egolfopoulos, paper No. 04S-22, Spring Technical Meeting, *Western States Section/Combustion* Institute, University of California at Davis, Davis, CA, March 29-30, 2004.

7. "Experimental and Detailed Numerical Studies of Fundamental Flame Properties of Gaseous and Liquid Fuels," 2003 Contractors Meeting in Chemical Propulsion, *Army Research Office and Air Force Office of Scientific Research*, Tucson, Arizona, June 7-9, 2004.

8. "Experimental and Detailed Numerical Studies of Fundamental Flame Properties of Gaseous and Liquid Fuels," 2005 Contractors Meeting in Chemical Propulsion, *Army Research Office and Air Force Office of Scientific Research*, Indianapolis, Indiana, June 20-22, 2005.

9. "Pressure and Temperature Effects on the Flammability Limits of CH_4/air and C_3H_8/air Flames," F.N. Egolfopoulos, A.T. Holley, and C.K. Law paper No. 05F-011 Fall Technical Meeting, *Western States Section/Combustion Institute*, Stanford University, California, California, October 17-18, 2005.

10. "A Detailed Study of $CO/H_2/O_2$ Kinetics in Dry Synthesis-Gas/Air Flames," D.A. Sheen, R. Kinslow, M. Call, A.T. Holley, X. You, M.G. Andac, H. Wang, and F.N. Egolfopoulos, paper No. 05F-013 Fall Technical Meeting, *Western States Section/Combustion Institute*, Stanford University, California, California, October 17-18, 2005.

11. "Diffusion and Reaction Effects on the Ignition of Premixed and Non-Premixed iso-Octane Flames," M.G. Andac and F.N. Egolfopoulos, paper No. 05F-015 Fall Technical Meeting, *Western States Section/Combustion Institute*, Stanford University, California, California, October 17-18, 2005.

12. "Ignition and Extinction of Non-Premixed Flames of Single-Component Liquid Hydrocarbons, Jet Fuels, and their Surrogates," A.T. Holley, Y. Dong, M.G. Andac, F.N. Egolfopoulos, and T. Edwards paper No. 05F-056 Fall Technical Meeting, *Western States Section/Combustion Institute*, Stanford University, California, California, October 17-18, 2005.

13. "Ignition and Extinction Studies of Mixtures of Air with Single-Component Liquid Hydrocarbons, Gasoline, and Gasoline Surrogates," A.T. Holley, Y. Dong, M.G. Andac, and F.N. Egolfopoulos, paper No. 05F-074 Fall Technical Meeting, *Western States Section/Combustion Institute*, Stanford University, California, California, October 17-18, 2005.

14. "Experimental and Detailed Numerical Studies of Fundamental Flame Properties of Gaseous and Liquid Fuels," 2003 Contractors Meeting in Chemical Propulsion, *Army Research Office and Air Force Office of Scientific Research*, Washington, D.C., June 7-9, 2006.

Technical Interactions with AFRL Researchers

Several meetings with Dr. Tim Edwards of AFRL took place during the reporting period. The purpose of these meetings was to discuss the measurements on the ignition and extinction limits of mixtures of air with JP7, JP8, JP10, RP1, and various synthetic jet fuels that were supplied to the USC Combustion and Fuels Laboratory by Dr. Edwards. Further discussions will follow in the future regarding the ongoing experimental and modeling work pertaining to jet fuels and their surrogates, as well as ongoing work on smaller hydrocarbons in the C_1-C_4 range. The latter is of relevance to the thermal cracking of jet fuels.

Other Technical Interactions

A close interaction has been established with Professor Hai Wang of the University of Southern California on the modeling aspects of this research. More specifically, the kinetic model development guides to great extent the experimental parameter space.

Inventions, Technology Transitions and Transfers

Part of the work described in this report resulted to the following technology transition and transfer:

Performers:	Dr. Hai Wang, University of Southern California, (213) 740-0499; Dr. Fokion N. Egolfopoulos, University of Southern California, (213) 740-0480
Customer:	Dr. Bala Varatharajan, GE Global Research Center, One Research Circle, Building K-1, Room ES243, Niskayuna NY 12309.
Phone:	(518) 387-4133
Result:	Reaction model for hydrogen and propane combustion
Application:	NO_x control in gas turbines

Available online at www.sciencedirect.com
SCIENCE DIRECT®
ELSEVIER
Proceedings of the Combustion Institute 30 (2005) 1283–1292
Proceedings of the Combustion Institute
www.elsevier.com/locate/proci

An optimized kinetic model of H_2/CO combustion

Scott G. Davis[a,*], Ameya V. Joshi[a], Hai Wang[a], Fokion Egolfopoulos[b]

[a] *Department of Mechanical Engineering, University of Delaware, Newark, DE 19716, USA*
[b] *Department of Aerospace and Mechanical Engineering, University of Southern California, Los Angeles, CA 90089, USA*

Abstract

We propose a H_2–CO kinetic model which incorporates the recent thermodynamic, kinetic, and species transport updates relevant to high-temperature H_2 and CO oxidation. Attention has been placed on obtaining a comprehensive and kinetically accurate model able to predict a wide variety of H_2–CO combustion data. The model was subject to systematic optimization and validation tests against reliable H_2–CO combustion data, from global combustion properties (shock-tube ignition delays, laminar flame speeds, and extinction strain rates) to detailed species profiles during H_2 and CO oxidation in flow reactor and in laminar premixed flames.

Keywords: Kinetics; Detailed reaction model; Hydrogen; Carbon monoxide

1. Introduction

The most successful model of H_2–CO combustion has been that of Mueller et al. [1], developed on the basis of a careful evaluation of relevant kinetic parameters and flow reactor experiments. The model is also able to predict a wide range of flame experiments. Over the last few years, however, the rate parameters of the key reaction $H + O_2 + M = HO_2 + M$ and its third-body efficiencies have been revised [2,3], giving an urgent reason for a re-examination of the H_2–CO combustion model. The downward revision of the enthalpy of formation of OH [4] may also exert an influence on the overall reaction kinetics of H_2 combustion.

Several new studies [5–7] have been reported in recent years. Two of these studies analyzed the hydrogen submodel [5,6], both being an extension of the model of Mueller et al. The third analysis [7] considered both H_2 and CO chemistry and is the predecessor to the present study. The objectives of the present study are (1) to provide an update for the H_2–CO combustion reaction model on the basis of recent kinetic data, and (2) to optimize the H_2–CO model against available H_2–CO combustion data.

2. Reaction model

The unoptimized (trial) reaction model consists of 14 species and 30 reactions as shown in Fig. 1. The model and its thermochemistry and transport property files can be found at the URL: http://ignis.me.udel.edu/h2co. The trial model was based on a careful review of recent kinetics literature, considering both direct data and compilations. A large number of GRI 3.0 rate parameters [8] were

* Corresponding author. Present address: Exponent, 21 Strathmore Road, Natick, MA 01760, USA. Fax: +1 508 647 3619.
E-mail address: daviss@exponent.com (S.G. Davis).

1540-7489/$ - see front matter © 2004 The Combustion Institute. Published by Elsevier Inc. All rights reserved.
doi:10.1016/j.proci.2004.08.252

no.	reaction	rate parameters[a] $A^{(b)}$	n	E	f^c	ref/ comments[c]
1	$H+O_2=O+OH$	2.65(16)	−0.671	17041	1.15	[8]
2	$O+H_2=H+OH$	3.87(04)	2.7	6260	1.3	[8]
3	$OH+H_2=H+H_2O$	2.16(08)	1.51	3430	1.3	[8]
4	$2OH=O+H_2O$	3.57(04)	2.4	−2110	1.3	[8]
5	$2H+M=H_2+M$	1.00(18)	−1		2	[8]
5a	$H_2O/0.0 T^{b\ 2.5}/$				2	d
	$H_2/0.0506 T^{2.5}/$, $CO/1/$, $CO_2/3.097 T^{1.5}/$, $Ar/0.63/$, $He/0.63/$					
6	$H+OH+M=H_2O+M$	2.20(22)	−2		2	[8]
	$H_2/2/$, $H_2O/6.3/$, $CO/1.75/$, $CO_2/3.6/$, $Ar/0.38/$, $He/0.38/$					
7	$O+H+M=OH+M$	4.71(18)	−1		2	[9]
	$H_2/2/$, $H_2O/12/$, $CO/1.75/$, $CO_2/3.6/$, $Ar/0.7/$, $He/0.7/$					
8	$2O+M=O_2+M$	1.20(17)	−1			[8]
	$H_2/2.4/$, $H_2O/15.4/$, $CO/1.75/$, $CO_2/3.6/$, $Ar/0.83/$, $He/0.83/$					
9	$H+O_2(+M)=HO_2(+M)$	4.65(12)	0.44		1.2	[2], k_∞
		5.75(19)	−1.4		1.2	k_0, e
9a	$Ar/0.85/$				1.2	d
9b	$He/0.85/$				1.2	d
9c	$O_2/0.75/$				1.2	d
9d	$H_2O/12/$				1.2	d
9e	$H_2/1.0/$				1.2	d
	$CO/1.2/$, $CO_2/2.4/$					
10	$H_2+O_2=HO_2+H$	7.40(05)	2.433	53502	1.25	[10]
11	$2OH(+M)=H_2O_2(+M)$	7.40(13)	−0.37		1.5	[11], k_∞
		1.34(17)	−0.584	−2293	1.5	k_0, f
	$H_2/2/$, $H_2O/6/$, $CO/1.75/$, $CO_2/3.6/$, $Ar/0.7/$, $He/0.7/$					
12	$HO_2+H=O+H_2O$	3.97(12)		671		[8]
13	$HO_2+H=OH+OH$	7.08(13)		295	2	[13]
14	$HO_2+O=OH+O_2$	2.00(13)			2	[8]
15a	$HO_2+OH=O_2+H_2O$	2.90(13)		−500	2	[14]
15b		1.00(16)		17330		[15]
16a	$2HO_2=O_2+H_2O_2$	1.30(11)		−1630		[16]
16b		4.20(14)		12000	1.5	[16]
17	$H_2O_2+H=HO_2+H_2$	1.21(07)		25200	2	[8]
18	$H_2O_2+H=OH+H_2O$	2.41(13)		3970		[9]
19	$H_2O_2+O=OH+HO_2$	9.63(06)		23970		[9]
20a	$H_2O_2+OH=HO_2+H_2O$	2.00(12)		427		[15]
20b		2.67(41)		−737600		g
21	$CO+O(+M)=CO_2(+M)$	1.80(10)		2384	2	[13], k_∞
		1.55(24)	−2.79	4191	2	k_0, h
	$H_2/2/$, $H_2O/12/$, $CO/1.75/$, $CO_2/3.6/$, $Ar/0.7/$, $He/0.7/$					
22a	$CO+OH=CO_2+H$	9.60(11)	0.14	7352	1.2	i
22b		7.32(10)	0.03	−16	1.2	i
23	$CO+O_2=CO_2+O$	2.53(12)		47700	3	[9]
24	$CO+HO_2=CO_2+OH$	3.01(13)		23000	2	[1]
25	$HCO+H=CO+H_2$	1.20(14)			2	[17]
26	$HCO+O=CO+OH$	3.00(13)				[8]
27	$HCO+O=CO_2+H$	3.00(13)				[8]
28	$HCO+OH=CO+H_2O$	3.02(13)				[9]
29	$HCO+M=CO+H+M$	9.35(16)	−1	17000	2	[17]
29a	$H_2O/12/$				2	d
	$H_2/2/$, $CO/1.75/$, $CO_2/3.6/$, $Ar/1/$, $He/1/$					
30	$HCO+O_2=CO+HO_2$	1.20(10)	0.807	−727		[18]

[a] Rate parameters $k=AT^n\exp(-E/RT)$. Units are cm, s, mol, and cal. Unless otherwise indicated, multiple entries of rate expressions for a reaction indicate the rate coefficient is the sum of these expressions. [b] The number in the parenthesis is the exponent of 10, i.e., 2.65(16) = 2.65×10^{16}. Parameters highlighted in red are active and subject to optimization. [c] f is the uncertainty factor or span assigned to active A factors. [d] The third-body collision efficiency is active and subject to optimization. [e] Center broadening factor $F_c = 0.5$. [f] Low-pressure limit fit to expressions given in [11] and [12]. $F_c = 0.2654\exp(-T/1758) + 0.7346\exp(-T/5182)$. [g] Fit to the expression of [16]. [h] $F_c = 1$ (Lindemann fall-off). [i] This work (see text).

Fig. 1. Trial reaction model of H_2–CO oxidation, active parameters, and their spans employed in model optimization (see Refs. [9,14,16–18]).

found to be appropriate and are used. The discussion below highlights the choice of key rate parameters.

The rate expression of $H + O_2 = O + OH$ was taken from GRI 3.0 [8]. The rate coefficient of $H + O_2(+M) = HO_2(+M)$ was based on Troe [2], who employed a high-pressure rate $k_{rec,\infty}$ ($cm^3\ mol^{-1}\ s^{-1}$) $= 4.65 \times 10^{12} T^{0.44}$ and developed the low-pressure and fall-off expressions for Ar and N_2 as the bath gases. The broadening factor F_c was found to be 0.5 for both third bodies. Troe's fall-off rate parameterization, however, could not be directly used in CHEMKIN [19], because the low-pressure limit rate coefficient k_0 does not share the same temperature dependence for different third bodies. We had to develop parameterized rate expressions (see Fig. 1) based on the k_0 expression of Ar and using the fall-off formula of Troe [20]. A collision efficiency factor $\beta = 0.53$ was used for Ar relative to N_2. The collision efficiency of He was assumed to be equal to that of Ar. The study of Michael et al. [3] supports a collision efficiency of O_2 smaller than that of N_2. We found that for O_2, $\beta = 0.75$ gives a good agreement with experiment [3] and theory [2]. For H_2O, Troe [2] suggested that the broadening factor is close to the strong-collision limit. We chose a β value of 12 (relative to N_2) with the resulting rate in good agreement with those of Troe and others [2,3,21].

The k_0 expression of $H + OH + M = H_2O + M$ was taken from [8] with the β values equal to 0.38 and 6.3 for Ar and H_2O, respectively [12]. The rate expression of Michael et al. [10] was employed for $H_2 + O_2 = H + HO_2$. For $OH + OH(+M) = H_2O_2(+M)$, the k_0 expression, given in the reverse direction by Baulch et al. [12], was refitted based on the new heat of formation of the OH radical along with the low temperature data of Zellner et al. [11]. The $k_{rec,\infty}$ expression and the β value of H_2O (6) were taken from [11] while the Troe fall-off parameters [22] were the same as those in GRI 3.0. The rate expressions for $H_2O_2 + OH = HO_2 + H_2O$ were taken directly from [15], though the high-temperature expression was refitted using a modified Arrhenius expression to avoid the rate constant values exceeding the collision limit when extrapolated to high temperatures.

For $CO + O(+M) = CO_2(+M)$, the k_∞ expression was taken from [13], and following Allen et al. [23], k_0 was taken from the QRRK analysis of Westmoreland et al. [24] and fall-off was that of Lindemann. The collision efficiency of H_2O was assumed to be 12. The rate constant for $CO + OH = CO_2 + H$ was re-analyzed in the present study, and the experimental data were refitted by the sum of two modified Arrhenius expressions. The new expression resolves more accurately the high temperature data of Wooldridge et al. [25] as well as the data found in [26]. Without this revision, it was not possible to reconcile the high-temperature H_2 ignition data with the H_2–CO laminar flame speeds. The known pressure dependence of this reaction was not considered as this dependence is quite unimportant for the CO oxidation experiments considered herein.

3. Computational and optimization method

A comprehensive review was conducted for a large number of H_2–CO combustion data. Thirty-six experiments were chosen as optimization targets as shown in Table 1. They can be classified into four categories: (1) laminar flame speeds of H_2–air, H_2–O_2–He, and H_2–CO–air mixtures, (2) the peak mole fractions of H and O in a low-pressure burner-stabilized H_2–O_2–Ar flame, (3) the consumption rates of H_2 and CO during the reaction of H_2–O_2–N_2 and CO–O_2–H_2O–N_2 mixtures in a turbulent flow reactor, and (4) ignition delay times of H_2–O_2–Ar and H_2–CO–O_2–Ar mixtures behind reflected shock waves.

Ignition delay and flow reactor calculations were conducted using a kinetic integrator interfaced with CHEMKIN [19] by assuming adiabatic condition. Ignition delays were modeled using the constant-density model, whereas flow reactor modeling used the constant-pressure assumption. The numerical ignition delays were determined following the same ignition criteria as in the respective experiments. Laminar flame speeds and structure were calculated using Premix [40], employing thermal diffusion, and multicomponent transport. Diffusion coefficients of several key pairs were updated [41].

Sensitivity analyses were conducted for ignition delay and consumption rates of the fuel in flow reactor with a brute force method. For laminar flame speeds and H and O peak mole fractions in burner-stabilized flames, the local sensitivity methods were utilized. Based on the sensitivity information, active rate parameters (to be optimized) were chosen for each target. The entire set of active parameters consists of 28 A-factors and third-body efficiency factors as shown in Figs. 1 and 2.

The optimization approach is similar to earlier studies [8,43]. Briefly, the solution mapping technique was employed to express a response by a second-order polynomial $\eta^{(2)} = a_0 + \sum_{j=1}^{n} a_i x_i + \sum_{i=1}^{n} \sum_{j \geq i}^{n} b_{ij} x_i x_j$, where a's and b's are the coefficients, x's are factorial active variables given by $x = \ln(\alpha/\alpha_{\text{trial}})/\ln(f)$, where α is the active A factor or third-body efficiency factor, and f is its span or uncertainty factor. The uncertainty factor was estimated on the basis of kinetic uncertainty and is provided in Fig. 1 for each active parameter. Though an optimization of the temperature dependence of rate coefficients is possible, we chose not to vary the T-dependence because of the insufficient number of systematic experimental targets [43].

For flow reactor targets, the response was found to be highly non-linear with respect to x's. These responses are expressed by adding a hyperbolic tangent term to account for the S-shaped dependence of response with respect to x's, $\eta = \eta^{(2)} + c \tanh(a_0' + \sum_{j=1}^{n} a_i' x_i + \sum_{i=1}^{n} \sum_{j \geq i}^{n} b_{ij}' x_i x_j)$. The coefficients for the flow reactor and ignition delay targets were calculated by a factorial design test [43]. The coefficients for flame targets were obtained using the sensitivity analysis based method [44].

Minimization was carried out on the objective function $L^2 = \Sigma_i[(\eta_{i,\text{expt}} - \eta_{i,\text{calc}})/\sigma_i]^2$ subject to the constraint $-1 < \{x\} < +1$, where the subscript i denotes the ith target. Each target was individually weighted by their uncertainty σ_i. The target values and their uncertainties are presented in Table 1.

4. Results and discussion

The trial kinetic model was tested against a wide range of experimental data. The predictions of the trial model for the 36 target values are shown in Table 1 (the "trial" column). Overall the model performed well against these experimental data. The exceptions are: it overpredicts H_2–O_2–He flame speeds, the H and O mole fractions in the burner-stabilized flame, and the consumption rate of H_2 for the 1.0% H_2–1.5 O_2%–N_2 flow reactor mixture at 943 K and 2.5 atm.

To reconcile these discrepancies, optimization was then carried out for 28 active parameters with respect to 36 targets. All active parameters were allowed to vary freely within their uncertainty spans. The optimal parameter set was obtained as the minimum of L^2, first from a random sample of the multidimensional parameter space, followed by a Newton search of the L^2 minimum in the parameter space. The values of optimized active parameters are shown in the last column of Fig. 2 (expressed as the optimized-to-trial parameter ratio). To obtain the optimized model, the active parameters (A-factors and third-body efficiency factors) shown in Fig. 1 should be multiplied by their corresponding ratios.

Validation of the optimized model will be discussed below. Figure 3 presents experimental [27–31,45] and computed laminar flame speeds of H_2–air and air-equivalent mixtures where N_2 was replaced by Ar or He. With trial model predictions already close to the experimental values, the optimization served only to fine-tune the model, resulting in excellent agreement with the experiment as can be seen in Fig. 3 and Table 1. The trial model tends to overpredict the H_2–O_2–He flame speeds at elevated pressures (Table 1). The discrepancies are clearly caused by kinetics as a previous study showed that the uncertainty in the transport coefficients cannot account for the observed differences [41]. Now the optimized model can successfully predict these H_2–O_2–He flame speeds [27] as seen in Fig. 4. This agreement was brought by lowering the rate of $OH + H_2 = H + H_2O$, $H + HO_2 = OH + OH$, and a small increase in the rate of $H + O_2 + H_2O = HO_2 + H_2O$.

The dominant sensitivity of the laminar flame speeds of H_2–CO–air mixtures, especially the

Table 1
Optimization targets

Target No.	Composition (mol %)					$T_0(T_5)$ (K)	$p_0(p_5)$ (atm)	Comments	Target		Model		Units
	H_2	O_2	CO	H_2O	Diluent				Value ± σ	Ref.	Trial	Opt.	
Flame speed													
fls 1a	29.6	14.8	—	—	N_2	298.2	1	H_2–air, $\phi = 1$	204 ± 20	[27–31]	221	206	cm/s
fls 1b	55.8	9.3	—	—	N_2	298.2	1	H_2–air, $\phi = 3$	217 ± 20	[27,28,31]	228	216	cm/s
fls 2a	20	10	—	—	He	298.2	1	$\phi = 1$	206 ± 20	[27]	237	231	cm/s
fls 2b	36	8	—	—	He	298.2	1	$\phi = 2.25$	249 ± 25	[27]	265	258	cm/s
fls 3a	13.8	6.9	—	—	He	298.2	15	$\phi = 1$	58 ± 6	[27]	69	61	cm/s
fls 3b	21.9	6.3	—	—	He	298.2	15	$\phi = 1.75$	88 ± 9	[27]	97	91	cm/s
fls 4a	1.6	14.2	30.9	—	N_2	298.2	1	$\phi = 1.148$	40 ± 4	[32]	42	42	cm/s
fls 4b	3	8	59	—	N_2	298.2	1	$\phi = 3.895$	52.5 ± 5	[32]	56	53	cm/s
fls 5a	14.8	14.8	14.8	—	N_2	298.2	1	$\phi = 1$	111.5 ± 11	[32]	114	110	cm/s
fls 5b	28.1	9.2	28.1	—	N_2	298.2	1	$\phi = 3.05$	154.5 ± 15	[32]	161	155	cm/s
fls 6a	9.2	17.4	7.8	—	N_2	298.2	1	$CO/H_2 = 0.84$	10.3 ± 2.0	[33]	11	11	cm/s
fls 6b	2.9	17.4	14.1	—	N_2	298.2	1	$CO/H_2 = 4.90$	18.5 ± 2.0	[33]	20	20	cm/s
Flat flame													
flf 1a	39.7	10.3	—	—	Ar	—	0.047	$x_{H,max}$	0.067 ± 0.051	[34]	0.103	0.077	—
flf 1b	39.7	10.3	—	—	Ar	—	0.047	$x_{O,max}$	0.002 ± 0.015	[34]	0.003	0.003	—
Flow reactor													
flw 1a	1.18	0.61		—	N_2	914	15.7	a	8.6 ± 0.5	[13]	10.4	8.7	ppm/ms
flw 2a	1.01	0.52	—	—	N_2	935	6	a	13.0 ± 0.5	[13]	11.2	12.4	ppm/ms
flw 3a	1.0	1.5	—	—	N_2	943	2.5	a	98 ± 10	[13]	532	97	ppm/ms
flw 4a	0.5	0.5	—	—	N_2	880	0.3	a	261 ± 20	[13]	334	318	ppm/ms
flw 5a	—	0.517	1.014	0.65	N_2	1038	1	b	354 ± 40	[35]	293	282	ppm/ms
flw 6a	—	0.494	0.988	0.65	N_2	1038	3.46	b	140 ± 20	[35]	54	53	ppm/ms
flw 6b	—	0.494	0.988	0.65	N_2	1038	3.46	c	229 ± 20	[35]	242	237	ms
flw 7a	—	0.482	1.002	0.65	N_2	1068	6.5	d	14.1 ± 0.5	[35]	19.0	14.6	ppm/ms
flw 8a	0.95	0.49	—	—	N_2	934	3.02	e	19.0 ± 1.0	[13]	17.8	19.0	ppm/ms
flw 8b	0.95	0.49	—	—	N_2	934	3.02	f	70 ± 5	[13]	62	68	ms
Shock-tube ignition													
ign 1a	6.67	3.33	—	—	Ar	1051	1.729	Onset of p rise	231 ± 120	[36]	320	310	μs
ign 1b	6.67	3.33	—	—	Ar	1312	2.008		50 ± 25	[36]	62	62	μs
ign 2a	20	10	—	—	Ar	1033	0.518	Maximum p	238 ± 140	[37]	345	342	μs
ign 2b	20	10	—	—	Ar	1510	0.493		29 ± 20	[37]	37	39	μs
ign 3a	0.5	0.25	—	—	Ar	1754	33	Maximum [OH]	10 ± 3	[38]	11	11	μs
ign 4a	2	1	—	—	Ar	1189	33	Maximum [OH]	293 ± 100	[38]	243	168	μs
ign 4b	2	1	—	—	Ar	1300	33		11 ± 4	[38]	24	20	μs
ign 5a	0.1	0.05	—	—	Ar	1524	64	Maximum [OH]	54 ± 25	[38]	64	60	μs
ign 6a	0.05	1	12.17	—	Ar	2160	1.492	Onset of CO_2 rise	63 ± 25	[39]	56	60	μs
ign 6b	0.05	1	12.17	—	Ar	2160	1.492	$[O] = 2.5 \times 10^{14}$ cm^{-3}	47 ± 25	[39]	34	41	μs
ign 6c	0.05	1	12.17	—	Ar	2625	1.949	Onset of CO_2 rise	23 ± 10	[39]	20	22	μs
ign 6d	0.05	1	12.17	—	Ar	2625	1.949	$[O] = 2.5 \times 10^{14}$ cm^{-3}	11 ± 6	[39]	10	13	μs

[a] The target value is $\Delta x_{H_2}/\Delta t|^{0.6}_{c_{H_2}=0.4}$, where x is the mole fraction (ppm); c is the fractional conversion.
[b] $\Delta x_{CO}/\Delta t|^{0.6}_{c_{CO}=0.4}$.
[c] $\Delta t|^{0.95}_{c_{CO}=0.75}$.
[d] $\Delta x_{CO}/\Delta t|^{0.6}_{c_{CO}=0.4}$.
[e] $\Delta x_{CO}/\Delta t|^{0.95}_{c_{CH_4}=0.85}$.
[f] $\Delta t|^{0.9}_{c_{H_2}=0.4}$.

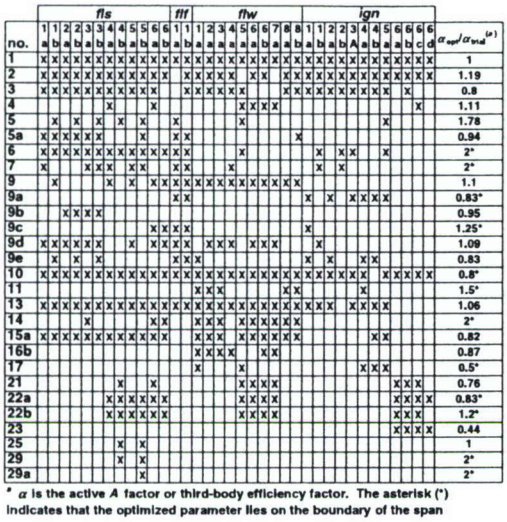

Fig. 2. Target-active parameter matrix.

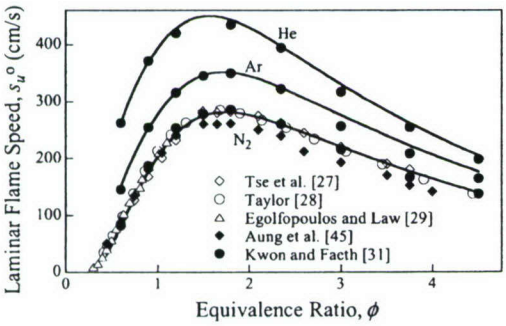

Fig. 3. Experimental (symbols) and computed (lines: the optimized model) H_2–air and air equivalent (N_2 is replaced by Ar or He) flame speed at a pressure of 1 atm.

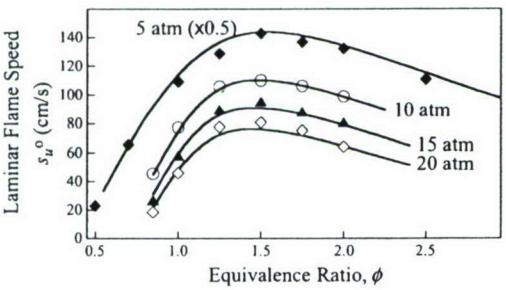

Fig. 4. Experimental (symbols [27]) and computed (lines: the optimized model) H_2–O_2–He flame speeds.

95% CO + 5% H_2 mixtures, to CO + OH = CO_2 + H has been observed elsewhere [32] and necessitated a re-evaluation this reaction. It was determined that the sum of two modified Arrhenius expressions was necessary to predict the laminar flame speed data. Figures 5 and 6 show that the optimized model reproduces experimental H_2–CO–air laminar flame speeds [32,33].

Figure 7 depicts species profiles for four selected H_2 oxidation experiments in a turbulent flow reactor [13]. Time shift was necessary to match the computed profiles with the experimental counterparts. The amounts of time shift were found to be similar with those used by Mueller et al. [13]. It is seen that the optimized model predicts the experimental species profile accurately, and it also improved the prediction of the experiment as compared to the trial model (cf. Fig. 7B). Similarly, the results of Fig. 8 show that for CO oxidation [35] the optimized model accurately predicts the CO consumption rate over an extended pressure range.

The trial model could accurately reconcile most of the ignition delay data for H_2–O_2–diluent mixtures, and optimization served only to improve these predictions as can be seen in Table 1. In addition, Fig. 9 shows a plot of experimental and computed ignition delay times for H_2–O_2–Ar mixtures [36–38,46] behind reflected shock waves. Here, the experimental shock-tube ignition delay data were fitted into $\tau\ (\mu s) = [H_2]^{-0.154}[O_2]^{-0.693}[Ar]^{0.04}\ [6.77 \times 10^{-8} T^{0.252} e^{9234/T}]$ for non-"run-

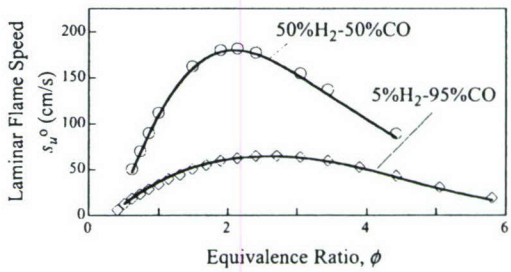

Fig. 5. Experimental (symbols [32]) and computed (lines: the optimized model) H_2–CO–air flame speeds at a pressure of 1 atm.

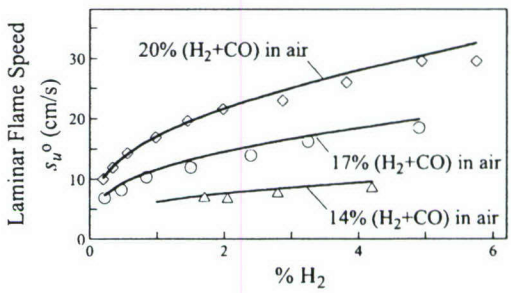

Fig. 6. Experimental (symbols [33]) and computed (lines: the optimized model) H_2–CO–air flame speeds at a pressure of 1 atm.

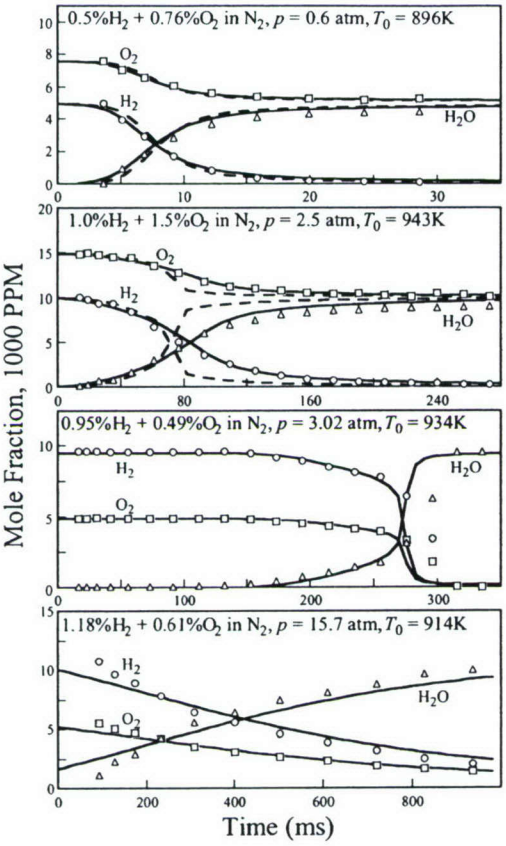

Fig. 7. Experimental (symbols [13]) and computed (lines) species mole fraction profiles during hydrogen oxidation in a flow reactor. Solid lines: optimized model; dashed lines: trial model.

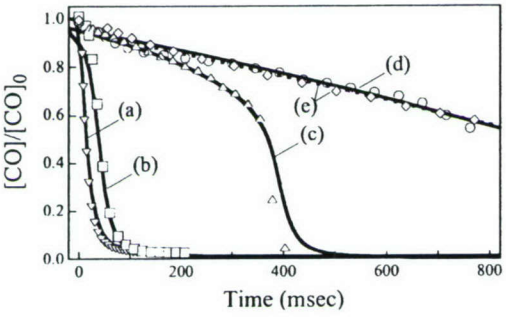

Fig. 8. Experimental (symbols [35]) and computed (lines) $[CO]/[CO]_0$ profiles during moist CO oxidation in a flow reactor. Cases (a): 1.014% CO + 0.517% O_2 + 0.65% H_2O in N_2, $p = 1$ atm, $T_0 = 1038$ K, (b) 1.01% CO + 0.496% O_2 + 0.65% H_2O in N_2, $p = 2.44$ atm, $T_0 = 1038$ K, (c) 0.988% CO + 0.494% O_2 + 0.65% H_2O in N_2, $p = 3.46$ atm, $T_0 = 1038$ K, (d) 0.984% CO + 0.497% O_2 + 0.65% H_2O in N_2, $p = 6.5$ atm, $T_0 = 1040$ K, and (e) 0.994% CO + 1.47% O_2 + 0.65% H_2O in N_2, $p = 9.6$ atm, $T_0 = 1039$ K.

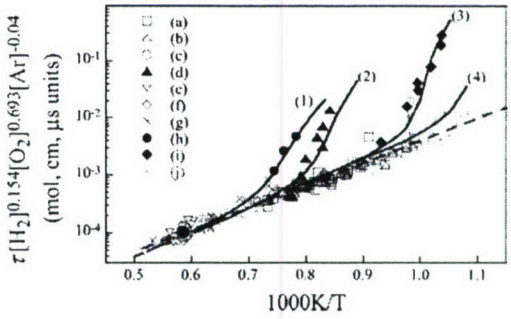

Fig. 9. Experimental (symbols) and computed (lines) ignition delay times of H_2–O_2–Ar mixtures behind reflected shock waves. Symbols: (a) 6.67% H_2 + 3.33% O_2, $p_5 = 1.35$–2.90 atm; (b) 5% H_2 + 5% O_2, $p_5 = 1.35$–2.90 atm (onset of pressure rise [36]), (c) 0.5% H_2 + 0.25% O_2, $p_5 = 33$ atm, (d) 2% H_2 + 1% O_2, $p_5 = 33$ atm, (e) 0.5% H_2 + 0.25% O_2, $p_5 = 57$ atm, (f) 0.33% H_2 + 0.17% O_2, $p_5 = 64$ atm, (g) 0.1% H_2 + 0.05% O_2, $p_5 = 64$ atm, (h) 0.5% H_2 + 0.25% O_2, $p_5 = 87$ atm (maximum OH absorption rate [38]), (i) 8% H_2 + 2% O_2, $p_5 = 5$ atm (maximum OH emission) [46], and (j) four $H_2 + O_2$ mixtures [37]. Lines: (1) 0.5% H_2 + 0.25% O_2, $p_5 = 87$ atm (maximum [OH] rate), (2) 2% H_2 + 1% O_2, $p_5 = 33$ atm (maximum [OH] rate), (3) 8% H_2 + 2% O_2, $p_5 = 5$ atm (maximum [OH]), and (4) 5% H_2 + 5% O_2, $p_5 = 2$ atm (maximum pressure gradient).

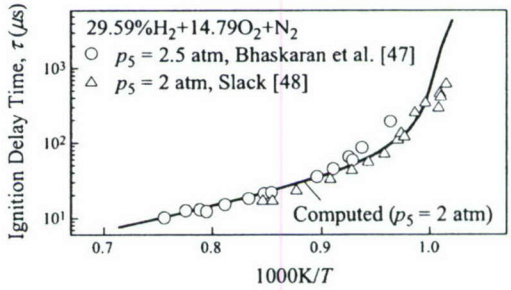

Fig. 10. Experimental (symbols) and computed (lines) ignition delay times behind reflected shock waves for H_2–O_2–N_2 mixtures. Experimental data were determined from onset of pressure rise [47] and maximum rate of OH emission [48].

away" data, i.e., those fall on the nearly linear portion of the curves of Fig. 9, where [ ] denotes concentration in mol/cm^3. For mixtures of H_2–O_2–N_2 [47,48], comparison was also made as seen in Fig. 10, where the result should only be considered as a secondary validation because the vibrational relaxation of N_2 was not accounted for in modeling. The optimized model also predicts fairly well the ignition delay of CO-H_2–O_2–Ar mixtures [39] as seen in Fig. 11.

The optimized model resulted in improved prediction of the species profiles measured in a low-pressure H_2–O_2–Ar flame, though the concen-

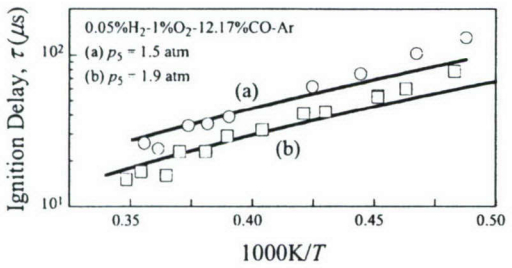

Fig. 11. Experimental (symbols [39]) and computed (lines) ignition delay times behind reflected shock waves. The experimental ignition delay was determined from the onset of infrared emission due to CO_2; the computational ignition delay determined from the maximum CO_2 concentration gradient.

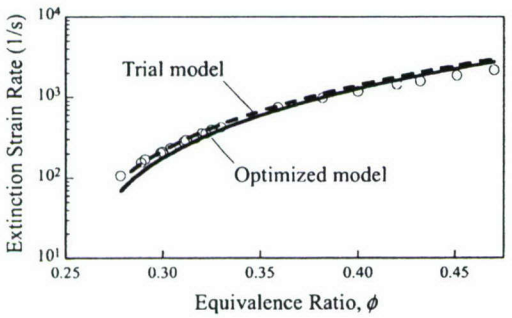

Fig. 12. Experimental (symbols [42]) and computed (lines) extinction strain rates as a function of the equivalence ratio for ultra-lean H_2–air mixtures.

trations of H and O are still overpredicted (see, Table 1). These discrepancies may well be caused by the experimental uncertainty due to flame perturbation by the sample probe.

Finally, the trial model (dashed lines) and the optimized model (solid lines) were compared against extinction strain rates of ultra-lean H_2–air mixtures [42]. These experiments were not used as optimization targets because of large influences from the uncertainties in the diffusion coefficients. The results of Fig. 12 indicate that both the trial and optimized model can accurately predict the data for the leaner equivalence ratios, and begin to deviate as the equivalence ratio approaches 0.5. Again, this deviation may be due to diffusion effects and shows the need to include diffuse coefficients in the optimization space [42].

The optimization procedure also allows us to probe the residual kinetic uncertainties. We found that the rate coefficient of $H + O_2 = OH + O$ always stayed within 5% of the trial value for all optimization runs made, including the use of a smaller number of targets and/or a reduced dimensionality of active parameter space. The rate coefficient is within 8% and 20% from the analysis of Troe and Ushakov [49] for $T > 1500$ and 1000 K, respectively. Again, our assignment of rate constant uncertainties prior to optimization is consistent with these differences. Of the remaining active parameters, the optimized k_2, k_3, and k_4 values are often within 20% of the trial values. For $H + O_2(+M) = HO_2(+M)$, optimization led to a 10% increase in the rate coefficient of the base reaction ($M = N_2$), which is acceptable. For $M = H_2O$, the optimized third-body efficiency was a factor of 1.09 of the trial value. Coupled with the change in the rate for base reaction ($M = N_2$), the third-body efficiency of H_2O relative to N_2 remains unchanged. Optimization yielded a smaller efficiency factor for argon, driven primarily by the ignition delay data (the trial model overpredicts ignition delays). The resulting efficiency factor is equal to 0.46 (relative to N_2), and the corresponding rate coefficient for $H + O_2 + Ar = HO_2 + Ar$ is within the experimental uncertainty given in [10]. The low-temperature rate coefficient of $HO_2 + OH = HO_2 + OH$ and the high-temperature rate of $HO_2 + HO_2 = O_2 + H_2O_2$ were lowered by 18% and 13% upon optimization, respectively. Both give a better agreement with the rates recommended by Troe and Ushakov [49].

Among the 28 active parameters, 12 "hit" their respective boundaries of uncertainty spans. The fraction of these parameters is much smaller than what is usually encountered in kinetic model optimization (see, for example [50]). Some of these parameters are either inadequately constrained because of a lack of relevant targets or because they are only marginally active for H_2–CO combustion (e.g., 9c, 9e, 23, 25, 29, and 29a). Others may be caused by target data inconsistency [51]. These issues, while worthy to explore, are clearly outside of the scope of the present study.

5. Summary

A H_2–CO kinetic model was proposed. The model was based on a comprehensive review of literature kinetic data, considering the recent revisions in the rate coefficient of $H + O_2(+M) = HO_2(+M)$, its third-body efficiencies, and the enthalpy of formation of the OH radical. The trial model performed very well against most of the H_2/CO combustion data. Discrepancies in the predictions, however, existed for several data sets. These discrepancies were successfully resolved by optimization within the uncertainty bounds of the relevant rate parameters with respect to 36 targets, including the global combustion properties of ignition delays and laminar flame speeds, and the detailed species profiles during H_2 and CO oxidation in flames and flow reactors. It is shown that this set of H_2–CO combustion targets can be reconciled within the underlying kinetic uncertain-

ties, and the optimized kinetic model is predictive for all reliable H_2–CO combustion data considered herein.

Acknowledgments

This work was supported by AFOSR (Grant Nos. F49620011014 and F496200210002) under the technical supervision of Dr. Julian M. Tishkoff. The work at UD was also supported by NSF (CTS-9874768).

References

[1] M.A. Mueller, R.A. Yetter, F.L. Dryer, *Int. J. Chem. Kinet.* 31 (1999) 705–724.
[2] J. Troe, *Proc. Combust. Inst.* 28 (2000) 1463–1469.
[3] J.V. Michael, M.-C. Su, J.W. Sutherland, J.J. Carroll, A.F. Wagner, *J. Phys. Chem. A* 106 (2002) 5297–5313.
[4] B. Ruscic, D. Feller, D.A. Dixon, K.A. Peterson, L.B. Harding, R.L. Asher, A.F. Wagner, *J. Phys. Chem. A* 105 (2001) 1–4.
[5] H. Curran, Personal communication, 2003.
[6] J. Li, Z. Zhao, A. Kazakov, D.L. Dryer, An updated comprehensive kinetics model of H_2 combustion, in: *Chemical and Physical Processes in Combustion, the 2003 Technical Meeting of the Eastern States Section of the Combustion Institute*. University Park, PA, October 2003, pp. 169–171.
[7] S.G. Davis, A.V. Joshi, H. Wang, F.N. Egolfopoulos, A comprehensive and optimized kinetic model of H_2/CO combustion, in: *Proceedings of the 3rd Joint Meeting of the U.S. Sections of the Combustion Institute*. Chicago, March 2003, paper PK8.
[8] G.P. Smith, et al. GRI-Mech 3.0. Available from: <http://www.me.berkeley.edu/gri_mech/> (2000).
[9] W. Tsang, R.F. Hampson, *J. Phys. Chem. Ref. Data* 15 (1986) 1087–1279.
[10] J.V. Michael, J.W. Sutherland, L.B. Harding, A.F. Wagner, *Proc. Combust. Inst.* 28 (2000) 1471–1478.
[11] R.E. Zellner, F. Ewig, R. Paschke, Gg. Wagner, *J. Phys. Chem.* 92 (1988) 4184–4190.
[12] D.L. Baulch, C.J. Cobos, R.A. Cox, P. Frank, G. Hayman, T. Just, J.A. Kerr, T. Murrells, M.J. Pilling, J. Troe, R.W. Walker, J. Warnatz, *J. Phys. Chem. Ref. Data* 21 (1992) 411–734.
[13] M.A. Mueller, T.J. Kim, R.A. Yetter, F.L. Dryer, *Int. J. Chem. Kinet.* 31 (1999) 113–125.
[14] L.F. Keyser, *J. Phys. Chem.* 92 (1988) 1193–1200.
[15] H. Hippler, H. Neunaber, J. Troe, *J. Chem. Phys.* 103 (1995) 3510–3516.
[16] H. Hippler, J. Troe, J. Willner, *J. Chem. Phys.* 93 (1990) 1755–1760.
[17] G. Friedrichs, D.F. Davidson, R.K. Hanson, *Int. J. Chem. Kinet.* 34 (2002) 374–386.
[18] C.-C. Hsu, A.M. Mebel, M.C. Lin, *J. Phys. Chem.* 105 (1996) 2346–2352.
[19] R.J. Kee, J.A. Miller, T.H. Jefferson, *CHEMKIN: A general-purpose, problem-independent, transportable, Fortran chemical kinetics code package*, Technical Report SAND80-8003. Sandia National Laboratories, 1980.
[20] R.G. Gilbert, K. Luther, J. Troe, *Ber. Bunsenges Phys. Chem.* 87 (1983) 169–177.
[21] P.J. Ashman, B.S. Haynes, *Proc. Combust. Inst.* 27 (1998) 185–191.
[22] J. Troe, *Proc. Combust. Inst.* 15 (1975) 667–680.
[23] M.T. Allen, R.A. Yetter, F.L. Dryer, *Combust. Flame* 109 (1997) 449–470.
[24] P.R. Westmoreland, J.B. Howard, J.P. Longwell, A.M. Dean, *AIChE J.* 32 (1986) 1971–1979.
[25] M.S. Wooldridge, R.K. Hanson, C.T. Bowman, *Proc. Combust. Inst.* 25 (1994) 741–748.
[26] D.M. Golden, G.P. Smith, A.B. McEwen, C.L. Yu, B. Eiteneer, M. Frenklach, G.L. Vaghjiani, A.R. Ravishankara, F.P. Tully, *J. Phys. Chem. A* 102 (1998) 8598–8606.
[27] S.D. Tse, D.L. Zhu, C.K. Law, *Proc. Combust. Inst.* 28 (2000) 1793–1800.
[28] M.W. Dowdy, D.B. Smith, S. Taylor, *Proc. Combust. Inst.* 23 (1990) 325–333.
[29] F.N. Egolfopoulos, C.K. Law, *Proc. Combust. Inst.* 23 (1990) 333–340.
[30] C.M. Vagelopoulos, F.N. Egolfopoulos, C.K. Law, *Proc. Combust. Inst.* 25 (1994) 1341–1347.
[31] O.C. Kwon, G.M. Faeth, *Combust. Flame* 124 (2001) 590–610.
[32] I.C. McLean, D.B. Smith, S.C. Taylor, *Proc. Combust. Inst.* 25 (1994) 749–757.
[33] C.M. Vagelopoulos, F.N. Egolfopoulos, *Proc. Combust. Inst.* 25 (1994) 1317–1323.
[34] J. Vandooren, J. Bian, *Proc. Combust. Inst.* 23 (1990) 341–346.
[35] T.J. Kim, R.A. Yetter, F. Dryer, *Proc. Combust. Inst.* 25 (1994) 759–766.
[36] R.K. Cheng, A.K. Oppenheim, *Combust. Flame* 58 (1984) 125–139.
[37] A. Cohen, J. Larsen, Report BRL 1386, 1967.
[38] E.L. Peterson, D.F. Davidson, M. Rohrig, R.K. Hanson, in: *20th International Symposium on Shock Waves*, 1996, pp. 941–946.
[39] A.M. Dean, D.C. Steiner, E.E. Wang, *Combust. Flame* 32 (1978) 73–83.
[40] R.J. Kee, J.F. Grcar, M.D. Smooke, J.A. Miller, *A Fortran program for modeling steady laminar one-dimensional premixed flames*. Sandia National Laboratory Report SAND85-8240 (1986).
[41] P. Middha, B. Yang, H. Wang, *Proc. Combust. Inst.* 29 (2002) 1361–1369.
[42] Y. Dong, A.T. Holley, M.G. Andac, F.N. Egolfopoulos, S.G. Davis, P. Middha, H. Wang, Experimental and numerical studies of extinction of premixed lean H_2/air flames, *2004 Spring Technical Meeting of the Western States of the Combustion Institute*. University of California at Davis, Davis, California, March, 2004, paper 04S-19.
[43] M. Frenklach, H. Wang, M.J. Rabinowitz, *Prog. Energy Combust. Sci.* 18 (1992) 47–73.
[44] S.G. Davis, A.B. Mhadeshwar, D.G. Vlachos, H. Wang, *Int. J. Chem. Kinet.* 36 (2003) 94–106.
[45] K.T. Aung, M.I. Hassan, G.M. Faeth, *Combust. Flame* 109 (1997) 1–24.
[46] G.B. Skinner, G.H. Ringrose, *J. Chem. Phys.* 42 (1965) 2190–2192.
[47] K.A. Bhaskaran, M.C. Gupta, T. Just, *Combust. Flame* 21 (1973) 45–48.
[48] M.W. Slack, *Combust. Flame* 28 (1977) 241–249.

[49] J. Troe, V.G. Ushakov, *J. Chem. Phys.* 115 (2001) 2628–3621.
[50] Z. Qin, V. Lissianski, H. Yang, W.C. Gardiner Jr., S.G. Davis, H. Wang, *Proc. Combust. Inst.* 28 (2000) 1663–1669.
[51] M. Frenklach, A. Packard, P. Seiler, Prediction uncertainty from models and data, in: *Proceedings of the American Control Conference*. Anchorage, AK, May, 2002, pp. 4135–4140.

Comments

J. Troe, University of Göttingen, Germany. I see problems with this type of optimization of elementary reaction rate coefficients on the basis of macroscopic reaction systems. The conditions of the macroscopic experiments just do not correspond to those of separate studies of the elementary reactions. In particular, pressure-dependent reactions like $H + O_2 + M$ or $HO + CO + M$ depend strongly on the third bodies M. In macroscopic reaction systems, these M may also be H_2O, reactive atoms, or reactive radicals. For the latter, collision efficiencies may differ markedly from the values derived for third bodies like N_2. The optimization of this paper may mix this all up. I would recommend leaving the results, from separate elementary reaction rate studies untouched and only optimize those collision efficiencies (or rate coefficients) that are otherwise inaccessible or unknown.

Reply. We agree that optimization of reaction rate coefficients on the basis of macroscopic reaction systems cannot provide rate values more accurate than isolated "microscopic" experiments or "ab initio" theoretical studies. The purpose of optimization is to examine the ability of up-to-date rate coefficients for predicting the responses of macroscopic reaction systems. This is, after all, the practical purpose of fundamental reaction kinetics. In our optimization procedure, we ask two basic questions. First, do the latest developments in reaction kinetics, i.e., better and more accurate rate coefficients, predict or give rise to better predictions for the macroscopic reaction systems? Second, given the uncertainty in each and every rate parameter, can the responses of macroscopic reaction systems be better predicted by systematic optimization within the uncertainty bounds of each rate parameter? We maintain that the ultimate goal of kinetics studies can only be achieved by fundamental theoretical and experimental studies supplemented frequently by studies such as the one reported here.

The collision efficiencies of different species are indeed markedly different, and it is precisely this reason why we chose to optimize the key, individual collision efficiencies for key pressure-dependent reactions. Uncertainty bounds intrinsically limit to which extent each efficiency factor can be varied, thus maintaining their physical nature, for example, H_2O is a more efficient third body. For this reason, we do not see any fundamental reason why optimization would mix this up. As a practical measure we note that for $H + O_2 + M = HO_2 + M$ the un-optimized third body efficiencies are 0.53, 0.53, 0.75, 12, and 1 for Ar, He, O_2, H_2O, and H_2, respectively, relative to that of N_2, and the optimized efficiency factors are 0.4, 0.46, 0.85, 11.9, and 0.75. These optimized factors are well within their respective range of uncertainties.

•

Juan Li, Princeton University, USA. The rate constant of $CO + OH \Longleftrightarrow CO_2 + H$ is pressure-dependent. The authors provide a new expression of the rate constant by fitting the literature experimental results. However, most of the experimental results were measured at low pressures. Is it proper to use the rate constant expression for high-pressure cases?

Reply. A recent theoretical study [1] showed that the rate coefficient for $CO + OH = CO_2 + H$ starts to deviate from the low pressure limit (by more than 2%) when pressure becomes greater than ca. 20, 80, 700, 3600 and 13000 bar for $T = 800$, 1000, 1500, 2000, and 2500 K, respectively. This suggests that the reaction would indeed be at or nearly at its low-pressure limit under the conditions of all experimental data considered herein. Furthermore, the optimized rate expression agrees to within 5% of the theoretical result of [1] in the temperature range of 800–2500 K.

Reference

[1] A. Joshi, H. Wang, *Int. J. Chem. Kinet.* (2004) submitted for publication.

•

S.S. Kumaran, Cabot Corporation, USA. How does the bath gas βc impart the flame speed map (uncertainties)? What is the relative βc of various bath gases towards other reactions (title reaction) $CO + OH \rightarrow CO_2 + H$?

Reply. The influence of third body efficiencies of certain pressure-dependent reactions on flame speed has been known for quite a while (Ref. [43] in paper). Active efficiency factors were considered in model optimization.

Based on recent theoretical studies, e.g. [1], the $CO + OH$ reaction would indeed be very close to its low-pressure limit under conditions of all experiments considered herein. For this chemical activation process, the impact of various bath gases would therefore be virtually unimportant for the present study.

Reference

[1] A. Joshi, H. Wang, *Int. J. Chem. Kinet.* (2004) submitted.

•

David Smith, University of Leeds, UK. For part of their optimization, the authors use the burning velocity data of McLean (Ref. [32] in paper). The experiments, particularly those with 25% CO/5% H_2 fuel were carefully chosen to have high sensitivity to the CO + OH reaction. Two comments on these data:

1. All expanding spherical flame methods for burning velocity measurements have hot burnt gas inside the flame; thereby prone to radiative heat loss. For these flames (relatively show burning and high CO_2 content), measured burning velocities may be low by up to 4–5%.
2. As reported in the paper, the authors found that computed burning velocities were sensitive to CO + OH rate only at temperatures around 1160 K. Comparison with these experimental data says essentially nothing about CO + OH at other temperatures.

Reply. Radiative heat loss would have little influence on measured flame speeds, as long as you are not near the flammability limits [1,2]. The 95% CO + 5% H_2 in air flame data measured by the expanding spherical flame methods and used as model optimization and validation targets were far from the flammability limits and thus they should be affected minimally by radiative heat loss.

The fact that the CO + OH reaction is influential in a fairly narrow temperature range for the 95% CO + 5% H_2 flames is a very important result. Although comparison with these flame speed data says very little about CO + OH at other temperature, it does point out the subtle fact that a single modified Arrehnius expression cannot reconcile available flame speed and shock tube data of CO. Specifically, a proper prediction for the 95% CO + 5% H_2 flames requires a smaller rate coefficient at temperatures around 1160 K, yet a single modified Arrehnius expression would not be able to reconcile flame speed and shock tube data that are sensitive to the rate coefficient of the CO + OH reaction at higher temperatures.

References

[1] C.K. Law, F.N. Egolfopoulos, *Proc. Combust. Inst.* 24 (1992) 137–144.
[2] G. Rozenchan, D.L. Zhu, C.K. Law, S.D. Tse, *Proc. Combust. Inst.* 29 (2002) 1461–1469.

•

Frederick L. Dryer, Princeton University, USA. Your method of optimization appears to involve adjustments only in the pre-exponent in rate correlations, which results in rate changes at all temperatures. We have shown [1] that there are "temperature windows" for each input parameter (rate constant, diffusion coefficient) where laminar flame speed is most sensitive to the specific parameter. These windows are small in comparison to the total temperature range of the particular flame. Thus in optimizing against all of the different types of experimental targets that were utilized, your method simultaneously adjusts each rate constant at all temperatures while optimizing against a particular target that covers a particular temperature range. Would it not be more appropriate to optimize both the pre-exponent and temperature dependence (functional shape) of each rate correlation? Essentially you forced such a result here for one rate by proposing a different correlation of CO + OH than appears in the published literature. We have shown the importance of adjusting both pre-exponent and temperature dependence of rate correlations for several elementary reactions involved in the H_2/CO/O_2 oxidation mechanism, including this one [2].

References

[1] Work in Progress Poster 1F2-13, *Int. J. Chem. Kin.* (2004) submitted.
[2] Work in Progress Poster 1F1-04, *Int. J. Chem. Kin.* (2004) submitted.

Reply. We agree with the fact that each target (flame speed, ignition delay, and flow reactor) is sensitive to a given input parameter (i.e., reaction rate, diffusion coefficient) at a specific temperature or over a given temperature range, depending on the experimental conditions, including pressure. This is precisely the reason why we chose targets that covered an extensive temperature (880–2625 K) and pressure (0.3–33 atm) range in order to ensure accurate optimization of the input parameter over an extended temperature and pressure range. While we agree that a simultaneous optimization of the pre-exponential and temperature dependence would be more rigorous, this level of optimization was not needed as can be seen by the excellent agreement between model predictions of the optimized model and experimental data over extensive temperature and pressure ranges.

A theoretical analysis by Troe [1] has shown that due to the complexity of the CO + OH reaction, there is no inherent reason to believe that a single modified Arrehnius expression can adequately describe the rate of this reaction over an extended temperature range. We proposed to refit the experimental data for the CO + OH reaction using a summation of two modified Arrehnius expressions to more accurately reconcile the experimental data for high, intermediate and low temperatures. This expression also agrees very well will our recent theoretical result [2].

References

[1] J. Troe, *Proc. Combust. Inst.* 27 (1998) 167–175.
[2] A. Joshi, H. Wang, *Int. J. Chem. Kinet.* (2004) submitted.

Available online at www.sciencedirect.com
SCIENCE DIRECT
ELSEVIER
Combustion and Flame 142 (2005) 374–387
Combustion and Flame
www.elsevier.com/locate/combustflame

Extinction of premixed H_2/air flames: Chemical kinetics and molecular diffusion effects

Yufei Dong [a], Adam T. Holley [a], Mustafa G. Andac [a], Fokion N. Egolfopoulos [a,*], Scott G. Davis [b], Prankul Middha [c], Hai Wang [a]

[a] *Department of Aerospace and Mechanical Engineering, University of Southern California, Los Angeles, CA 90089-1453, USA*
[b] *Exponent, Natick, MA 01760, USA*
[c] *Department of Mechanical Engineering, University of Delaware, Newark, DE 19716, USA*

Received 17 November 2004; received in revised form 18 March 2005; accepted 30 March 2005

Available online 3 May 2005

Abstract

Laminar flame speed has traditionally been used for the partial validation of flame kinetics. In most cases, however, its accurate determination requires extensive data processing and/or extrapolations, thus rendering the measurement of this fundamental flame property indirect. Additionally, the presence of flame front instabilities does not conform to the definition of laminar flame speed. This is the case for Le < 1 flames, with the most notable example being ultralean H_2/air flames, which develop cellular structures at low strain rates so that determination of laminar flame speeds for such mixtures is not possible. Thus, this low-temperature regime of H_2 oxidation has not been validated systematically in flames. In the present investigation, an alternative/supplemental approach is proposed that includes the experimental determination of extinction strain rates for these flames, and these rates are compared with the predictions of direct numerical simulations. This approach is meaningful for two reasons: (1) Extinction strain rates can be measured *directly*, as opposed to laminar flame speeds, and (2) while the unstretched lean H_2/air flames are cellular, the stretched ones are not, thus making comparisons between experiment and simulations meaningful. Such comparisons revealed serious discrepancies between experiments and simulations for ultralean H_2/air flames by using four kinetic mechanisms. Additional studies were conducted for lean and near-stoichiometric H_2/air flames diluted with various amounts of N_2. Similarly to the ultralean flames, significant discrepancies between experimental and predicted extinction strain rates were also found. To identify the possible sources of such discrepancies, the effect of uncertainties on the diffusion coefficients was assessed and an improved treatment of diffusion coefficients was advanced and implemented. Under the conditions considered in this study, the sensitivity of diffusion coefficients to the extinction response was found to be significant and, for certain species, greater than that of the kinetic rate constants.

Keywords: H_2/air flames; Flame extinction; Premixed flames

1. Introduction

Accurate knowledge of the chemical kinetic mechanisms of hydrocarbon fuels is essential for design of

* Corresponding author.
E-mail address: egolfopo@usc.edu (F.N. Egolfopoulos).

0010-2180/$ – see front matter
doi:10.1016/j.combustflame.2005.03.017

the next generation of engines. While progress in fundamental reaction kinetics has facilitated the growth of this knowledge, it is still essential that the resulting reaction model be tested against a wide variety of fundamental flame properties to ensure model completeness and accuracy. Laminar flame speed, S_u^0, has been the main property against which kinetic mechanisms have been tested and optimized (e.g., [1]). While this is an acceptable approach, there are drawbacks. First, the determination of S_u^0 frequently requires either extrapolations or data processing. Additionally, S_u^0 cannot be defined under conditions that do not conform to the steady, laminar, one-dimensional, stretch-free, planar, adiabatic flame model. This is the case when instabilities develop. The most profound example covers flames with Le $\ll 1$ such as ultralean H_2/air flames; Le is the mixture's effective Lewis number. These flames are severely affected by cellular instabilities as the stretch rate approaches zero.

Yet the properties of these ultralean, weak flames are particularly useful to kinetic model development, in that the maximum temperature of these flames approaches or is below the crossover temperature of chain branching versus chain termination. The overall reaction becomes slow and rate limiting. And for this reason, the properties of ultralean flames are expected to be more sensitive to reaction kinetics than those of stronger flames. The intensity of ultralean flames may also be limited by the rate of fuel supply to the intense reaction zone. Consequently diffusion–kinetic coupling is expected to be ever important.

The current study was directly motivated by the aforementioned considerations. Specifically, an alternative/supplemental approach is proposed here for the validation of flame kinetics. It is proposed that the extinction strain rate, K_{ext}, determined in counterflow configurations be used to supplement S_u^0, considering that K_{ext} is often sensitive to kinetic subsets similar to S_u^0 (e.g., [2]). In the counterflow configuration the surface of Le $\ll 1$ flames become smooth under the influence of positive stretch, as the cellular instabilities are suppressed.

To ensure that the comparisons between the experimental and predicted K_{ext} values are reliable, the flame extinction experiments must be performed so that several subtle issues are adequately addressed. First, given that the extinction state cannot be measured and only the strain rates of preextinction states can be determined, a methodology is required to ensure that there is no need for extrapolations. Second, some geometric requirements must be met for the experimental configuration to be truly represented by the numerical simulations. Both these points were carefully considered, and the details are presented next.

In summary, implementation of K_{ext} for kinetic validation allows for probing of the ultralean H_2/air regime that has not been adequately assessed in past flame studies. This kinetic regime corresponds to temperatures of about 1000 to 1400 K that are well below those encountered in hydrocarbon/air flames, and is also of direct relevance to hydrocarbon ignition. In addition, molecular diffusion is expected to be important in the flame extinction process. In the present investigation, the effects of uncertainties associated with the diffusion coefficients and their formulations are also addressed.

2. Experimental approach

The experiments were conducted using the counterflow technique, which allows for the establishment of planar single or twin flames. Single flames were considered and they were established by counterflowing a fuel/air jet against an opposing ambient-temperature air jet. In the present investigation this approach was preferred over the symmetric twin-flame configuration (e.g., [3]) because, for the same equivalence ratio, ϕ, the single-flame configuration results in lower K_{ext} values compared with the twin-flame configuration. Consequently, lower Reynolds numbers are required, thus minimizing the effect of intrinsic instabilities that are present in flow systems.

For the experiments to be consistent with the assumptions of the quasi-one-dimensional stagnation code that is presented in the following section, the L/D ratio was chosen to be less than 1.0, typically between 0.5 and 1.0; L is the burner separation distance and D is the burner diameter. It has been confirmed experimentally that as long as $L/D \leqslant 1$, the experimental and predicted velocity profiles along the stagnation streamline are in close agreement. The nozzle diameters used were $D = 7$, 14, and 22 mm, and the reported data were taken by using $L = 7$, 14, and 18 mm; typically smaller (greater) L and D values are used for stronger (weaker) flames.

The digital particle image velocimetry (DPIV) technique [4] was used for determination of the axial velocity profile along the stagnation streamline. The flow was seeded by 0.3-μm-diameter silicon oil droplets, produced by a nebulizer similar to that of Hirasawa et al. [5]. The absolute value of the maximum velocity gradient in the hydrodynamic zone is defined as the strain rate, K.

The extinction strain rate, K_{ext}, cannot be directly determined given that measurements at the extinction state cannot be made, and, therefore, extrapolations may be needed. This problem was resolved by establishing flames at states very close to extinction, determining the prevailing K, and by subsequently achiev-

ing extinction through a slight reduction of the fuel flow rate for these fuel-lean flames. It was shown both experimentally and numerically that K is minimally affected through such slight variations of the fuel flow rate. Thus, the measured K for a slightly richer flame is a very close representation of the actual K_{ext}. This approach provides a *direct* measurement of K_{ext} that can be used with confidence for validating chemical kinetics.

The measurements were performed for atmospheric ultralean H_2/air mixtures. Additionally, and to moderate potential Le number effects, N_2-diluted near-stoichiometric H_2/air mixtures were also considered.

3. Numerical approach

The counterflow configuration was numerically simulated by solving the quasi-one-dimensional conservation equations of mass, momentum, species concentrations, and energy along the stagnation streamline [6–8]. The effect of thermal radiation from CH_4, H_2O, CO_2, and CO at the optically thin limit [7] was also included. The code was integrated with the CHEMKIN [9] and Sandia Transport [10] subroutine libraries. Modifications were made in the Transport subroutines to account for recent updates of diffusion coefficients for pairs whose interactions cannot be accurately described by the Lennard–Jones potential function, as is discussed in Section 4.

The extinction condition was achieved by first establishing a vigorously burning flame and by increasing the flow velocities at the burner exits; all experimental conditions were modeled *directly* by considering the *exact* values of L (i.e., 7, 14, and/or 18 mm) that were used in the experiments as they can have a notable effect on K_{ext} [7]. At the extinction state, the response of any flame property to the strain rate is characterized by a turning point behavior. The code has been modified to allow for capturing this singular behavior and allowing, thus, for the accurate determination of K_{ext} (e.g., [11]). More specifically, a two-point continuation approach was implemented by imposing a predetermined temperature or species mass fraction at two points in the flow field, so that the nozzle exit velocities are solved for, rather than imposed as boundary conditions. In doing so, the local strain rate, K, and as a result K_{ext}, become *dependent* variables rather than *independent* ones and the turning point behavior is not a singular one.

Four H_2/O_2 kinetic models were used in the numerical simulations. The first two models are those of Mueller et al. [12] (hereafter referred to as MKYD99) and Li et al. [13] (hereafter referred to as LZKD04). Two additional models were also considered and the details are given in Ref. [14]. Briefly, a "trial" model (hereafter referred to as TRM04) was compiled based on a comprehensive review of literature data considering recent kinetic developments, especially in the rate constants of the $H + O_2 + M \rightarrow HO_2 + M$ reaction and the revision of the enthalpy of formation of the OH radical. An "optimized" model (hereafter referred to as OPM04) was derived from the "trial" model by optimizing rate parameters with respect to a wide range of H_2 and CO oxidation data in shock tubes, flow reactors, and flames. It is important to note that the objective of the current simulations was *not* to compare the performance of various reaction models. Rather selected models were employed to illustrate two important points: (1) the suitability of K_{ext} as a tool of kinetic mechanism validation, and (2) the strong diffusion-kinetic coupling that exists for all models tested.

Assessing the effects of chemical kinetics and molecular diffusion on K_{ext} requires the use of sensitivity analysis. While the standard CHEMKIN-based codes do allow for automated sensitivity analysis with respect to all rate constants for S_u^0 and all temperature and species concentrations (e.g., [15]), this is not the case for the important K_{ext}. In this investigation, this was achieved for the first time by realizing, as described earlier, that K_{ext} becomes a dependent variable when the aforementioned two-point continuation approach is invoked. As a result it was possible to perform rigorous sensitivity analysis with respect to rate constants for K_{ext} at the exact location that is determined experimentally, i.e., where it reaches its maximum value in the hydrodynamic zone. However, the capability of performing sensitivity calculations of the various dependent flame properties on species diffusivities is not readily available in the existing codes. Thus, a "brute force" approach was implemented. More specifically, the mass diffusivity of each species i to the mixture, $D_{i,m}$, was perturbed by ±25% and the attendant K_{ext} values were subsequently determined. Subsequently, logarithmic sensitivity coefficients were formed by determining the derivatives $\partial(\ln K_{ext})/\partial(\ln D_{i,m})$.

As is shown in the Section 5, the sensitivity of K_{ext} to diffusion was found to be significant for certain species. This motivated further assessment of the validity of the diffusion coefficient formulation of the Sandia Transport subroutine library [10] which is extensively used in flame modeling. As a result, an improved treatment of the diffusion coefficients was advanced and is presented next.

Additional simulations were performed using the Premix code [15] for the determination of laminar flame speeds, S_u^0, to address the relative sensitivities of kinetics versus diffusivities to S_u^0. The code automatically outputs the logarithmic sensitivity coef-

Table 1
Summary of polynomial coefficients for updated binary diffusion coefficients and ratios of collision integrals

Pair	Diffusion coefficient, D_{ij}					A^*_{ij}			
	d_0	d_1	$d_2 \times 10^2$	$d_3 \times 10^3$	Ref.[a]	a_0	$a_1 \times 10$	$a_2 \times 10^2$	$a_3 \times 10^3$
H–He	−9.6699	2.1002	−7.7060	5.4611	[17]	0.93003	0.80150	−0.94733	0.63459
H–Ar	−9.0511	1.6161	−0.2878	1.3054	[18]	0.68819	1.53423	−1.76995	0.88796
H–H_2	−11.7498	3.1507	−25.7472	15.8916	[17]	0.68565	1.53390	−1.36735	0.32210
H–O_2	−11.0410	2.4043	−10.2797	5.3264	[19]	1.29254	−1.84989	4.27103	−2.60823
H–N_2	−13.2703	3.5187	−29.6649	16.4314	[20]	1.33865	−0.85454	0.92291	0.04406
H_2–He	−12.7513	3.4244	−28.4726	15.9317	[17]	0.59534	2.07809	−2.48477	1.00128
H_2–N_2	−10.9994	2.2026	−8.1155	4.4061	[21]	1.31648	−1.32021	2.41620	−1.20259
H_2–H_2	−9.9610	2.0560	−6.4977	4.1368	[22]	1.32209	−1.20749	2.20471	−1.05955
	B^*_{ij}					C^*_{ij}			
	b_0	$b_1 \times 10$	$b_2 \times 10^2$	$b_3 \times 10^3$		c_0	$c_1 \times 10$	$c_2 \times 10^2$	$c_3 \times 10^3$
H–He	0.87638	1.02383	−1.48030	0.98804		1.06002	−0.59928	1.02650	−0.73451
H–Ar	0.69683	1.71580	−2.43568	1.36548		0.67027	1.14334	−1.50407	0.51876
H–H_2	0.67795	1.37471	−1.10587	0.16577		0.65119	0.82160	−0.43894	−0.27358
H–O_2	1.99270	−2.72201	2.05951	0.16444		1.27566	−2.27862	4.44995	−2.74619
H–N_2	−2.20300	15.91601	−25.33938	13.64477		1.27616	−2.25934	4.64183	−3.10151
H_2–He	0.67715	1.35792	−1.14253	0.18886		0.65192	0.83651	−0.44501	−0.25987
H_2–H_2	3.63140	−11.39793	16.94208	−8.12678		1.29811	−1.78141	2.95671	−1.70201
H_2–N_2	1.94230	−4.19106	6.71192	−3.36850		1.29073	−1.93012	3.39899	−1.96836

[a] The fits are based on diffusion coefficients taken directly from the referenced article, or those computed using the potential functions given in the referenced article.

ficients $\partial(\ln S_u^0)/\partial(\ln A)$. The logarithmic sensitivity coefficients $\partial(\ln S_u^0)/\partial(\ln D_{i,m})$ were determined using the "brute force" approach.

4. Updated diffusion coefficients

The need to update the diffusion coefficients stems from the fact that they were measured usually at or near room temperature. Extrapolation of these diffusion coefficients to high temperatures is accomplished using Chapman–Enskog theory. An empirical potential function, for example, the Lennard–Jones (L–J) 12–6 potential function, may provide a good prediction at room temperature, as the potential parameters are usually fitted to data around the same temperature. However, extrapolation to high temperature is subject to uncertainties in the repulsive part of the potential function. For example, the current understanding is that the repulsive part of the L–J potential function is too stiff to accurately account for diffusion coefficients at high temperatures [16]. Replacing the repulsive part of the potential with an empirical, yet softer, exponential function led to an increase in most of the diffusion coefficients involving H and H_2 [16], compared with those predicted by the Sandia Transport subroutine library [10]. Recent studies [17,18] showed that even the exponential function might be too restricted and suggested that the diffusion coefficients of key pairs be directly modeled, using potential functions calculated from first principles, without resorting to the use of tabulated L–J 12–6 collision integrals. The rationale behind this approach is that when the resulting diffusion coefficient is appropriately compared with experimental data at or near room temperature, the extrapolation of diffusion coefficient into the high-temperature region is made more reliable, as the potential function is solidly based on ab initio quantum chemistry theories.

In this work an update for binary diffusion coefficients is provided for selected pairs (see Table 1). All of the updates are based on ab initio theory, and all the corresponding diffusion coefficients validated against the room-temperature experimental data [17–22]. Fig. 1 compares the binary diffusion coefficients of the Sandia compilation [10] and those of the current update for pairs (H_2, N_2) and (H, N_2). Although the differences in the two sets of diffusion coefficients are seemingly small (i.e., within 10%), this same difference could cause notable differences in predicted K_{ext}, as is discussed later.

Within the framework of the Sandia Premix [15] and similar codes, implementing these updates is quite easy and adequate, even if diffusion coefficients are available for only a few pairs. The temperature dependence of binary diffusion coefficients at 1 atm was fitted, as in Ref. [10], by

$$\ln D_{ij} = d_0 + d_1 \ln T + d_2 (\ln T)^2 + d_3 (\ln T)^3,$$

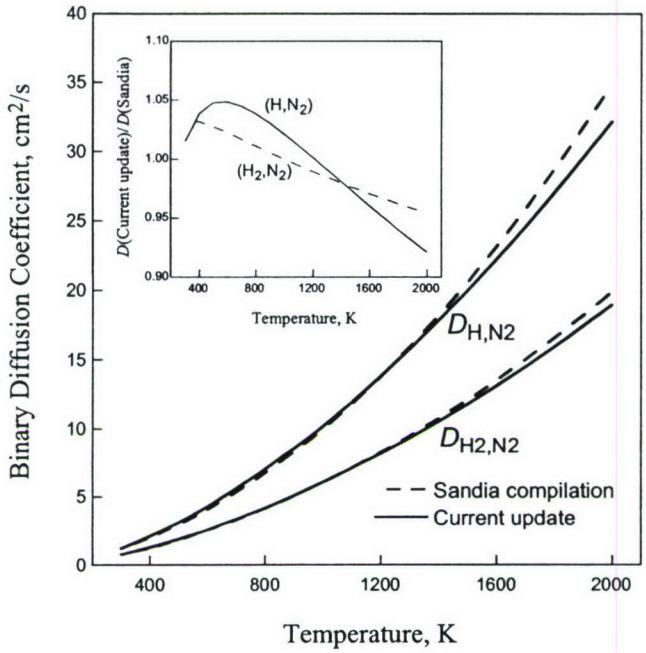

Fig. 1. Comparison of binary diffusion coefficients of the Sandia compilation [10] and the current update for pairs (H, N_2) and (H_2, N_2) at a pressure of 1 atm.

where d_k ($k = 0, 3$) is the polynomial coefficient, tabulated in Table 1. For the mixture-averaged transport formulation, the above polynomial is sufficient for flame simulations. The multicomponent transport formulation, as well as computation of the thermal diffusion ratio in both transport formulations, however, requires the input of the ratios of collision integrals [10,23], i.e.,

$$A_{ij}^* = \Omega_{ij}^{(2,2)} / \left(2\Omega_{ij}^{(1,1)}\right),$$

$$B_{ij}^* = \left(5\Omega_{ij}^{(1,2)} - \Omega_{ij}^{(1,3)}\right) / \left(3\Omega_{ij}^{(1,1)}\right),$$

$$C_{ij}^* = \Omega_{ij}^{(1,2)} / \left(3\Omega_{ij}^{(1,1)}\right).$$

These ratios are given for each pair in the following forms:

$$A_{ij}^* = a_0 + a_1 \ln T_{ij}^* + a_2 \left(\ln T_{ij}^*\right)^2 + a_3 \left(\ln T_{ij}^*\right)^3,$$

$$B_{ij}^* = b_0 + b_1 \ln T_{ij}^* + b_2 \left(\ln T_{ij}^*\right)^2 + b_3 \left(\ln T_{ij}^*\right)^3,$$

$$C_{ij}^* = c_0 + c_1 \ln T_{ij}^* + c_2 \left(\ln T_{ij}^*\right)^2 + c_3 \left(\ln T_{ij}^*\right)^3.$$

Here a_k, b_k, and c_k ($k = 0, 3$) are the polynomial coefficients, the values of which are listed in Table 1, and T_{ij}^* is the reduced temperature determined by the collision well depth ε_{ij} as $T_{ij}^* = kT/\varepsilon_{ij}$.

5. Results and discussion

The experimental K_{ext} values were modeled by using four different kinetic models and several diffusion coefficient models. Typically, in most flame modeling studies, the Sandia Transport library [10] is used, which includes two options for the calculation of $D_{i,m}$ values. The first option is the multicomponent approach, and the second is the mixture-averaged approach. Although not explicitly reported, the latter approach is the one that is used more frequently given its significantly lower computational cost. In the present study the effect of such choices was assessed. Additional comparisons were made between predictions based on the $D_{i,m}$ values as calculated by the present update and that of Ref. [10]. In all simulations the Soret effect was included.

The extent of spatial resolution had a first-order effect on the predicted K_{ext} values. More specifically, by varying the number of grid points, N, from 300 to 2000–3000, K_{ext} was found to increase by as much as 25%, reaching asymptotically the values that are reported hereafter. It should be noted that in all subsequent figures that contain the experimental and predicted K_{ext} values, the vertical scale is logarithmic given the large scale of variation of K_{ext} considered. It should also be noted that the logarithmic scale tends to underemphasize discrepancies. Thus, to accurately illustrate the comparisons between experimental and

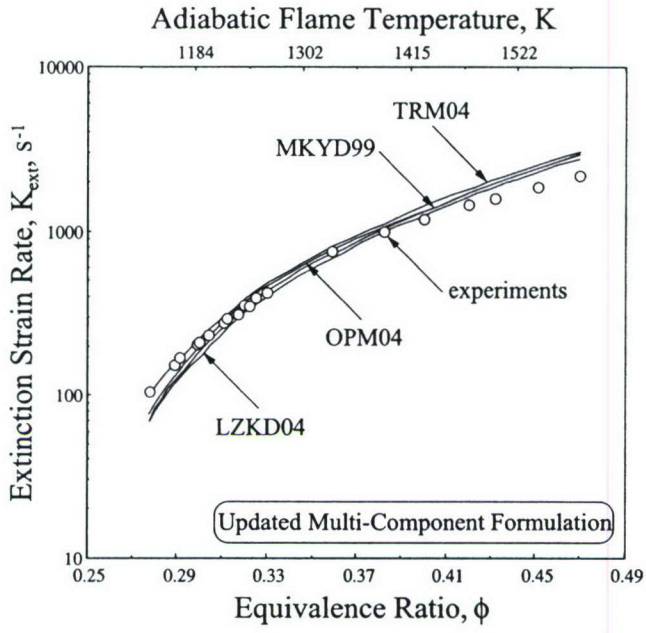

Fig. 2. Experimental and numerical K_{ext} values for single ultralean H_2/air flames. The effect of reaction model is shown.

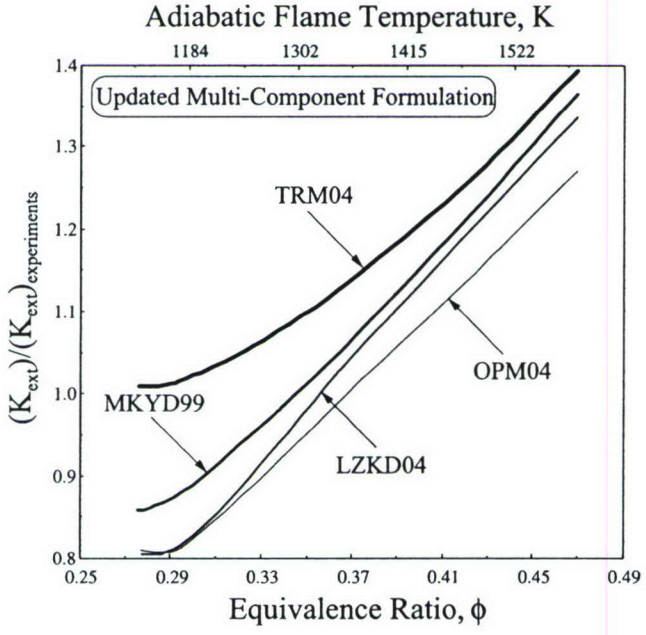

Fig. 3. Ratio of numerical to experimental K_{ext} values for single ultralean H_2/air flames. The effect of reaction model is shown.

predicted K_{ext} values, their ratio is also shown when appropriate.

Fig. 2 depicts comparisons between the experimental and predicted K_{ext} values for ultralean H_2/air flames; the simulations shown in the figures included use of updated multicomponent diffusion model (UMC). Fig. 3 depicts the ratio between predicted and experimental K_{ext} values. It is of interest to note that significant disagreements exist between experimental and predicted K_{ext} values, and that there is a difference in the "slope" of the results. At low ϕ values, TRM04 closely predicts the experimental K_{ext} values, whereas at high ϕ, it overpredicts by nearly 40%. The predictions achieved by the other three mechanisms appear to be shifted toward lower K_{ext} values throughout the domain considered. It is apparent that

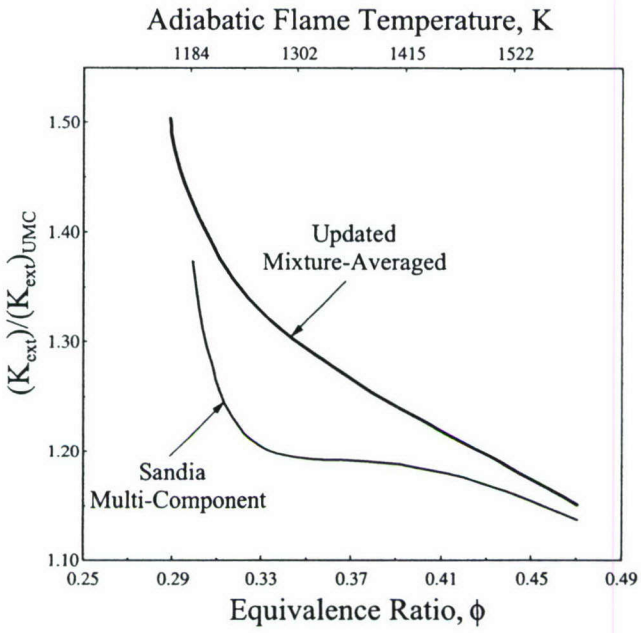

Fig. 4. Numerically determined K_{ext} values for single ultralean H_2/air flames scaled by those obtained using the UMC model. The effect of diffusion model is shown.

no mechanism can reproduce the slope of the experimental data.

The results in Figs. 2 and 3 illustrate the effect of chemical kinetics on predicting K_{ext}. The effect of diffusivity on predicting K_{ext} was also assessed by performing simulations using the TRM04 model and three different diffusion models. For clarity, the results are shown in Fig. 4 scaled by the values of K_{ext} determined by using the UMC diffusion model. The other two diffusion models were the Sandia multicomponent [10] formulation (SMC) and the updated mixture-averaged formulation (UMA). Comparison of the predictions obtained by the two multicomponent models reveals that the SMC predicts larger K_{ext} values, by 15–35% compared with UMC. Furthermore, the UMA model gives K_{ext} values 15–50% larger than those given by UMC. These results suggest that the widely used mixture-averaged diffusion models can result in computed flame properties that are notably in error. Similarly, even if a full multicomponent model is used, the values of various molecular diffusion properties could also result in notably different results. Inspection of the results shown in Figs. 3 and 4 also reveals that the UMC model presents roughly 20 and 15% improvements for the predicted K_{ext} at $\phi = 0.35$ and 0.45, respectively, compared with the SMC model. The degree of improvement, however, depends on the kinetic model employed.

The reported differences on the order of 15–50% cannot be considered minor. Without proper consideration of diffusion uncertainties, these differences could be falsely attributed to kinetics. Clearly, probing this *unique* flame region, from both kinetic and molecular diffusion points of view, the uncertainties associated with both processes must be taken into account. It should also be noted from the results shown in Figs. 2–4, the range of the attendant adiabatic flame temperatures, T_{ad}, is of direct relevance to the ignition of practical hydrocarbon fuels.

To moderate potential diffusion effects, additional experiments were performed, by determining K_{ext} values for N_2-diluted near-stoichiometric H_2/air mixtures. The results are illustrated in Figs. 5 and 6 for $\phi = 0.777$ and Figs. 7 and 8 for $\phi = 0.965$. In these studies the attendant T_{ad} values vary from 1600–1700 K down to ~1200 K, thus assessing flame temperatures similar to those of ultralean flames. The numerical simulations shown in Figs. 5–8 were conducted by using the UMC diffusion model and all four kinetic models. The results reported for both $\phi = 0.777$ and 0.965 exhibit similar behavior compared with those of Fig. 2 in which the UMC diffusion model was also used. More specifically, for $\phi = 0.777$ all mechanisms underpredict K_{ext} at low T_{ad} values by 25–50%, whereas they overpredict K_{ext} at high T_{ad} values by 50–60%. For $\phi = 0.965$, all mechanisms appear to have a better agreement at low T_{ad} values, with discrepancies within ±15%, but at high T_{ad}, the overpredictions persist and are of the order of 40–50%.

The results shown in Figs. 2–8 clearly indicate that both chemical kinetics and diffusion have a notable

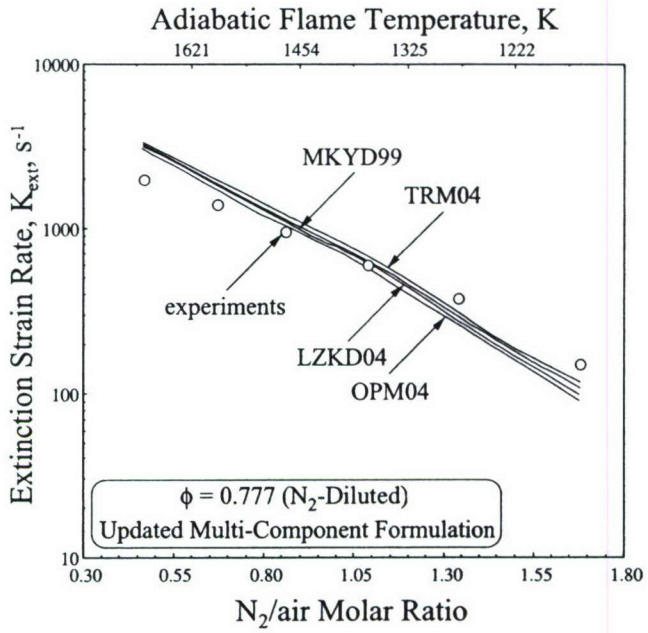

Fig. 5. Experimental and numerical K_{ext} values for N_2-diluted, $\phi = 0.777$ H_2/air flames. The effect of reaction model is shown.

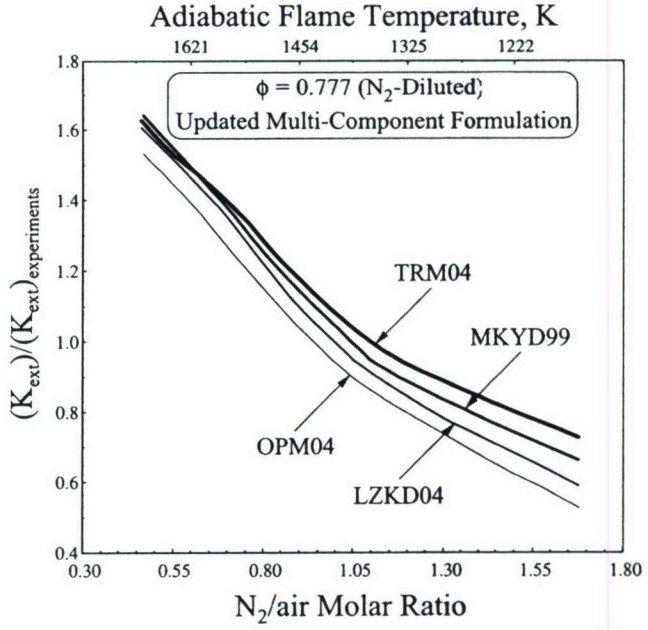

Fig. 6. Ratio of numerical to experimental K_{ext} values for N_2-diluted, $\phi = 0.777$ H_2/air flames. The effect of reaction model is shown.

effect on the predicted K_{ext} values. It is also of interest to note the similarity of the results shown in Figs. 2–4 with those of Figs. 5–8. This similarity does not provide any further insight into the relative importance between chemistry and diffusion. To further investigate the effects of kinetics and diffusion, sensitivity analyses of both processes were performed.

Fig. 9 depicts logarithmic sensitivity coefficients of K_{ext} for the kinetics for ultralean H_2/air flames with $\phi = 0.289$ and 0.314. The analysis was con-

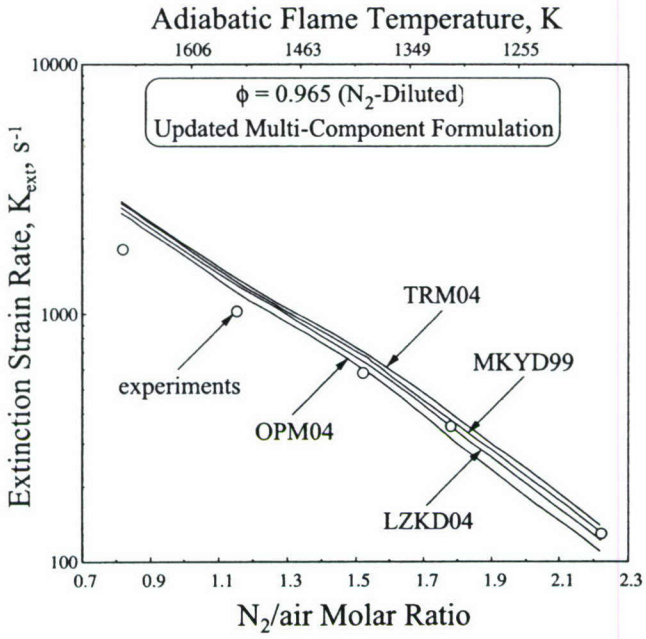

Fig. 7. Experimental and numerical K_{ext} values for N_2-diluted, $\phi = 0.965$ H_2/air flames. The effect of reaction model is shown.

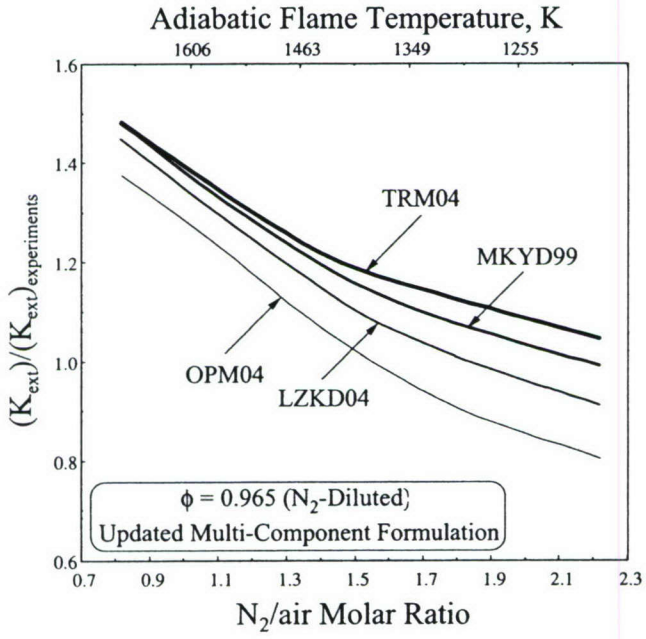

Fig. 8. Ratio of numerical to experimental K_{ext} values for N_2-diluted, $\phi = 0.965$ H_2/air flames. The effect of reaction model is shown.

ducted by using TRM04. As expected, K_{ext} is positively sensitive to the reactions

$H_2 + O \rightarrow OH + H$,

$H_2 + OH \rightarrow H_2O + H$,

$HO_2 + H \rightarrow OH + OH$,

and the radical chain branching reaction

$H + O_2 \rightarrow OH + O$.

As also expected, the reaction

$H + O_2 (+M) \rightarrow HO_2 (+M)$

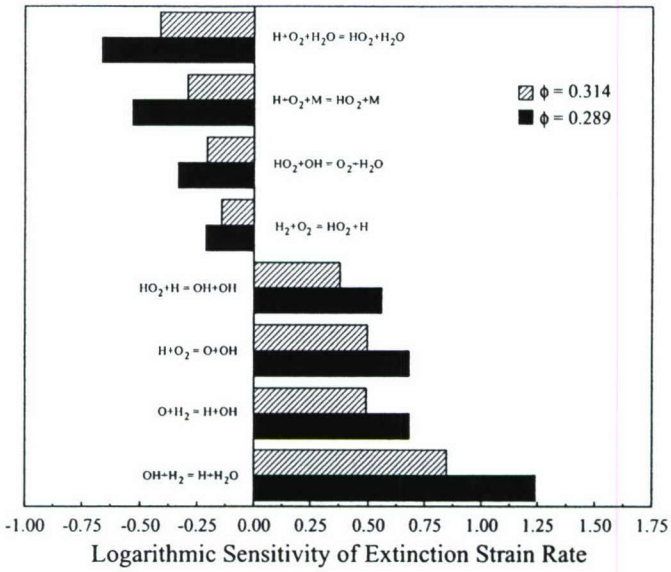

Fig. 9. Logarithmic sensitivity coefficients of K_{ext} with respect to reaction rate coefficients, computed for ultralean H_2/air flames using the TRM04 model.

exhibits a large negative sensitivity along with other radical termination reactions:

$$HO_2 + OH \rightarrow O_2 + H_2O,$$

$$HO_2 + H \rightarrow H_2 + O_2.$$

The HO_2 chemistry is significant for $\phi = 0.289$, but its role is diminished for the higher $\phi = 0.314$ for which T_{ad} is higher. Based on these results, it is reasonable to attribute some the observed discrepancies to uncertainties associated with the rate parameters of the aforementioned reactions.

On the other hand, the influence of kinetic uncertainties cannot be adequately assessed without considering the uncertainties in the diffusion coefficients. This point is illustrated in Fig. 10, which depicts logarithmic sensitivity coefficients of K_{ext} with respect to the mass diffusion coefficients for ultralean H_2/air flames with $\phi = 0.289$ and $\phi = 0.47$, as well as two N_2-diluted $\phi = 0.777$ H_2/air flames. It was found that the diffusivity of only four species had a notable effect on K_{ext}, namely, H_2, O_2, H_2O, and H. Comparing the results of Figs. 9 and 10, the large sensitivity values derived from diffusion are rather striking. Logarithmic sensitivity coefficients for diffusion are not only comparable to those of reaction rates, but, in the case of H_2, are nearly three times larger than those of reaction rates. Additionally, the logarithmic sensitivities of the diffusivities of other species such as H and O_2, although smaller than that of H_2, are still of the order of those of reaction rates.

A simple analysis of the diffusion problem reveals that the diffusion coefficients of all species of interest in the mixture, $D_{i,m}$, are nearly equal to the binary diffusion coefficient of the species in N_2, D_{i,N_2}, for these highly diluted flames in which N_2 is the dominant species. Thus, a 10% difference in D_{H_2,N_2} between the Sandia compilation and the current update (see, e.g., Fig. 1) could lead to about a 30% difference in the predicted K_{ext}! Even if D_{H_2,N_2} is accurate to within 5%, we are still faced with an uncertainty of 15% in K_{ext}. While the prospect of narrowing D_{H_2,N_2} to within 5% at high temperatures is small, the current work highlights the importance of considering diffusion coefficient uncertainties in future reaction model optimization and validation. It is also apparent from the above discussion that the discrepancies between experiment and the four models tested *cannot* be conclusively viewed as deficient kinetics, because the diffusion uncertainties may be solely responsible.

Comparing the various sensitivities in Fig. 10 reveals that although the diffusivities of H_2 and H_2O are positively sensitive to K_{ext} for all cases studied herein, this is not the case for H and O_2. The positive sensitivity on the H_2 diffusion coefficient is physically sound and can be explained based on the very low Le number for these fuel-lean mixtures (e.g., [24]). More specifically, increasing the diffusivity of H_2 results in higher flux of H_2 into the reaction zone compared with the loss of thermal energy. As a result the flame temperature increases and the flames become more resistant to extinction. Note that the ultralean $\phi = 0.289$ and highly diluted (N_2/air = 1.68) $\phi = 0.777$ flames have the highest sensitivities to H_2 diffusivity compared with the more stoichiomet-

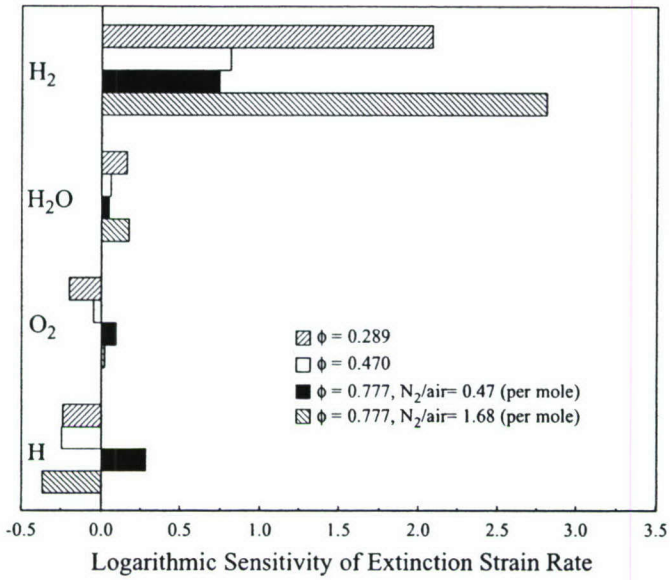

Fig. 10. Logarithmic sensitivity coefficients of K_{ext} with respect to mass diffusion coefficients, computed for ultralean and N_2-diluted near-stoichiometric H_2/air flames using the TRM04 model.

ric $\phi = 0.47$ and less diluted (N_2/air = 0.47) flames. This can be explained by the fact that for the leaner and more inert-diluted flames, the H_2 concentration is low and the overall reactivity is more diffusion controlled.

The species with the second most important sensitivity to K_{ext} is the H radical. For all cases except one, its sensitivity is negative, and these are the cases in which the H radical pool is small so that any increase in its diffusivity leads to a "loss" from the reaction zone. For the vigorously burning case of $\phi = 0.777$ flames with relatively low dilution (N_2/air = 0.47), the sensitivity of the H diffusion coefficient is positive given that the radical pool is large, and increasing H radical diffusivity facilitates the initiation of reactions upstream of the intense burning zone.

The sensitivities of the mass diffusion of O_2 are negative for the ultralean flames, whereas they are positive for the $\phi = 0.777$ flame. This can be explained by the fact that for ultralean flames, O_2 is abundant and increasing its diffusion coefficient tends to transport more O_2 into the reaction zone, making it thus fuel-leaner and less reactive. However, for the more stoichiometric $\phi = 0.777$ flame, O_2 is no longer abundant, and increasing its diffusivity augments the chain branching within the reaction zone.

The extinction process in stagnation-type flows is expected to be sensitive to molecular transport. On the other hand, flame propagation is less sensitive to molecular diffusion. As such, predictions of laminar flame speeds, S_u^0, are expected to be less sensitive to molecular diffusion uncertainties. This thesis was also assessed and logarithmic sensitivity coefficients were derived for lean ($\phi = 0.4$), stoichiometric ($\phi = 1.0$), and rich ($\phi = 5.0$) H_2/air flames. The simulations were performed using the OPM04 kinetic model and the logarithmic sensitivity coefficients are shown in Figs. 11 and 12 for kinetics and diffusivities, respectively. The sensitivity results are in agreement with previous studies [25,26]. Although the magnitude of the sensitivities of S_u^0 with respect to the diffusion coefficients of H_2 and H is indeed smaller compared with K_{ext}, they are still of the same order as those of kinetics. Thus, validating the kinetic mechanism against S_u^0 values without considering uncertainties related to diffusivities could also result in falsification of the rate constants.

It is of interest to note that although the sensitivity coefficient of K_{ext} with respect to H_2 was shown to be positive, it is notably negative on S_u^0, especially for fuel-lean flames, meaning that increasing the diffusivity of the fuel decreases S_u^0, which appears to be counterintuitive. For one-dimensional, stretchless, freely propagating flames, it can be theoretically shown that the thickness of the diffusive layer of any reactant i, δ_i, scales with its mass diffusivity to the mixture, $D_{i,m}$, according to the relation $\delta_i \sim D_{i,m}^{3/2}$. (Note that this is *not* the case for near-extinction stagnation-type and Le < 1 flames that are stabilized on the stagnation plane and its structure is largely affected by stretch.) Analysis of the computed detailed structures of freely propagating flames indeed confirmed that scaling. For example, 20% increase in the diffusivity of H_2 leads to an increase of about 30% in the thickness of the

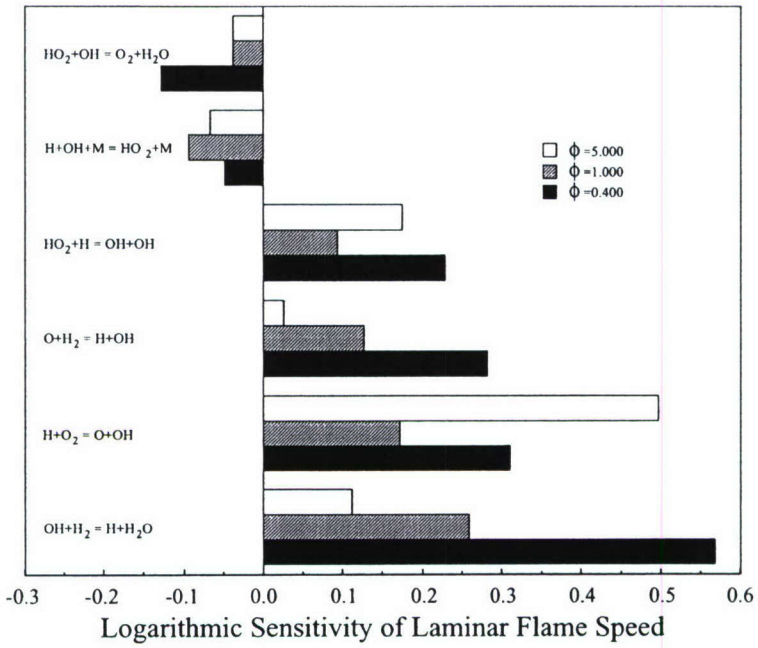

Fig. 11. Logarithmic sensitivity coefficients of S_u^0 with respect to reaction rate coefficients, computed for ultralean, stoichiometric and rich H_2/air flames using the OPM04 model.

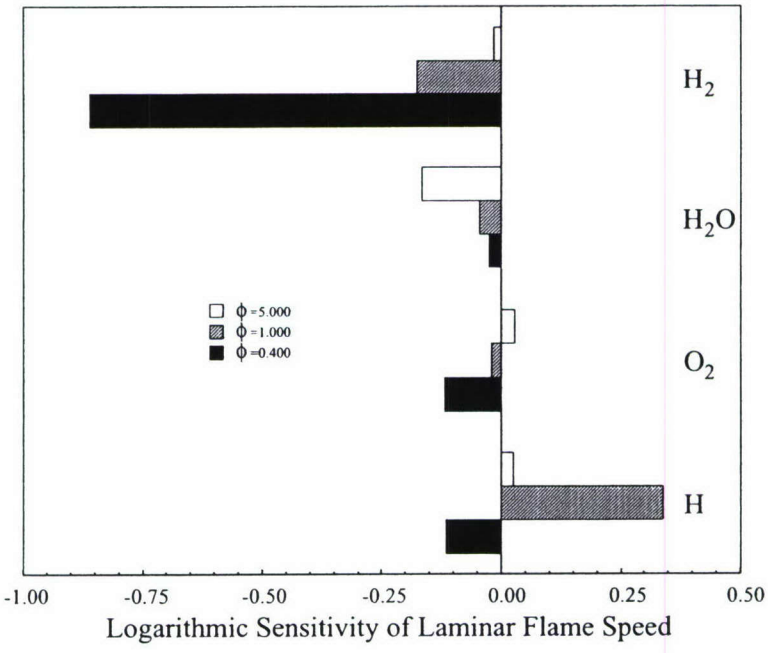

Fig. 12. Logarithmic sensitivity coefficients of S_u^0 with respect to mass diffusion coefficients, computed for ultralean, stoichiometric and rich H_2/air flames, using the OPM04 model.

H_2 diffusive layer, which in turn results in milder H_2 concentration gradients. The flux of H_2 into the flame is proportional to the product of the diffusion coefficient and the concentration gradient. In the absence of flame stretch, which is present in stagnation flows but not in freely propagating one-dimensional flames, the decrease in the concentration gradient overwhelms the increase in diffusivity. This results in an overall decrease in the flux of H_2 to the flame. Thus, the diffusivities of H_2 and S_u^0 are inversely related.

6. Concluding remarks

A detailed experimental and numerical investigation was conducted on the extinction of ultralean H_2/air mixtures under atmospheric pressure. The flame kinetics of such mixtures have not been previously validated as laminar flame speeds under such conditions cannot be determined, given the presence of thermodiffusional instabilities. Extinction strain rates were determined instead in the counterflow configuration, which were subsequently compared against predictions based on four kinetic models. Such comparisons are meaningful, as these low-Le-number mixtures do not develop instabilities when subjected to high strain rates. Comparisons between experimental and predicted extinction strain rates revealed significant discrepancies for well-validated and widely used models. Under certain conditions, discrepancies of a factor of 2 were realized.

Through detailed sensitivity analysis, it was also shown that the extinction states of such mixtures are sensitive not only to the kinetics but also to the species diffusivities. Thus, validation of models against flame data of such highly diffusive mixtures must be done by considering the uncertainties associated with both kinetics and molecular diffusion. In view of this consideration, an additional contribution of this study was the advancement of a somewhat improved treatment of the mass diffusion coefficients.

Detailed simulations also showed that the predicted extinction strain rates based on the present formulation of diffusion coefficients were different by 15–35% compared with the Sandia transport coefficient compilation. Similarly, it was found that using mixture-averaged versus full multicomponent formulation could affect the predicted extinction strain rates by 15–50%. From a kinetic point of view, differences of the order of 15–50% in predicting global flame properties are rather large and could have a major impact on the approach traditionally taken in kinetic model validation.

Additional studies were conducted for N_2-diluted near-stoichiometric H_2/air flames, to obtain results at flame temperatures similar to those of ultralean mixtures but with moderated diffusion effects. However, it was found that for these less diffusive mixtures, the predictions of the four kinetic models were very similar to those for ultralean mixtures, under similar adiabatic flame temperatures.

Finally, additional computations of laminar flame speeds of lean, stoichiometric, and rich H_2/air mixtures revealed that their sensitivities to kinetics could be of the same order as those to diffusivities. This finding suggests that caution is needed when H_2 oxidation kinetics are validated through comparisons with laminar flame speeds without considering uncertainties in molecular diffusion coefficients.

Acknowledgments

This work was supported by AFOSR (Grants F496200210002 and F49620011014) under the technical supervision of Dr. Julian M. Tishkoff.

References

[1] G.P. Smith, D.M. Golden, M. Frenklach, N.W. Moriarty, B. Eiteneer, M. Goldenberg, C.T. Bowman, R.K. Hanson, S. Song, W.C. Gardiner, Jr., V. Lissianski, Z.Qin, GRI-Mech 3.0, http://www.me.berkeley.edu/gri_mech/ (2000).
[2] F.N. Egolfopoulos, P.E. Dimotakis, Combust. Sci. Technol. 162 (2001) 19–36.
[3] C.K. Law, D.L. Zhu, G. Yu, Proc. Combust. Inst. 21 (1986) 1419–1426.
[4] Y. Dong, C.M. Vagelopoulos, G. Spedding, F.N. Egolfopoulos, Proc. Combust. Inst. 29 (2002) 1419–1426.
[5] T. Hirasawa, C.J. Sung, H. Wang, C.K. Law, Proc. Combust. Inst. 29 (2002) 1427–1434.
[6] R.J. Kee, J.A. Miller, G.H. Evans, G. Dixon-Lewis, Proc. Combust. Inst. 22 (1988) 1479–1494.
[7] F.N. Egolfopoulos, Proc. Combust. Inst. 25 (1994) 1375–1381.
[8] F.N. Egolfopoulos, C.S. Campbell, J. Fluid Mech. 318 (1996) 1–29.
[9] R.J. Kee, F.M. Rupley, J.A. Miller, Chemkin-II: A Fortran Chemical Kinetics Package for the Analysis of Gas-Phase Chemical Kinetics, Report SAND89-8009, Sandia National Laboratories, 1989.
[10] R.J. Kee, G. Dixon-Lewis, J. Warnatz, M.E. Coltrin, J.A. Miller, A Fortran Computer Code Package for the Evaluation of Gas-Phase Viscosities, Conductivities, and Diffusion Coefficients, Report SAND86-8246, Sandia National Laboratories, 1986.
[11] F.N. Egolfopoulos, P.E. Dimotakis, Proc. Combust. Inst. 27 (1998) 641–648.
[12] M.A. Mueller, T.J. Kim, R.A. Yetter, F.L. Dryer, Int. J. Chem. Kinet. 31 (1999) 113–125.
[13] J. Li, Z. Zhao, A. Kazakov, F.L. Dryer, Int. J. Chem. Kinet. 36 (2004) 566–575.
[14] S.G. Davis, A.V. Joshi, H. Wang, F.N. Egolfopoulos, Proc. Combust. Inst. 30 (2005) 1283–1292.
[15] R.J. Kee, J.F. Grcar, M.D. Smooke, J.A. Miller, PREMIX: A Fortran Program for Modeling Steady Laminar One-Dimensional Premixed Flames, Report SAND85-8240, Sandia 1985.
[16] P. Paul, J. Warnatz, Proc. Combust. Inst. 27 (1998) 495–504.
[17] P. Middha, B.H. Yang, H. Wang, Proc. Combust. Inst. 29 (2002) 1361–1369.
[18] P. Middha, H. Wang, Combust. Theory Model. (2005), in press.
[19] J.R. Stallcop, H. Partridge, E. Levin, Phys. Rev. A 64 (2001), 042722.

[20] J.R. Stallcop, H. Partridge, S.P. Walch, E. Levin, J. Chem. Phys. 97 (1992) 3431–3436.
[21] J.R. Stallcop, H. Partridge, E. Levin, Phys. Rev. A 62 (2000), 062709.
[22] J.R. Stallcop, E. Levin, H. Partridge, J. Thermophys. Heat Trans. 12 (1998) 514–519.
[23] G. Dixon-Lewis, Proc. R. Soc. London A 307 (1968) 111–135.
[24] C.K. Law, Proc. Combust. Inst. 22 (1988) 1381–1402.
[25] H. Wang, Chem. Phys. Lett. 325 (2000) 661–667.
[26] Z. Yang, B. Yang, H. Wang, The influence of H-atom diffusion coefficient on laminar flame simulation, in: Proceedings of the Second Joint Meeting of the U.S. Sections of the Combustion Institute, Berkeley, CA, March 2001, Paper 237.

Combust. Sci. and Tech., 178: 635–653, 2006

ISSN: 0010-2202 print/1563-521X online
DOI: 10.1080/00102200500241230

Taylor & Francis
Taylor & Francis Group

NON-PREMIXED IGNITION BY VITIATED AIR IN COUNTERFLOW CONFIGURATIONS

J. A. LANGILLE
Y. DONG
M. G. ANDAC
F. N. EGOLFOPOULOS*

Department of Aerospace and Mechanical Engineering, University of Southern California, Los Angeles, California, USA

T. T. TSOTSIS

Department of Chemical Engineering, University of Southern California, Los Angeles, California, USA

Ignition studies have been conducted in counterflow configurations in recent years by using heated air as the ignition source. In the present investigation, an alternative methodology has being advanced for studying ignition, by utilizing vitiated air that is produced from the oxidation of ultra-lean H_2/air mixtures supplied from one burner. Non-premixed ignition is achieved by counterflowing the hot vitiated air against a fuel-containing jet. The ultra-lean H_2/air mixtures are oxidized on a catalyst positioned at the burner exit, allowing thus for the effective variation of the temperature of the hot gases, which are mainly composed by N_2, excess O_2, small amounts of H_2O, and negligible amounts of radical species. Thus, the heat release of the H_2 oxidation serves as the ignition source and eliminates the need of heating the air. This new methodology was tested for non-premixed ignition of H_2 and

Received 22 November 2004; accepted 4 April 2005.
This work was supported by AFOSR (Grant No. FA9550-04-1-0006), under the technical supervision of Dr. Julian M. Tishkoff.
*Address correspondence to egolfopo@alnitak.usc.edu

H_2-enriched CO. H_2 and CO were studied first, given that the kinetics of these fuels, constitute the fundamental "building blocks" of the hydrocarbons oxidation kinetics. For the H_2 studies, the ignition temperatures were measured for global strain rates varying between 100 and 250 s^{-1} and mole fractions of H_2 in the $(H_2 + N_2)$ stream varying between 10–60%. Similar studies were conducted for non-premixed H_2-enriched CO, with H_2 molar fractions ranging from 0.3–3% in the fuel stream. The fuel stream was not diluted with N_2 in these studies, given the relatively low ignition propensity of CO, and the need to avoid excessively high ignition temperatures as they could impact the performance of the catalyst and its supporting ceramic material. The present experimental results compare favorably with previously reported ones in similar configurations, providing thus confidence in the proposed ignition methodology. Agreements with numerical predictions were partially satisfactory.

Keywords: ignition, laminar flames, non-premixed flames

INTRODUCTION

As noted by Kreutz, Nishioka, and Law (1994), until recently, most of our knowledge of the low-temperature chemistry that governs flame ignition has come from past studies on the development of chemical mechanisms in homogeneous systems. Subsequently, Law and coworkers (e.g., Fotache et al., 1995, 2000; Kreutz and Law, 1996, 1998) performed rigorous flame ignition studies in the counterflow configuration. H_2 and CO ignition was studied first given the importance of the oxidation chemistry of these fuels in the hierarchy of hydrocarbon chemistry. These studies have indicated that H_2 exhibits a 3-limit dependency on pressure that is similar to the homogeneous explosive limits, and they have also characterized the effect of H_2 concentration on CO ignition in a convective-diffusive system.

The ignition studies of Law and coworkers (1995, 1996, 1998, 2000) were conducted by counter-flowing fuel/inert jets against a heated air-jet. The heating of the air was achieved by using electrically heated coils placed within a quartz tube through which the air was passing. The design of the system is rather involved, and there may be some physical limitations associated with the quartz material with respect to the maximum temperature that it could be attained. It has also been reported that the radial temperature profiles are uniform in only 30–50% of the radial range, and this is the result of the unavoidable heat

losses to the quartz tube walls. However, and given that ignition initiates at the highest temperature, which for the experiments of Law and coworkers (1995, 1996, 1998, 2000) is located around the centerline, achieving uniformity at 30–50% of the radial range, makes the reported data reliable, and a close representation of what is modeled using the quasi-one dimensional stagnation-flow code.

The purpose of this work is to introduce an alternative approach for ignition studies in the counterflow configuration by utilizing the chemical energy of fuels to create a hot stream of gases that will also have a rather uniform radial temperature distribution. This approach can be much simpler compared to that of Law and coworkers (1995, 1996, 1998, 2000) and can be readily used in environments, such as for example in microgravity, in which there are time limitations, and reduced availability of electrical power. Non-premixed H_2 and CO ignition is studied first, as these fuels are kinetically simple and constitute the fundamental "building blocks" of the hydrocarbons oxidation kinetics. Furthermore, comparing the experimental results for these simple fuels with those of Law and coworkers (1995, 1996, 1998, 2000) would test the validity of the proposed technique.

EXPERIMENTAL APPROACH

A variation of the counterflow configuration has been adapted for the present ignition studies. The schematic is shown in Figure 1. Each burner includes an aerodynamically shaped converging nozzle that results in a top-hat velocity profile at the nozzle exit that has a diameter of 10 mm. The top burner contains both internal cooling and an external cooling coil to prevent heating of the system by the flames upon ignition, and/or the vitiated air. Nitrogen co-flow is used to negate the effects of ambient gases, preserving thus the radial uniformity of all properties of the two opposing jets.

The bottom burner includes a 52-mesh, 25 × 25 mm platinum gauze woven from 0.1 mm diameter wire (Alfa Aesar) supported 1 mm above the nozzle exit; see for details Figure 1. A non-porous 99.9% aluminum-oxide ceramic disk, machined with an 11 mm hole, was used to support the platinum mesh due to its high temperature durability, ability to withstand fast temperature loading (thermal shock), and low thermal conductivity (to minimize heat loss in the radial direction). The spacing between the top burner and the platinum screen was set at 12 mm.

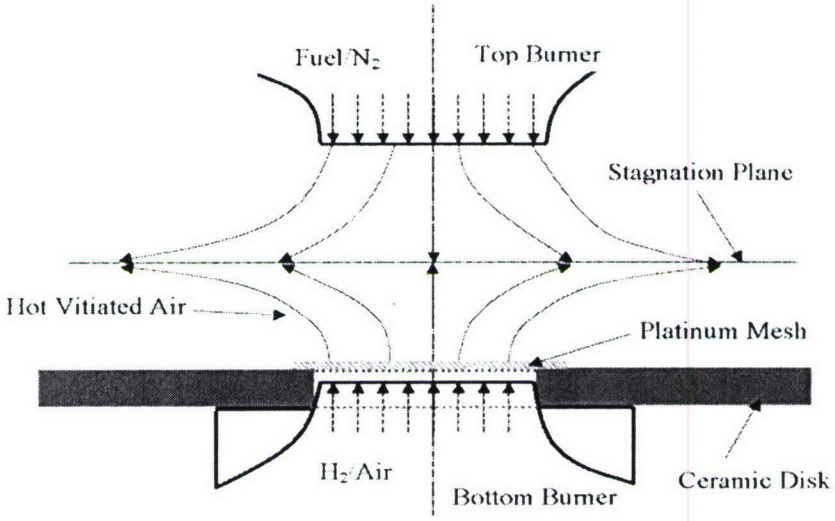

Figure 1. Schematic of the experimental configuration.

Ultra-lean H_2/air mixtures are catalyzed on the platinum surface and become the heat source for ignition, resulting in essence in an H_2/air flame that is stabilized on the catalyst surface. Using a combination of ultra-lean H_2/air mixtures and a catalyst, results in flame temperatures in the range of 650 to 1300 K, that are of relevance to ignition, as Law and coworkers have shown (1995, 1996, 1998, 2000); the lower end of this temperature range can only be achieved in the presence of the catalyst. Furthermore, under such conditions the combustion products largely consist of O_2 and N_2, small amounts of H_2O, and negligible amounts of radical species.

In addition to controlling the vitiated air temperature within the range that is of interest to ignition, the use of a platinum screen to catalyze H_2/air mixtures was implemented in order to assure that the hot gases are produced at the nozzle exit, so that there is no need for stabilizing a (strained) flame between the nozzle exit and the stagnation plane. The location of such flame would become an important parameter in the ignition problem as, to the first order, would affect the heat flux to the opposing fuel/inert jet. Furthermore, it is rather difficult to simultaneously control the flame location and temperature for these ultra-lean H_2/air flames that are characterized by Lewis numbers, Le, notably less than one (e.g., Law, 1988). Variation of the temperature right after the

platinum screen is achieved by changing the equivalence ratio, ϕ, of the H_2/air mixture. It should be noted that some initial energy must be supplied to activate the H_2/air/catalyst system and initiate the heat production, after which the system is completely self-sustaining. The use of a pilot flame or heated wire was concluded to be effective for this task.

The system was found to be stable within a temperature variation of less than 1 K for over 3 hours of operation in the range of 650 to 1300 K. The adiabatic flame temperature limits the maximum temperature that can be achieved over the catalyst, based on the principle of chemical equilibrium. It should be also noted, that because H_2 oxidation takes place on the platinum screen, the prevailing strain rate has no effect on the flame temperature which, as a result, cannot exceed its equilibrium value; this would not be the case, if these ultra-lean, $Le < 1$ H_2/air air mixtures were allowed to form a flame that is stabilized by the fluid mechanics (e.g., Law, 1988). Repeatability of the temperatures obtained was found to be within 10 K. Initial temperature measurements for a new Pt mesh may be observed to be higher than those of a used mesh, but preventive maintenance can eliminate further deactivation of the platinum. It was found that "baking" the catalyst in a furnace at 1000 K for 3 hours, shortly after shutdown and during storage, is effective in burning-off any organic matter that can poison the platinum. The radial temperature profile was measured and was found to be uniform within approximately 60% of the radial range, which is an improvement over the temperature profile uniformity reported by Law and coworkers (1995, 1996, 1998, 2000).

Non-premixed ignition of N_2-diluted H_2 was investigated for H_2 mole fractions in the fuel stream, X_{H_2}, ranging from 10 to 60%, and global strain rates, K_{glb}, ranging from 100 to 250 s^{-1}. A similar study on H_2-enriched CO was carried out for strain rates between 150 and 260 s^{-1}.

For all cases, the catalytic activity was first established opposite to a flow of N_2. The temperature of the ignition source was then reduced far below the anticipated ignition value, while the desired concentration of fuel/N_2 exiting the top burner was set. For the case of CO that ignites at higher temperatures compared to H_2, N_2 was entirely eliminated in order to maintain relatively low ignition temperatures that would not compromise the performance of the catalyst and its ceramic support. Ignition was subsequently obtained by gradually increasing the temperature of the hot gases until a vigorously burning flame is established. It

should be noted that a dark environment is necessary to observe the ignition of H_2 flames, as they are colorless.

The temperature was measured at a distance of 0.5 mm above the platinum just prior to ignition and is used as the ignition temperature, T_{ign}, similarly to the approach of Law and coworkers (1995, 1996, 1998, 2000). An yttrium-beryllium-oxide-coated Omega S-type thermocouple with a 0.041 mm junction was used for the temperature measurements. All temperatures were corrected for radiation losses in the manner consistent with that of Qin (2000). Correction of measured temperatures does have a tendency to introduce uncertainties that stem particularly from the choice of model assumed for the thermocouple wire. Relevant models assume the junction to be either a sphere or a cylinder in cross flow (Qin, 2000). Differences in the corrected temperatures vary by as much as 40 K between the models for some measurements, but were on average no more then 30 K apart. Given that the thermocouple used can most accurately be described as somewhere between the cylinder and sphere (e.g., Fotache et al., 1995), the uncertainty introduced by the thermocouple corrections is as much as ± 20 K at a conservative estimate, but more realistically ± 15 K.

In order to investigate uncertainties regarding the composition of the vitiated air, which is an important boundary condition in the numerical simulations, stable species measurements just downstream of the platinum screen were carried out using mass spectrometry. To sample the flow, the technique reported by Ren (2001) was utilized. Briefly, a microprobe was inserted into the stagnation streamline of the vitiated air at 1 mm above the platinum screen. The vacuum inside the probe was set so that the flow velocity inside the probe entrance was equivalent to that of the sample stream. This is important, because as it has been noted in previous studies (e.g., Ren, 2001; Westenberg et al., 1957), the introduction of microprobes into laminar flows does not significantly affect the concentrations of the measured species only if the flow velocity at the probe entrance is equivalent to the flow velocity of the undisturbed stream at the same point, unperturbed by the probe. The sample was then transferred to the UTI 100c mass spectrometer for analysis. This particular model utilizes a quadrupole design coupled with a tuning fork chopper cycling at 400 Hz that feeds into a lock-in amplifier that ensures that only the modulated mass spectrometer output that coincides to the beat frequency of the chopper is read. This process helps to enhance the signal-to-noise ratio of the measurements.

NUMERICAL APPROACH

The opposed-jet configuration was simulated along the stagnation streamline by solving the quasi-one dimensional conservation equations of mass, momentum, energy, and species concentration similar to previous studies (e.g., Egolfopoulos and Campbell, 1996). The code is integrated with the CHEMKIN (Kee et al., 1989) and Transport (Kee et al., 1983) subroutine libraries. The GRI 3.0 (Smith et al., 2000) and Mueller et al. (1999) kinetic mechanisms were used to describe the details of the $H_2/CO/O_2$ oxidation.

In the simulations, the ignition state was reached through successive solutions of the governing equations that were obtained by increasing the values of temperature, and by also considering the attendant changes of the composition of the vitiated air. The composition of the vitiated air at a particular temperature was determined by calculating the equilibrium products of the catalyzed H_2/air mixture using STANJAN (Reynolds, 1987). Thus, the equilibrium products determined at the measured temperature and for the prevailing ϕ of the (ultra-lean) H_2/air stream, were used as boundary conditions. The validity of the assumption and its implications on the ignition process will be further assessed in the Results and Discussion section.

The ignition state is described by a "turning-point" behavior as the temperature of the vitiated air increases (e.g., Law et al., 1995, 1998, 2000). To capture this behavior, the stagnation code was modified by imposing a one-point continuation technique (Egolfopoulos and Dimotakis, 1998; Nishoika et al., 1996) with respect to any radical concentration. Given its importance to chain-branching, the H radical can be used as a good measure of the ignition kernel characteristics. A pre-determined increment on the H-radical concentration was imposed at the location where this concentration had a maximum slope on the side that is near to the hot boundary, i.e., the bottom burner. Thus, this new boundary condition replaces the temperature at the bottom burner for which the "S"-curve is single-valued. Progressive steady-state solutions were obtained and monitored until turning point behavior was exhibited on the system response curve of the maximum H mass fraction, $(Y_H)_{max}$, versus the maximum temperature of the vitiated air, T_{max}, as shown in Figure 2; note that $T_{max} = T_{ign}$. The solution at the turning point corresponds to the ignition state. It should be noted that this method can capture the entire "S" shaped system response curve, but simulations were stopped

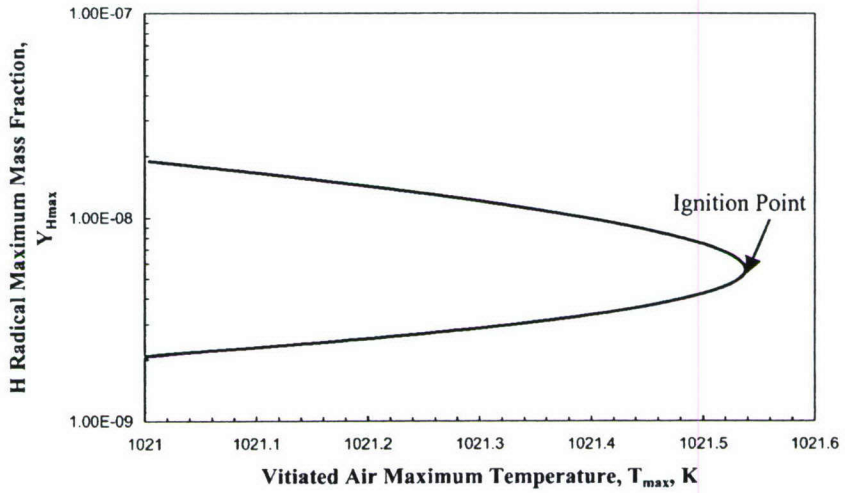

Figure 2. Variation of numerically determined Y_{Hmax} vs. T_{max} around the ignition state of non-premixed H_2 vs. vitiated air for $X_{H_2} = 0.4$ and $K_{glb} = 150\,s^{-1}$. Simulations included the use of the GRI 3.0 mechanism (Smith et al., 2000).

after the ignition point was established. Grid adaptation was used to resolve the obtained solutions, which lead to a typical range of 200–500 grid-points. Further grid refinement was found to have no effect on the numerically determined ignition states. The numerical results were used in conjunction with sensitivity and reaction path analyses of the ignition states, in order to gain insight into the controlling physico-chemical mechanisms.

RESULTS AND DISCUSSION

Hydrogen Ignition

Figure 3 depicts the effect of N_2 dilution on H_2 ignition, and it is shown to exhibit three regions of distinct trends. In the first region corresponding to $X_{H_2} < 0.15$, T_{ign} monotonically decreases with increasing X_{H_2}. In the third region corresponding to $X_{H_2} > 0.20$, T_{ign} appears to minimally depend on X_{H_2}. For $0.15 < X_{H_2} < 0.20$, a transition from the first to the third region takes place. Error bars reflect the standard deviation that results from the data scatter. The numerically predicted T_{ign}'s, using the mechanisms of Mueller et al. (1999) and GRI 3.0 (Smith et al., 2000), are also shown in Figure 3. The Mueller et al. mechanism

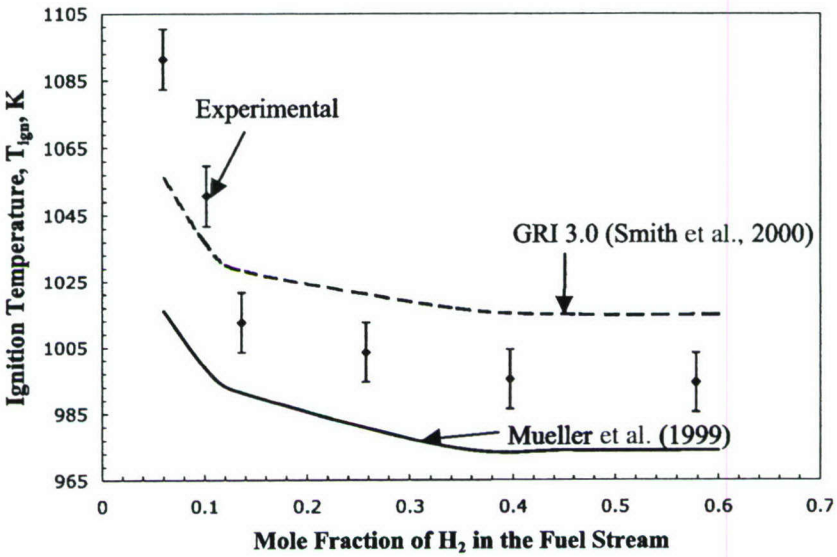

Figure 3. Experimentally and numerically determined T_{ign} vs. H_2 mole fraction for non-premixed H_2/N_2 vs. vitiated air with $K_{glb} = 126\,s^{-1}$. Error bars represent the standard deviation of the experimental data scatter.

under-predicts the experimental T_{ign}'s for all X_{H_2}'s, while the GRI 3.0 mechanism under-predicts the experiments for low X_{H_2}'s and over-predicts them for high X_{H_2}'s. In general, the predictions using the GRI 3.0 mechanism are closer to the experimental data when compared to the Mueller et al. mechanism, which under-predicts the T_{ign} by as much as 70 K at the lowest X_{H_2} tested.

In the present investigation the results are presented in terms of the global strain rate, K_{glb}, rather than the local strain rate before the flame, K. While $K_{glb} \equiv u_{exit}/(L/2)$, where u_{exit} is the nozzle exit velocity and L is the nozzle separation distance, K is the absolute value of the axial velocity gradient at the boundaries of the ignition kernel, and can be only determined through the use of laser-based velocity measurements diagnostics. To assess if reporting experimental data for a given value of K_{glb} are meaningful, the effect of K_{glb} on T_{ign} was determined numerically and the results are shown in Figure 4. It can be seen that for the range of K_{glb} studied here, T_{ign} is, for the most part, nearly invariant with K_{glb}, eliminating thus the need for determining the local strain rates. The lack of dependency of ignition on strain rate allows for a detailed view of the

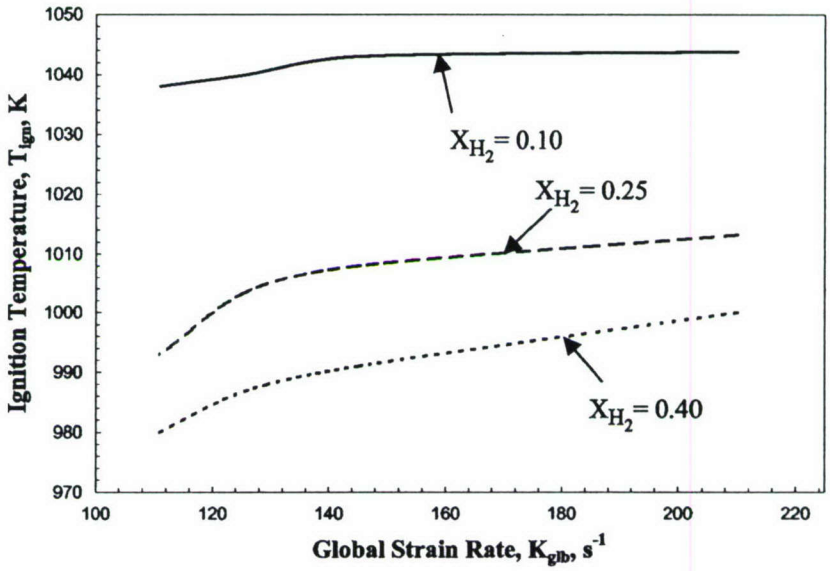

Figure 4. Variation of numerically determined T_{ign} vs. K_{glb} for non-premixed H_2/N_2 vs. vitiated air with X_{H_2} of 0.10, 0.25, and 0.40. Simulations included the use of the GRI 3.0 mechanism (Smith et al., 2000).

steady-state system as dependent on diffusion and kinetics only. It should be noted that this finding should not be generalized, as it is known from the work of Law and coworkers (1995, 1996, 1998, 2000) that for a wider range of strain-rate variation the effect on ignition can be significant. What is reported here is a relatively narrow range of strain rates as far as ignition is concerned, which however is wide enough to eliminate the need for using more detailed measurements of convective velocities. This constitutes a major simplification of the experimental approach, and the data can, therefore, be used with confidence to assess the effects of kinetics on ignition.

The analyses of the ignition states were performed within the ignition kernel, similarly to Kreutz, Nishioka, and Law (1995). Figure 5 depicts the kernel structure at the ignition state for $X_{H_2} = 0.10$. The structure shown in Figure 5 was found to be very similar to that reported by Kreutz, Nishioka, and Law (1995), implying that the ignition state using vitiated air is very similar to that of heated air.

As expected, reaction path analysis performed in the third region with $X_{H_2} > 0.40$ reveals that the H_2 oxidation at the ignition state is

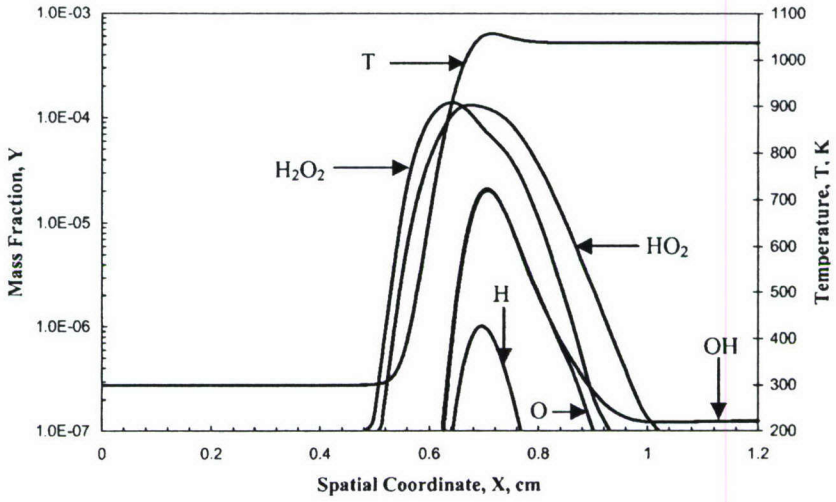

Figure 5. Structure of the numerically determined ignition kernel at the ignition state for non-premixed H_2/N_2 vs. vitiated air configuration with $X_{H_2} = 0.10$. Simulations included the use of the GRI 3.0 mechanism (Smith et al., 2000).

governed by the following four reactions (The preceding reaction numbers correspond to those in the H_2/O_2 sub-mechanism of the original GRI 3.0 mechanism):

$$\text{R10} \quad H + O_2 \Leftrightarrow OH + O$$

$$\text{R20} \quad H_2 + O \Leftrightarrow OH + H$$

$$\text{R3} \quad H_2 + OH \Leftrightarrow H + H_2O$$

$$\text{R8} \quad H + O_2 + (M) \Leftrightarrow HO_2 + (M)$$

R3 is dominant as it consumes the majority of H_2 and accounts for almost all the water production. In this case, the OH radical production is almost evenly split between the two branching reactions R10 and R20, and both are highly dependant on H, which is competed for by the 3-body reaction R8. These results are identical to those previously reported by Kreutz, Nishioka, and Law (1995).

The first region with $X_{H_2} < 0.15$ exhibits a monotonically increasing T_{ign} with decreasing X_{H_2}. Note that as a result of the dependence of Arrhenius kinetics on temperature, the ignition kernel is located close

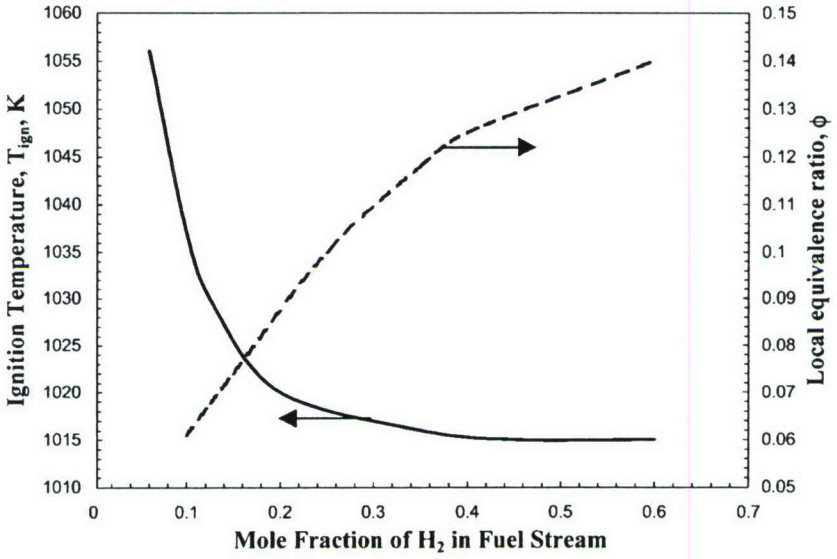

Figure 6. Numerically determined T_{ign} and local equivalence ratio vs. X_{H_2} for non-premixed H_2/N_2 vs. vitiated air configuration with $K_{glb} = 126\,s^{-1}$. Simulations included the use of the GRI 3.0 mechanism (Smith et al., 2000).

to the hot boundary, i.e., the oxidizer boundary. Furthermore, within the kernel the reactants are well mixed for the chemistry to be activated. Thus, a local equivalence ratio, ϕ, can be determined within the kernel; $\phi \equiv (X_{H_2}/X_{O_2})/(X_{H_2}/X_{O_2})_{stoichiometric}$. The value of ϕ is chiefly affected by the flux of H_2, which has to diffuse across the stagnation plane in order to reach the oxidizer boundary. Figure 6 depicts the variation of ϕ, determined at the position of maximum H concentration, with respect to X_{H_2}. It can be seen that ϕ in the kernel decreases more rapidly as the $X_{H_2} = 0.10$ limit is approached. This is due to the decrease in H_2 concentration on the fuel side, which, in turn, decreases the driving force of diffusion or in other words the process becomes diffusion-limited. For $X_{H_2} > 0.30$, the slope of the ϕ curve is becoming less steep, and for $X_{H_2} > 0.40$ the change is not significant enough, and ignition is controlled by kinetics with pathways that are nearly identical to cause any notable variation of T_{ign} with X_{H_2}.

Effect of H_2 Leakage. A concern of the proposed ignition methodology is that not all of the hydrogen used for the heat production is being

consumed over the catalyst. In order to investigate this, a series of experiments and numerical simulations were conducted. Figure 7 depicts the results of numerical simulations, in which H_2 was allowed to be present in the vitiated air stream in order to simulate the effect of potential H_2 leakage through the catalyst. The ignition states were determined for the $X_{H_2} = 0.10$ and 0.60 cases. The results show that there is a relatively small effect on T_{ign}, which is more apparent for the $X_{H_2} = 0.10$ case. This is reasonable, because H_2 leakage from the catalyst will have a greater effect on the local equivalence ratio within the ignition kernel for the lower $X_{H_2} = 0.10$ case. However, the variations of T_{ign} that are reported in Figure 7 are well within the uncertainty range of the experiments. It was subsequently determined by mass spectrometry measurements, that the H_2 mole fractions were less than 0.01 (i.e., 1%) for the entire range of experiments. This experimental evidence supports the argument that the equilibrium product assumption just downstream of the platinum screen is a physically sound one, and that the boundary conditions used in the numerical simulations closely resemble the experimental ones.

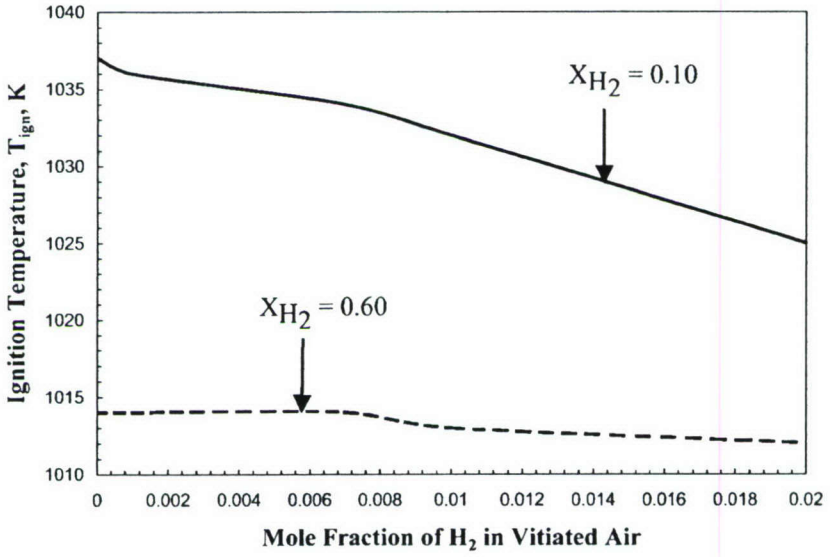

Figure 7. Numerically determined effect of H_2 leakage through the platinum mesh on T_{ign} for $X_{H_2} = 0.10$ and 0.60. Simulations included the use of the GRI 3.0 mechanism (Smith et al., 2000).

Effect of H_2O. The present results on non-premixed H_2 ignition were also compared with those of Law and coworkers (1995, 1996, 1998, 2000), in order to further assess the validity of the proposed methodology. It was found that the T_{ign}'s determined in both the present experiments and simulations were on the average, 60–70 K higher than those measured by Law and coworkers (1995, 1996, 1998, 2000).

This was explained based on kinetics arguments. The use of the chemical energy of H_2/air flames as the heating source for ignition results in a slightly oxygen-depleted oxidizer, when compared to normal air, which also contains small amounts of H_2O. The presence of H_2O results in the enhancement of the 3-body $H + O_2 + (H_2O) \Leftrightarrow HO_2 + (H_2O)$ reaction, which has a termination effect on the radical production and suppresses ignition. This is illustrated numerically in Figure 8, where the mole fraction of H_2O in the hot oxidizer stream is varied from 0 to 0.09. Results reveal a notable increase of T_{ign} with the amount of H_2O present in the oxidizer. It is also of interest to note, that there is about a 60 K difference in T_{ign} between the normal air case and the vitiated air, which supports the argument on the observed differences in T_{ign}

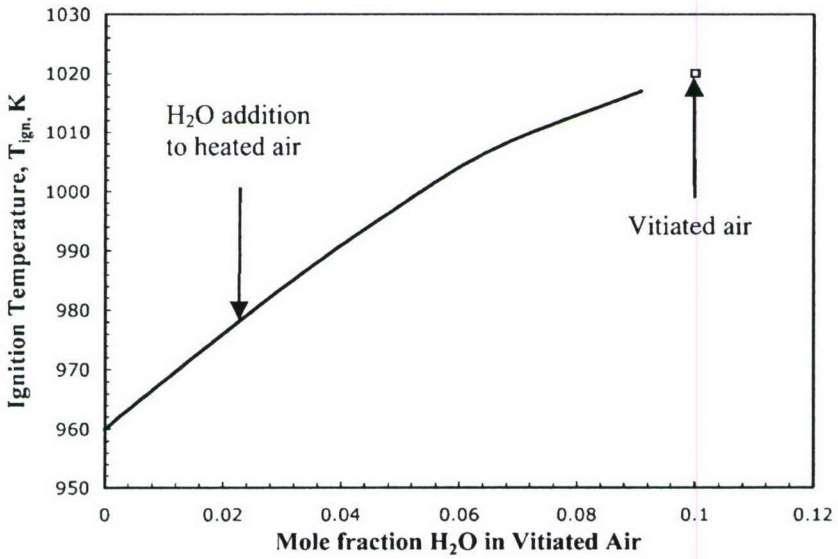

Figure 8. Numerically determined effect of H_2O on T_{ign} for $X_{H_2} = 0.20$. Simulations included the use of the GRI 3.0 mechanism (Smith et al., 2000).

values between the present data and those of Law and coworkers (1995, 1996, 1998, 2000).

Finally, an estimate of the uncertainty of the present experiments with respect to the H_2O concentration in the vitiated air can be made. Given that the maximum H_2 mole fraction measured downstream of the catalyst was found to be below 1%, the corresponding variation of the H_2O has to be at most 1% compared to its equilibrium value. Based on the results of Figure 8, 1% variation in the H_2O mole fraction results in a T_{ign} variation that is well within the experimental uncertainty, i.e., less than 5–7 K.

Effect of Total Vitiated Air Composition. To assess the potential influence of errors introduced by the thermocouple measurements and the experimental scatter on the reported data, the effect of the total vitiated air composition on ignition was also investigated. This was achieved through perturbations of the total composition of the vitiated air by varying the temperature at which the equilibrium products are calculated by $\pm 10\%$. The computed results are shown in Figure 9, and they reveal

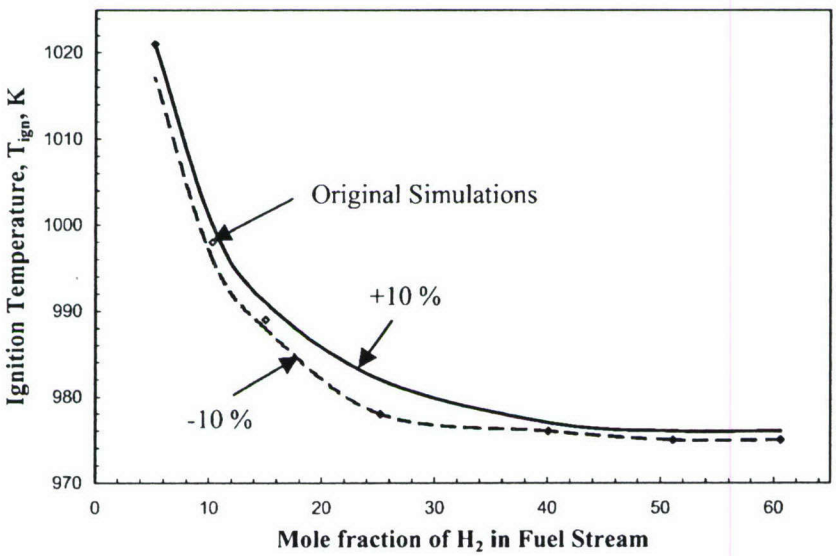

Figure 9. Variation of numerically determined T_{ign} vs. X_{H_2} for $K_{glb} = 126\,s^{-1}$ when vitiated air equilibrium products are calculated at $\pm 10\%$ of the measured vitiated air temperature. Simulations included the use of the GRI 3.0 mechanism (Smith et al., 2000).

that there is relatively minor change in T_{ign} as a result of the overall temperature at which the equilibrium products are calculated.

H_2-Enriched CO Ignition

H_2-enriched CO ignition experiments were conducted for X_{H_2} values ranging from 0.3 to 3% of H_2 in CO, and for K_{glb} varying between 150 and 260 s^{-1}. In these studies, no N_2 was present in the fuel stream, as CO ignites at higher temperatures compared to H_2 and our goal was to maintain the ignition temperatures to as low levels as possible as mentioned in a previous section. Figure 10 depicts the variation of T_{ign} with X_{H_2}. Error bars represent the standard deviation of the experimental data scatter. As expected, T_{ign} was found to decrease with X_{H_2}. The numerical simulations predict similar qualitative behavior, but notable differences between experimental and predicted T_{ign}'s exist. While the GRI 3.0 mechanism over-predicts the experimental T_{ign}'s, the Mueller et al. mechanism notably under-predicts them. Similarly to the H_2

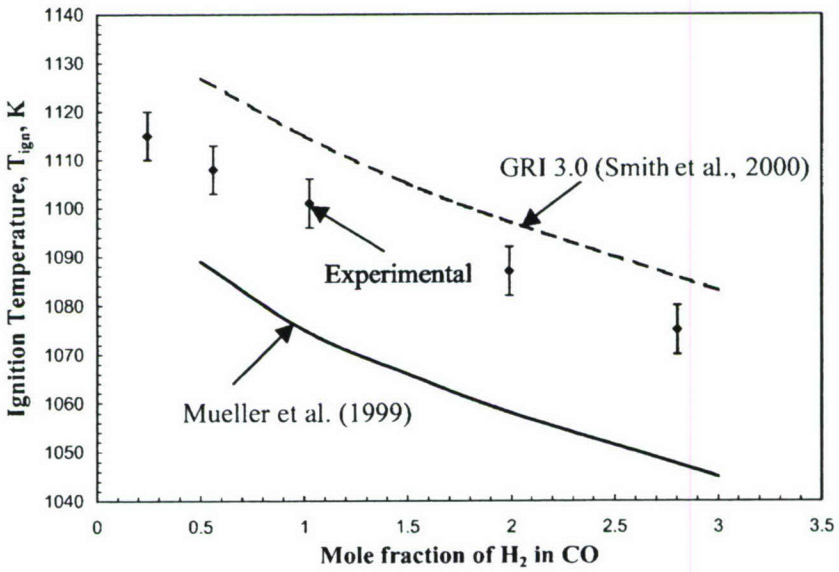

Figure 10. Experimentally and numerically determined T_{ign} vs. H_2 mole fraction for non-premixed H_2 enriched CO vs. vitiated air with $K_{gbl} = 200\ s^{-1}$. Error bars represent experimental scatter.

ignition case, it was found that the effect of the strain rate on T_{ign} is minor for the range of K_{glb} studied here.

Reaction path analysis revealed that the following reactions control the ignition process:

$$\text{R10} \quad H + O_2 \Leftrightarrow O + OH$$

$$\text{R3} \quad O + H_2 \Leftrightarrow H + OH$$

$$\text{R8} \quad H + O_2 + (M) \Leftrightarrow HO_2 + (M)$$

$$\text{R31} \quad OH + CO+ \Leftrightarrow H + CO_2$$

As expected, R31, which represents the main destruction pathway for CO, is of great importance. R10 and R3 are chain-branching pathways that compete with R8, the main chain termination pathway. These results are also in agreement to those of Fotache et al. (2000).

Effects of H_2O. Similarly to what was reported in the previous section on H_2 ignition, the ignition temperatures recorded for H_2-enriched CO versus vitiated air are also higher than those for ignition versus heated air (Fotache et al., 2000). The addition of H_2O to the hot oxidizer stream has a tendency to suppress ignition. Again, the presence of finite amounts of H_2O was found to enhance the 3-body $H + O_2 + (H_2O) \Leftrightarrow HO_2 + (H_2O)$ reaction, which depletes the H radical pool. The uncertainty of the H_2O concentration in the vitiated air is also less than 1% with an attendant variation for T_{ign} that is well within the experimental uncertainty, i.e., less than 5–7 K.

CONCLUDING REMARKS

A new experimental methodology has been advanced for studying flame ignition in counterflow configurations. It involves the use of vitiated air as the ignition source, which is produced by the oxidation of ultra-lean H_2/air flames on a platinum screen placed at the nozzle exit of one of the burners. This allows for the efficient variation of the temperature of the hot gases in a range that is of relevance to ignition. The vitiated air produced by ultra-lean H_2/air flames contains minor amounts of H_2O are present in the vitiated air, with its effect on the ignition process being relatively small but also well characterized. The proposed

technique is an alternative one to that of Law and coworkers, who instead used electrically heated air as the ignition source. The use of vitiated air eliminates the need for complex burner design and avoids problems associated with burner materials. As a result, it can be readily used to study ignition phenomena in environments, such as for example microgravity, in which the experimental times are short, and the availability of electrical power can be limited.

Non-premixed ignition of H_2 and H_2-enriched CO was studied. The obtained results are consistent with those determined by Law and coworkers, providing thus confidence to the proposed technique. The ignition results of H_2/N_2 mixtures revealed two distinct limits. For low H_2 concentrations the behavior was found to be diffusion-limited, while for high H_2 concentrations it was found to be kinetically controlled. The results on CO/H_2 demonstrated the anticipated sensitivity of CO ignition to H_2 addition. For both chemical systems insight was provided into the physico-chemical mechanisms controlling the ignition phenomena.

REFERENCES

Egolfopoulos, F.N. and Campbell, C.S. (1996) Unsteady counterflowing strained diffusion flames: Diffusion-limited frequency response. *J. Fluid Mech.*, **318**, 1–29.

Egolfopoulos, F.N. and Dimotakis, P.E. (1998) Non-premixed hydrocarbon ignition at high strain rates. *Proc. Combust. Inst.*, **27**, 641–648.

Fotache, C.G., Kreutz, T.G., Zhu, D.L., and Law, C.K. (1995) An experimental study of ignition in non-premixed counterflowing hydrogen versus heated air. *Combust. Sci. Tech.*, **109**, 373–393.

Fotache, C.G., Tan, Y., Sung, C.J., and Law, C.K. (2000) Ignition of CO/H2/N2 versus heated air in counterflow: experimental and modeling results. *Combust. Flame*, **120**, 417–426.

Kee, R.J., Rupley, F.M., and Miller, J.A. (1989) Report No. SAND89-8009, Sandia National Laboratories, Livermore, CA.

Kee, R.J., Warnatz, J., and Miller, J.A. (1983) Report No. SAND83-8209, Sandia National Laboratories, Livermore, CA.

Kreutz, T.G. and Law, C.K. (1996) Ignition in non-premixed counterflowing hydrogen versus heated air: Computational study with detailed chemistry. *Combust. Flame*, **104**, 157–175.

Kreutz, T.G. and Law, T.G. (1998) Ignition in non-premixed counterflowing hydrogen versus heated air: Computational study with skeletal and reduced chemistry. *Combust. Flame*, **114**, 436–456.

Kreutz, T.G., Nishioka, M., and Law, C.K. (1994) The role of kinetic versus thermal feedback in nonpremixed ignition of hydrogen versus heated air. *Combust. Flame*, **99**, 758–766.

Law, C.K. (1988) Dynamics of stretched flames. *Proc. Combust. Inst.*, **22**, 1381–1402.

Mueller, M.A., Kim, T.J., Yetter, R.A., and Dryer, F.L. (1999) Flow reactor studies and kinetic modeling of the $H_2/O_2/NO_X$ and $CO/H_2O/O_2/NO_X$ reactions. *Int. J. Chem. Kin.*, **31**(2), 113–125.

Nishioka, M., Law, C.K., and Takeno, T. (1996) A flame-controlling continuation method for generating S-curve responses with detailed chemistry. *Combust. Flame*, **104**, 328–342.

Qin, W. (2000) Ph.D. Dissertation Thesis, University of Southern California, Department of Chemical Engineering.

Ren, J.Y. (2001) Ph.D. Dissertation Thesis, University of Southern California, Department of Mechanical Engineering.

Reynolds, W.C. (1987) STANJAN Thermochemical Equilibrium Software, Stanford University, Stanford, CA.

Smith, G.P., Golden, D.M., Frenklach, M., Moriarty, N.W., Eiteneer, B., Goldenberg, M., Bowman, C.T., Hanson, R.K., Song, S., Gardiner, W.C., Jr., Lissianski, V., and Qin, Z. (2000) GRI-Mech 3.0, <http://www.me.berkeley.edu/gri_mech/>.

Westenberg, A.A., Raezer, S.D., and Fristrom, R.M. (1957) Interpretation of the sample taken by a probe in a laminar concentration gradient. *Combust. Flame*, **1**, 467–478.

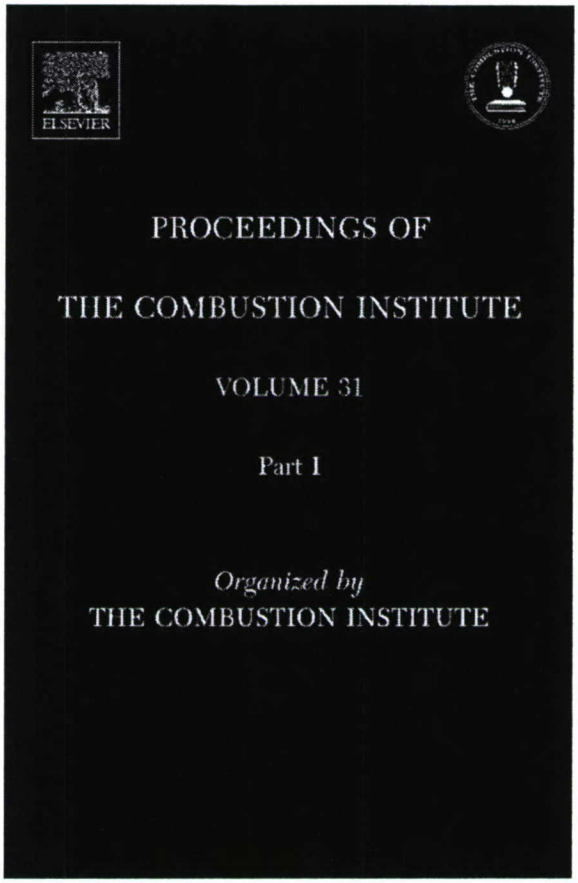

Available online at www.sciencedirect.com
ScienceDirect
Proceedings of the Combustion Institute 31 (2007) 1205–1213
Proceedings of the Combustion Institute
www.elsevier.com/locate/proci

Ignition and extinction of non-premixed flames of single-component liquid hydrocarbons, jet fuels, and their surrogates

A.T. Holley [a,*], Y. Dong [a], M.G. Andac [a], F.N. Egolfopoulos [a], T. Edwards [b]

[a] *Department of Aerospace and Mechanical Engineering, University of Southern California, Los Angeles, CA 90089-1453, USA*

[b] *Air Force Research Laboratory, AFRL/PRTG Bldg 490, 1790 Loop Rd N, Wright Patterson AFB, OH 45433-7103, USA*

Abstract

In the present study, extinction strain rates and ignition temperatures of a wide range of jet fuels were experimentally determined in the counterflow configuration under non-premixed conditions. Similar measurements were also made for single-component hydrocarbon fuels and surrogate fuels, and were compared with those obtained for the jet fuels. The experiments were conducted at atmospheric pressure and elevated temperatures. Comparing single-component hydrocarbon fuels, it was found that those with lower carbon number exhibit greater resistance to extinction and greater ignition propensity. The results for the jet fuels revealed that there is a large variation in both extinction and ignition limits. Jet fuels with similar extinction behavior were found to display a rather different ignition response. Two recently proposed JP-8 surrogates were also tested, and both the ignition and extinction states of a reference JP-8 fuel were not predicted satisfactorily. Both surrogates were found to exhibit a more robust combustion behavior compared to JP-8, as manifested by their increased ignition propensity and their increased resistance to extinction.

Keywords: Jet fuels; Surrogate fuels; Non-premixed flames; Ignition; Extinction

1. Introduction

Jet fuels (JF) are mixtures of large numbers of hydrocarbons spanning a wide range of carbon numbers and chemical classifications. Typically, the carbon number ranges from C_7–C_{16} (on the average C_{11}–C_{12}), and the chemical classifications from *n*-paraffins to aromatics. The defining characteristics of JFs are not necessarily their chemical compositions, but their physical properties such as density and boiling range. It is also known that the chemical composition of different batches of JFs can vary significantly from each other (e.g., [1]).

The large number of complex hydrocarbons present in real JFs renders the modeling of their pyrolysis/oxidation characteristics a rather daunting task. Development of reliable surrogate fuels is the only option to develop kinetics models for simulating real combustors.

* Corresponding author. Fax: +1 213 740 8071.
E-mail address: aholley@usc.edu (A.T. Holley).

1540-7489/$ - see front matter
doi:10.1016/j.proci.2006.07.208

Surrogates have been developed for practical fuels based on chemical composition by matching properties, such as volatility, chemical class distribution, average molecular weight, H/C ratio, sooting tendency, heat release, flammability, and regression rate (e.g. [2–6]). This matching, however, is mostly based on physical properties and much less on the chemical properties of the real fuels. Ideally, matching chemical properties requires the study of phenomena that depend to great extent on kinetics in both homogenous systems and flames. Few past studies have considered flame phenomena (e.g., [7]).

In the present investigation, the ignition and extinction limits of non-premixed flames were experimentally determined for a wide range of liquid fuels in the well-controlled counterflow configuration. It is known that both flame ignition and extinction are rather sensitive to chemical kinetics (e.g., [8–10]). Thus, such data could be used to develop appropriate surrogates as well as reliable kinetics mechanisms.

2. Experimental approach

2.1. Configuration

The experiments involved the use of the counterflow configuration. Single planar non-premixed flames were established by counter-flowing a heated fuel/N_2 jet against an ambient-temperature O_2 jet. The extinction and ignition states were determined as functions of the fuel/N_2 mass ratio. The burner diameters used were $D = 14$ and 22 mm. The burner separation distance, L, was kept equal to D, i.e., $L/D = 1$.

2.2. Fuels tested

A wide range of liquid fuels was tested. Nine single-component hydrocarbons (SCH), namely n-C_5H_{12}, n-C_6H_{14}, n-C_7H_{16}, n-C_8H_{18}, iso-C_8H_{18}, n-C_9H_{20}, n-$C_{10}H_{22}$, n-$C_{12}H_{26}$, n-$C_{14}H_{30}$, and JP10 (*exo*-tetrahydrodicyclopentadiene $C_{10}H_{16}$) were included. Ten practical JFs shown in Table 1, and two published JP-8 surrogates, namely a 12-component (S12) [4] and a six-component (S6) [6] were also tested; details of the surrogates composition are shown in Table 2. The practical (petroleum distillate) fuels studied include JP-8 (standard military JF, MIL-DTL-831333E), three Jet-A fuels (ASTM D1655, similar to JP-8 but for commercial use in US), JP-7 fuel (specialty JF, low volatility/highly processed), two RP-1 fuels (kerosene rocket propellant, MIL-DTL-25576D), JP-10, a Fischer–Tropsch-derived JF manufactured by Syntroleum, and a coal-derived JF [11]. The distillate fuels were supplied by Wright–Patterson Air Force Base and are identified by a four-digit sample number and fuel type in the data that follows.

JP-8-3773 is a typical batch of JP-8 fuel. Jet-A-3638 and −3602 were selected to have levels of aromatics at either end of the distribution described above with 12 and 24%, respectively. Jet-A-4658 is an "average" Jet-A fuel composed by mixing in equal proportions five samples from different US manufacturers. JP-7 and RP-1 are fuels with low aromatic content and more well defined specifications than other JFs, so it was anticipated that these fuels would be consistent from batch-to-batch. As can be seen from Table 1, the JP-8 and the "composite blend" Jet-A fuels have similar composition to the average JF composition revealed in a recent world survey—roughly 60% n-+i-paraffins, 20% *cyclo*-paraffins (naphthalenes) and 20% aromatics. Separate analyses have determined that typical JF's average approximately 20% n-paraffins. Two synthetic fuels were tested, namely the Fischer–Tropsch jet fuel (4734) and one based on direct coal-liquefaction (4765), and they are primarily composed of *iso*-paraffins and naphthenes, respectively. Thus, the present experimental investigation includes the widest variation in fuel composition of any similar flame study to date.

Table 1
Test fuels with detailed composition data (ASTM D2425)

	3327 JP-7	4734 F-T	4572 RP-1	4765 DCL	3773 JP-8	4658 Jet A blend	3602 Jet A	3638 Jet A	World survey average Jet-A JP-8 JP-5 TS-1
Paraffins (n-+i-)	67.9	99.7	57.6	0.6	57.2	55.2	49.4	64.5	58.8
Cycloparaffins	21.2	<0.2	24.8	46.4	17.4	17.2	15.8	13.2	10.9
Dicycloparaffins	9.4	0.3	12.4	47.0	6.1	7.8	10.8	7.1	9.3
Tricycloparaffins	0.6	<0.2	1.9	4.6	0.6	0.6	0.9	0.6	1.1
Alkylbenzenes	0.7	<0.2	2.1	0.3	13.5	12.7	14.0	10.8	13.4
Indans/tetralins	<0.2	<0.2	0.3	1.1	3.4	4.9	7.9	2.1	4.9
Indenes	<0.2	<0.2	<0.2	<0.2	<0.2	<0.2	<0.2	<0.2	<0.2
Naphthalene	<0.2	<0.2	<0.2	<0.2	<0.2	<0.2	<0.2	0.4	0.13
Naphthalenes	<0.2	<0.2	0.3	<0.2	1.7	1.3	1.2	1.3	1.55
Acenaphthenes	<0.2	<0.2	<0.2	<0.2	<0.2	<0.2	<0.2	<0.2	<0.2
Acenaphthylenes	<0.2	<0.2	0.4	<0.2	<0.2	<0.2	<0.2	<0.2	<0.2
Tricyclic aromatics	<0.2	<0.2	<0.2	<0.2	<0.2	<0.2	<0.2	<0.2	<0.2

Table 2
Surrogate fuel composition

Compound	% volume
S6	
m-Xylene	15
iso-Octane	10
Methylcyclohexane	20
n-Dodecane	30
n-Tetradecane	20
Tetralin	5
Compound	**% mass**
S12	
m-Xylene	5
iso-Octane	5
Methylcyclohexane	5
n-Dodecane	20
n-Tetradecane	15
Tetralin	5
cyclo-Octane	5
n-Decane	15
Butylbenzene	5
Tetramethylbenzene	5
Methylnapthalene	5
n-Hexadecane	10

2.3. Fuel vaporization methodology

The vaporization of liquid fuels is a challenging process. Preferential evaporation is an important complication in multi-component fuels studies that could modify the gaseous fuel composition. On the other hand, using high temperatures to avoid preferential evaporation could result in fuel cracking. Additionally, if the supply lines downstream of the vaporization chamber are not sufficiently heated, condensation can occur.

To satisfy all the requirements, one must identify: (1) a minimum allowable temperature for effective phase change; (2) a maximum temperature and flow residence time that would favor fuel cracking, and (3) a minimum temperature that would result in condensation. To ensure that all fuel components are vaporized at the same rate, the vaporization chamber wall temperature needs to be maintained close to the boiling temperature of the heaviest component in the fuel mixture, that is approximately 300 °C for JFs. Fine droplets are injected into the chamber surrounded by a co-flowing heated N_2 jet as shown in Fig. 1. The chamber diameter is large enough to assure uniform mixing of the fuel vapor with N_2. The chamber wall temperature is the maximum in the entire flow system. The mixture temperature at the exit of the vaporization chamber is approximately 100 °C below the chamber's wall temperature, but varies depending on the flow rate.

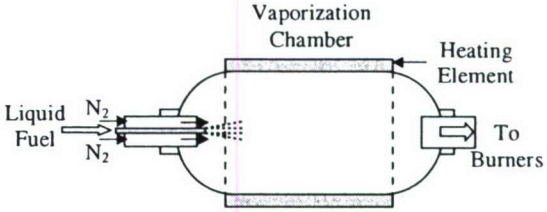

Fig. 1. Schematic of the vaporization chamber.

The extent of fuel cracking depends on both temperature and residence time. In the current configuration, the residence time from the point of fuel injection into the chamber to burner exit was determined to be 3–5 s. For a given flow rate, a change in the heating path results a non-monotonic extinction response for SCHs with carbon number greater than C_{10} and for all JFs. The post-chamber temperatures at which such response was observed were found to be 200–300 °C. This suggests that there is finite amount of cracking when the fuel is exposed to these temperatures for 3–5 s. To avoid such non-monotonic behavior caused by partial fuel cracking, the post-chamber temperatures were kept below 200 °C for all experiments.

The burners were not heated, resulting thus in temperatures at the burner exit in the range of 110–130 °C, which is the boundary condition for the heated fuel-jet. Under such conditions, low fuel/N_2 mass fractions were considered to avoid condensation. For these low fuel/N_2 mass fractions, flames could only be sustained in the presence of O_2-enriched oxidizer. Similarly, Cooke et al. [7] reported that for JP-8/N_2 mass fractions of about 0.02, the minimum O_2 mole fraction in the oxidizer stream was 60% to sustain flames. In the present investigation, pure O_2 was used in both the ignition and extinction studies.

2.4. Determination of extinction and ignition limits

Upon the establishment of a non-premixed flame, the fuel flow rate was slowly reduced until extinction occurred while maintaining the flow rates of O_2 and N_2 constant at the respective burners. Extinction strain rates, K_{ext}, were determined by measuring the maximum strain rate in the oxidizer stream using Digital Particle Image Velocimetry (DPIV) just before extinction occurred. Since the oxidizer stream was kept constant, the K_{ext} was constant for all of the fuels. The ranges of K_{ext} and fuel/N_2 mass ratio considered were 40–360 s^{-1} and 0.05–0.1, respectively.

The ignition studies were performed by counterflowing the fuel/N_2 jet against ultra-lean H_2/O_2 flames whose temperature was controlled by varying the H_2 flow rate for small temperature changes and by adding trace amounts of CO for larger temperature changes. This approach allows for

the production of hot vitiated oxidizer that serves as the ignition source. Given that H_2/O_2 flames can be sustained at compositions with very low H_2, it has been shown [12] that the composition of the vitiated oxidizer stream is dominated by O_2 with small amounts of products such as H_2O and CO_2 and negligible amounts of radicals. It has also systematically shown [12] that such data are of fundamental value as they can be readily modeled by using the equilibrium product composition of the $H_2/CO/O_2$ mixture and the measured flame temperature as boundary conditions.

Ignition was achieved by establishing $H_2/CO/O_2$ premixed flame midway between the nozzle and the stagnation plane, and by subsequently increasing the fuel flow rate in the fuel/N_2 stream until ignition is observed. The peak temperature of the $H_2/CO/O_2$ flame was measured with a thermocouple, and is reported as the ignition temperature, T_{ign}. The ranges of T_{ign} and fuel/N_2 mass ratio considered in this study were approximately 1000–1100 °C and 0.045–0.065, respectively.

3. Results and discussion

Experimental results obtained for all fuels will be presented in Tables for completeness and clarity. Graphical presentation will be used only for selected conditions.

Table 3 depicts K_{ext} as a function of fuel/N_2 mass ratio for all fuels; for the $K_{ext} = 60$, 78, and 97 s^{-1} cases, $D = 22$ mm was used, while for the $K_{ext} = 155$, 223, 290, and 357 s^{-1} cases, $D = 14$ mm was used. Comparison of the SCHs reveals that for the same K_{ext} SCHs with smaller carbon number extinguish at lower fuel/N_2 mass ratio, i.e., they have greater resistance to extinction. It can be seen that n-C_5H_{12} is the most resistant while n-$C_{14}H_{30}$ is the least resistant one. There is, however, less separation between the various fuels extinction response at low strain rates than at higher ones. Non-premixed burning is diffusion-controlled and given that the lighter molecules are more diffusive, they result in more intense burning. The effect of strain rate can also be explained based on a rather similar argument. At high strain rates, the fuel concentration gradients just before the reaction zone are steeper compared to low strain rates. Thus, the importance of mass diffusion is more apparent and there are notable differences as the fuel molecular weight increases. At low strain rates these differences become less distinct.

Comparing n-C_8H_{18} and iso-C_8H_{18} flames, the former are more resistant to extinction. This finding illustrates the importance of the branched nature of the carbon chain on the flame response. Comparing JFs to the SCHs, JF-flames are less resistant to extinction compared to SCHs. The

Table 3
K_{ext} vs fuel/N_2 mass ratio for all fuels

Fuel	K_{ext} (s^{-1})						
	60	78	97	155	223	290	357
	Fuel/N_2 mass ratio						
n-C_5H_{12}	0.0571	0.0597	0.0613	0.0678	0.0734	0.0783	0.0829
n-C_6H_{14}	0.0572	0.0599	0.0627	0.0698	0.0760	0.0811	0.0860
n-C_7H_{16}	0.0572	0.0601	0.0625	0.0700	0.0770	0.0822	0.0870
n-C_8H_{18}	0.0580	0.0609	0.0635	0.0701	0.0769	0.0837	0.0889
iso-C_8H_{18}	0.0601	0.0625	0.0646	0.0707	0.0769	0.0838	0.0897
n-C_9H_{20}	0.0575	0.0610	0.0635	0.0708	0.0779	0.0847	0.0908
n-$C_{10}H_{22}$	0.0574	0.0609	0.0633	0.0704	0.0784	0.0851	0.0909
n-$C_{12}H_{26}$	0.0625	0.0662	0.0696	0.0737	0.0815	0.0872	0.0945
n-$C_{14}H_{30}$	0.0629	0.0661	0.0705	0.0750	0.0819	0.0877	0.0949
JP-7	0.0674	0.0706	0.0755	0.0817	0.0889	0.0925	0.0955
JP-8	0.0687	0.0712	0.0739	0.0802	0.0881	0.0916	0.0967
JP-10	0.0673	0.0704	0.0745	0.0820	0.0900	0.0943	0.0984
Jet-A-3602	0.0648	0.0686	0.0735	0.0791	0.0860	0.0932	0.0999
Jet-A-3638	0.0644	0.0672	0.0722	0.0788	0.0846	0.0916	0.0984
Jet-A-4658	0.0647	0.0680	0.0731	0.0797	0.0855	0.0921	0.0986
RP-1-3642	0.0654	0.0691	0.0732	0.0791	0.0853	0.0913	0.0976
RP-1-4572	0.0643	0.0682	0.0723	0.0777	0.0840	0.0902	0.0953
DCL-4765	0.0651	0.0680	0.0743	0.0787	0.0842	0.0904	0.0968
FT-4734	0.0628	0.0656	0.0701	0.0758	0.0820	0.0868	0.0921
S6	0.0620	0.0650	0.0684	0.0747	0.0817	0.0858	0.0886
S12	0.0631	0.0660	0.0685	0.0755	0.0833	0.0870	0.0897

The uncertainty in fuel/N_2 mass ratio is 2.5% and in K_{ext} is 3.5%.

flame extinction characteristics of n-$C_{12}H_{26}$ and n-$C_{14}H_{30}$ are close to the JFs suggesting that they may be good candidates in surrogate fuel development. For the fuel/N_2 mass ratio range considered, the flame extinction characteristics of the different JFs are in general similar. While are some systematic differences between the JFs, no fuel was clearly identified as the least resistant to extinction.

Figure 2 depicts K_{ext} for flames resulting from the three different batches of Jet-A. Similar extinction behaviors are observed, with the higher aromatic-content Jet-A-3602 flames being slightly less resistant to extinction than the low aromatic-content Jet-A-3638. The flames of the average Jet-A-4658 exhibit an extinction behavior between the flames of the other two batches of Jet-A at low strain rates, but they are the easiest to extinguish at high strain rates. This suggests that the greater the aromatic content of the fuel is the lower is the resistance to extinction.

Figure 3 depicts K_{ext}s for the two synthetic fuels. FT-4734 flames are far more resistant to extinction than the DCL-4765 flames. Comparing the purely n-+i-paraffin fuel to the purely *cyclo*-paraffin fuel reveals that the saturated alkanes have greater resistance to extinction than the ring structured alkanes.

The results of Fig. 4 reveal that flames of the two JP-8 surrogates (S6 and S12) are more resistant to extinction compared to JP-8 and Jet-A-4658. Though those surrogates were compiled by matching the chemical class distribution of JP-8, they both contain a large number of lighter compounds compared to JP-8. The high diffusivities of those smaller molecules cause the flames of both surrogates to be more resistant to extinction compared to JP-8 and Jet-A-4658. For S6, 50% of the mixture by volume has a carbon number of 10 or smaller, while only 20% has a carbon number of 14; the approximate average carbon number of JP-8 is 12. Comparing S6 and S12 flames, it can be seen that the extinction behavior is very similar. Thus, the inclusion of a large amount of small hydrocarbons in a surrogate will result in a fuel that may not mimic satisfactorily the flame behavior of the real fuel.

The difference in extinction characteristics cannot be only attributed to the chemical composition. Since JP-7 contains nearly no aromatics and JP-8 about 20% aromatics, JP-8 would be expected to be less resistant to extinction, which however is not the case. The average molecular weight of the two fuels is also different. With the

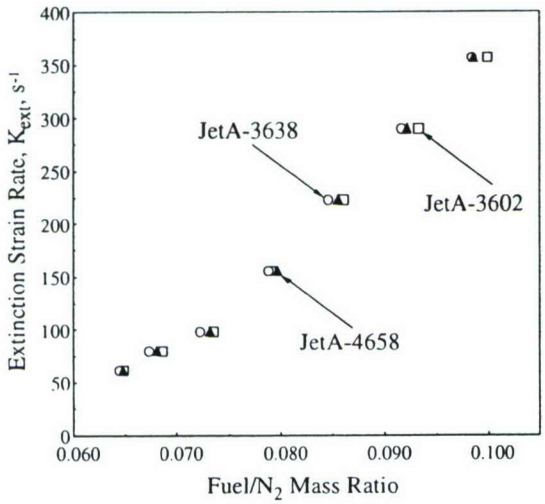

Fig. 2. Variation of K_{ext} with fuel/N_2 mass ratio for the different batches of Jet-A.

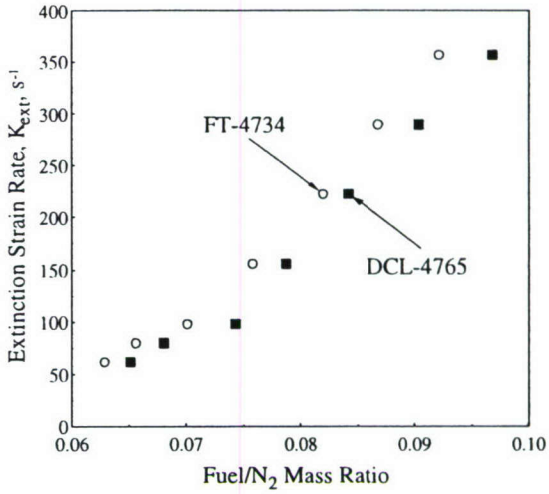

Fig. 3. Variation of K_{ext} with fuel/N_2 mass ratio for the synthetic fuels.

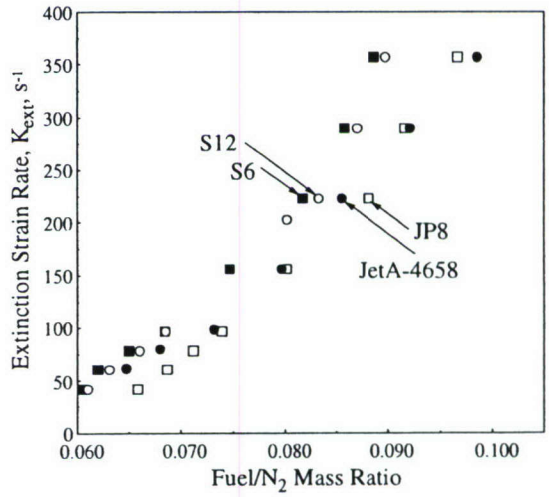

Fig. 4. Variation of K_{ext} with fuel/N_2 mass ratio for average Jet-A, JP-8, and its surrogates.

average molecular weights of JP-7 and JP-8 being 170 and 152, respectively, the increased average diffusivity of JP-8 counters the effect of chemical composition.

The T_{ign} for all fuels are shown in Table 4 as a function of the fuel/N_2 mass ratio. The data were obtained with $D = 14$ mm at a constant *global* strain rate of 194 s^{-1}, determined by dividing the burner exit velocity by $L/2$; strain rate effects will be assessed in future investigations. For the 998 °C flame the equivalence ratio, ϕ, was 0.0782 with a H_2/CO molar ratio of 3.548, for the 1050 °C flame $\phi = 0.0825$ with a H_2/CO molar ratio of 2.343, and for the 1101 °C flame $\phi = 0.0859$ with a H_2/CO molar ratio of 1.609.

When considering uncertainty many fuels have very similar ignition characteristics, but as all fuels were tested against the same ignition source their relative performance can be assessed. Among the SCHs, the lighter the fuel is the easier it is for a flame to ignite. This is, again, reasonable given that the lighter molecules are more diffusive and their transport into the ignition kernel (residing on the oxidizer side) is facilitated. There is only a small difference between the ignition conditions of low carbon number fuels C_5–C_7, but there is a notable difference between the larger fuels such as C_9–C_{14}. Comparing fuels of different chemical class reveals that the *iso*-C_8H_{18} flames are much harder to ignite than the *n*-C_8H_{18} flames, as expected. It is also seen that *iso*-C_8H_{18} flames are only slightly easier to ignite compared to *n*-$C_{12}H_{26}$ flames. All JF flames are harder to ignite than *n*-$C_{12}H_{26}$ except JP-10, which has a significantly smaller molecular mass than *n*-$C_{12}H_{26}$. JP-10 is lighter than *n*-$C_{10}H_{22}$ but is still much harder to ignite, demonstrating that napthenic compounds have reduced ignition propensity compared to n-paraffins. The JFs have similar ignition propensity as *n*-$C_{14}H_{30}$.

There is a large range of T_{ign}s for the different JF's with JP-10 and JP-8 flames exhibiting the greatest and lowest ignition propensity, respectively. The DCL-4765 flames are just slightly harder to ignite than *n*-$C_{12}H_{26}$, and are the second easiest to ignite compared to all JFs. It is of interest to note that while flames of DCL-4765 and JP-10 are the easiest to ignite, they have reduced resistance to extinction as reported earlier and that both fuels consist largely of *cyclo*-alkanes. Flames of low-aromatic fuels, namely RP-1s, JP-7, FT-4734, and Jet-A-3638, exhibit similar ignition characteristics. As expected, flames of the three high-aromatic fuels, JP-8 and the two batches of Jet-A, are the hardest to ignite. Figure 5 depicts the difference in ignition characteristics among the three batches of Jet-A. As expected, the fuels with higher aromatic content exhibit reduced ignition propensity.

The ignition behavior of two synthetic fuels is shown in Fig. 6, and the difference between a *n*-+*i*-paraffin fuel and a *cyclo*-paraffin fuel is apparent. In contrast to extinction characteristics, the *cyclo*-paraffins have greater ignition propensity than the *n*-+*i*-paraffins. This suggests that there is a different order of reactivity from an ignition and extinction point of view. Flames of *cyclo*-paraffin compounds were found to exhibit extinction

Table 4
T_{ign} vs fuel/N_2 mass ratio for all fuels

Fuel	Temperature (°C)		
	998	1050	1101
	Fuel/N_2 mass ratio		
n-C_5H_{12}	0.0498	0.0482	0.0466
n-C_6H_{14}	0.0501	0.0485	0.0468
n-C_7H_{16}	0.0503	0.0486	0.0468
n-C_8H_{18}	0.0511	0.0486	0.0479
iso-C_8H_{18}	0.0556	0.0538	0.0518
n-C_9H_{20}	0.0517	0.0499	0.0481
n-$C_{10}H_{22}$	0.0537	0.0518	0.0500
n-$C_{12}H_{26}$	0.0564	0.0545	0.0520
n-$C_{14}H_{30}$	0.0580	0.0561	0.0535
JP-7	0.0582	0.0555	0.0528
P-8	0.0607	0.0579	0.0551
JP-10	0.0556	0.0540	0.0517
Jet-A-3602	0.0603	0.0575	0.0548
Jet-A-3638	0.0580	0.0546	0.0526
Jet-A-4658	0.0600	0.0572	0.0545
RP-1-3642	0.0575	0.0555	0.0527
RP-1-4572	0.0585	0.0562	0.0538
DCL-4765	0.0567	0.0548	0.0530
FT-4734	0.0583	0.0557	0.0525
S6	0.0574	0.0547	0.0521
S12	0.0578	0.0552	0.0525

The uncertainty in fuel/N_2 mass ratio is 2.5% and in T_{ign} is ±20 °C.

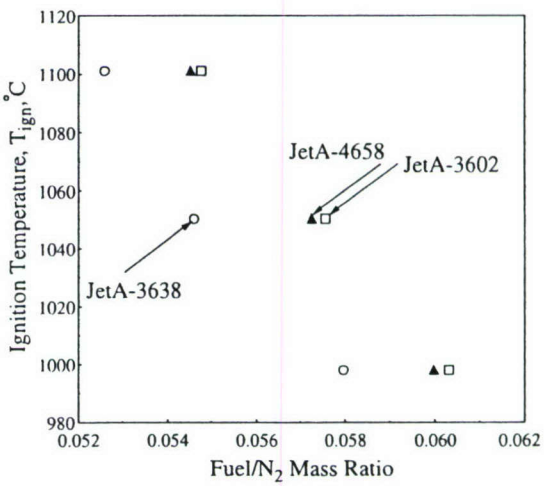

Fig. 5. Variation of T_{ign} with fuel/N_2 mass ratio for the different batches of Jet-A.

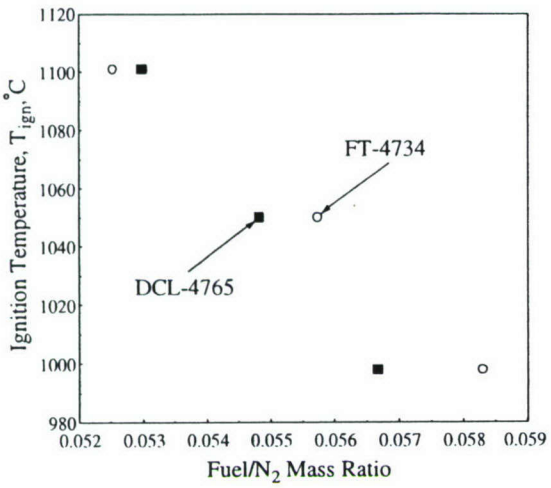

Fig. 6. Variation of T_{ign} with fuel/N_2 mass ratio for the synthetic fuels.

behavior that is between that of *n*-+*i*-paraffins and aromatics, but it appears that flames of *i*-paraffins are less likely to ignite than those of *cyclo*-paraffin compounds. The results for SCHs reveal that flames of *n*-paraffins are far easier to ignite than *iso*-paraffins, and that *n*-paraffins are the easiest of all compounds to ignite. This suggests that the *i*-paraffin content of FT-4734 inhibits ignition compared to the purely *cyclo*-paraffin fuel of DCL-4756.

Figure 7 depicts T_{ign}s of flames of JP-8, Jet-A-4658, and the S6 and S12 surrogates. Flames of S6 and S12 exhibit, again, similar ignition responses (S6 flames ignite only slightly easier than S12), which however, are different compared to the JP-8 flames that are distinctly harder to ignite compared to both S6 and S12. The smaller average molecular weight of the surrogates result in flames with stronger burning characteristics compared to JP-8, as manifested by their greater resistance to extinction and their greater ignition propensity.

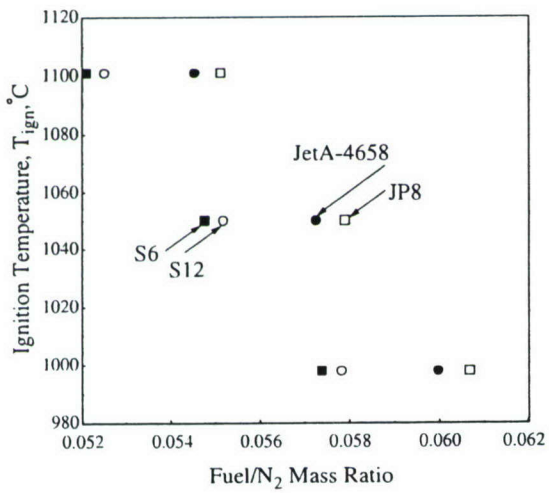

Fig. 7. Variation of T_{ign} with fuel/N_2 mass ratio for average Jet-A, JP-8, and its surrogates.

4. Concluding remarks

Extinction strain rates and ignition temperatures of a wide range of liquid fuels were determined in the counterflow configuration under non-premixed conditions. Single component hydrocarbons, practical jet fuels, and their surrogates were tested and the results were compared to assess their relative performance. The reported experimental flame data are the first ones to be reported for such a wide range of jet fuel and large liquid hydrocarbons, and they are essential towards the development of reliable surrogate fuels and the attendant kinetics models.

It was found that the fuels with lower carbon number result in flames that are more resistant to extinction compared to the ones with higher carbon number. The difference in the extinction characteristics of *n*-C_8H_{18} and *iso*-C_8H_{18} flames demonstrates the importance of branched nature of hydrocarbons on the flame response. Results showed that the jet fuel flames exhibit a rather wide range of resistance to extinction, which in general was found to be close to *n*-$C_{14}H_{30}$. Flames of the two JP-8 surrogates have similar extinction characteristics, with both being more resistant to extinction compared to JP-8.

Flames of fuels with lower carbon number were also determined to ignite easier than the ones with higher carbon number. Comparing *n*-C_8H_{18} and *iso*-C_8H_{18} flames revealed that the branched nature of the fuel has a greater effect on ignition than extinction, with the ignition characteristics of *iso*-C_8H_{18} flames being similar to *n*-$C_{14}H_{30}$ flames. Jet fuel flames exhibit a large range of ignition temperatures with JP-10 being the easiest and JP-8 being the hardest to ignite. Flames of proposed JP-8 surrogates ignite more readily compared to JP-8.

Comparing all data reveals certain hierarchy for both extinction and ignition characteristics. In terms of extinction, flames of *n*-paraffins were found to be the most resistant to extinction followed by *i*-paraffins, then *cyclo*-paraffins, then aromatics. In terms of ignition, flames of *n*-paraffins were found to be the easiest to ignite followed by *cyclo*-paraffins, then *i*-paraffins, then aromatics. The general flame response due to chemical classification could be used in surrogate fuel development.

Surrogate fuels that have been generated by considering the physical properties and chemical classification of the real fuels, do not necessarily match their transport properties. Choosing lower

molecular weight surrogate constituents with relatively known kinetics may result in falsification of the real fuel's transport properties, which could notably affect the flame response.

Acknowledgment

This work was supported by AFOSR (Grant FA9550-04-1-0006) under the technical supervision of Dr. Julian M. Tishkoff.

References

[1] Defense Energy Support Center, Petroleum Quality Information System, annual fuel property surveys, 1999–2004, available at http://www.desc.dla.mil/DCM/DCMPage.asp?pageid=99.
[2] J.T. Edwards, *USAF Supercritical Hydrocarbon Fuels Interests*, AIAA Aerospace Sciences Meeting, Reno, Paper 93-0807, January 1993.
[3] C.P. Wood, V.G. McDonell, R.A. Smith, G.S. Samuelson, *J. Propulsion Power* 5 (4) (1989) 399–405.
[4] W.D. Schulz, *J. Propulsion Power* 9 (1) (1993) 5–9.
[5] R.C. Farmer, P.G. Anderson, G.C. Cheng, B.L. Myruski, R.W. Pike, *Propulsion Chemistry for CFD Applications*, Final Report On Contract NAS8-40574, National Aeronautics and Space Administration, Marshall Space Flight Center, AL, September 1997.
[6] A. Violi, S. Fan, E.G. Eddings, A.F. Sarofim, S. Granata, T. Faravelli, E. Ranzi, *Combust. Sci. Tech.* 174 (11–12) (2002) 399–417.
[7] J.A. Cooke, M. Bellucci, M.D. Smooke, A. Gomez, A. Violi, T. Faravelli, E. Ranzi, *Chem. Phys. Processes Combust.* (2003) 337–340.
[8] F.N. Egolfopoulos, P.D. Dimotakis, *Combust. Sci. Technol.* 162 (2001) 19–36.
[9] Y. Dong, A.T. Holley, M.G. Andac, F.N. Egolfopoulos, S.G. Davis, P. Middha, H. Wang, *Combust. Flame* 142 (2005) 374–387.
[10] A.T. Holley, Y. Dong, Y. Fan, M.G. Andac, F.N. Egolfopoulos, *Combust. Flame* 144 (2006) 448–460.
[11] H. Schobert, B. Beaver, L. Rudnick, R. Santoro, C. Song, G. Wilson, *Am. Chem. Soc./Petrol. Chem. Division Preprints* 49 (4) (2004) 493–497.
[12] J.A. Langille, Y. Dong, M.G. Andac, F.N. Egolfopoulos, T.T. Tsotsis, *Combust. Sci. Technol.* 178 (2006) 635–653.

Comments

Jerry Lee, UTRC-UTC, USA. Jet-8 may consist of HC ranging from C6 to C16. Thus, each component class may exhibit very different dew and condensation temperature (of fixed pressure). Did you test your setup to make sure that, after vaporization to transportation of the vaporized fuel to the burner, you have the same mixture (i.e., the heavier HC did not condense out)? Also, that no significant decomposition occurred before reaching the reactor?

The surrogate model you used was formulated mostly to reproduce the thermo-physical properties specified for Jet-8; not quite its chemical kinetics characteristics. How would you modify these surrogate models to better reproduce your ignition extinction data?

Reply. Special attention was paid on the (fuel) heating path of these heavy fuels. More specifically, the temperatures prevailing along the heating path were restricted within two limits. The lower limit is imposed by the requirement that the fuel is maintained in the gaseous phase while the upper limit by the requirement that the fuel is not thermally decomposed. Extensive discussion regarding this issue is provided in the paper.

Developing a surrogate by matching all physical and burning characteristics of a real fuel is not possible. Thus, decisions have to be made regarding the targets that typically depend on the application. In terms of flame properties, predicting laminar flame speeds is required in order to assure that the surrogate closely reproduces the heat release rate of the real fuel. Additionally, close prediction of ignition and extinction limits is also essential in view of high-speed applications. Modifications of the surrogates to better reproduce any fundamental property needs to be done in a comprehensive manner. More specifically, such modifications need to be made by varying the concentrations of certain components (for example, aromatics to predict ignition) in a way that the surrogate fuel also predicts data obtained in homogeneous systems, such as shock tubes and flow reactors. Finally, it is mentioned in the paper that mass diffusivities need to also be considered in surrogate fuel development using flame data.

•

Ronald S. Sheinson, Naval Research Laboratory, USA. There are a variety of fire extinction performance test standards utilized by different entities and countries that use different commercial "standard" fuels that are in fact continually changing mixtures, such as hydrocarbon source dependent or seasonally modified refinery cuts. Relating performance and rankings from different test standards can be a difficult task. Similarly, ignition properties for safety or engine behavior can be affected by "standard" fuel composition differences. This work helps address understanding real world fuel properties.

Could you expand on the significance and influence of differing physical properties such as transport properties of the various components on liquid hydrocarbon mixture behavior?

Reply. The effects of transport properties on the burning of liquid hydrocarbon mixtures depend on the application and prevailing conditions. For example,

during the development of surrogate fuels by utilizing experimental data obtained in laminar flames, transport properties could have a notable effect on non-premixed flames and somewhat less on premixed flames, as combustion theory dictates. Parallel studies performed by our research group as well as others, have shown that for both non-premixed and premixed flames the sensitivities of fundamental flame properties on transport coefficients could be of the same order or even larger compared to those on the kinetics. One also has to consider that existing theories for computing transport coefficients may not be reliable for those long, non-spherical, large molecules. On the other hand, the effect of molecular transport on burning in engines under the presence of turbulence may be reduced as turbulent mixing plays a dominant role instead. However, modeling an engine using the kinetics of a surrogate fuel whose kinetics have been compromised by unquantified effects of diffusion in laminar flames could reduce the value of the simulations in engines.

Flame and Ignition Kinetics of Dry Synthesis Gas-Like Mixtures

Yufei Dong, Xiaoqing You, David A. Sheen, Hai Wang, Ryan Kinslow, Michael Call, Adam T. Holley, Mustafa G. Andac, Fokion N. Egolfopoulos
Department of Aerospace and Mechanical Engineering
University of Southern California
Los Angeles, CA 90089-1453, USA

Danielle M. Kalitan, Eric L. Petersen
Department of Mechanical, Materials, and Aerospace Engineering
University of Central Florida
Orlando, FL 23816-2450, USA

Scott G. Davis
Exponent, Natick, MA 01760, USA

Corresponding Author: Professor Hai Wang
Department of Aerospace and Mechanical Engineering
University of Southern California
Los Angeles, CA 90089, USA
Phone: 213-740-0499
FAX: 213-740-8071
E-Mail: haiw@usc.edu

Colloquium Topic Area: Chemical Kinetics

Total length: 5710 words

Main Text: 2981 words (MSWord 2000 word count)
Equations: (14 equation lines + 28 blank lines) x 7.6 words = 319 words
References: (39 references + 2) x (2.3 lines/reference) x (7.6 words/line) = 769 words
Table 1: (6 lines + 2 lines) x 7.6 words/line x 1 column = 61 words
Figure 1: [53mm+10mm] x 2.2 words/mm x 1 column = 139 words
Figure 2: [75mm+10mm] x 2.2 words/mm x 1 column = 187 words
Figure 3: [62mm+10mm] x 2.2 words/mm x 1 column = 158 words
Figure 4: [62mm+10mm] x 2.2 words/mm x 1 column = 158 words
Figure 5: [100mm+10mm] x 2.2 words/mm x 1 column = 242 words
Figure 6: [68mm+10mm] x 2.2 words/mm x 1 column = 172 words
Figure 7: [62mm+10mm] x 2.2 words/mm x 1 column = 158 words
Figure 8: [62mm+10mm] x 2.2 words/mm x 1 column = 158 words
Figures (total): 1373 words
Figure captions: 207 words (MSWord 2000 word count)

Submitted for consideration at the 31st International Symposium on Combustion, University at Heidelberg, Heidelberg, Germany, August 6-11, 2006.

Flame and Ignition Kinetics of Dry Synthesis Gas-Like Mixtures

Yufei Dong, Xiaoqing You, David A. Sheen, Hai Wang, Ryan Kinslow, Michael Call, Adam T. Holley, Mustafa G. Andac, Fokion N. Egolfopoulos
Department of Aerospace and Mechanical Engineering
University of Southern California
Los Angeles, CA 90089-1453, USA

Danielle M. Kalitan, Eric L. Petersen
Department of Mechanical, Materials, and Aerospace Engineering
University of Central Florida
Orlando, FL 23816-2450, USA

Scott G. Davis
Exponent, Natick, MA 01760, USA

Abstract

Reaction kinetics of H_2 and CO mixtures are examined experimentally and computationally under mixture and reaction conditions of immediate interest to synthesis gas combustion. Shock-tube ignition delay times are obtained for five CO-H_2-air mixtures (equivalence ratio $\phi = 0.5$) over the pressure range of 1 to 20 atm and temperatures from 950 to 1330 K. The influence of synthesis gas composition variations on flame ignition and propagation is also examined. Two types of experiments are carried out for H_2/CO/CO_2 mixtures with air. Laminar flame speeds are determined in the twin-flame counterflow configuration using Digital Particle Image Velocimetry. Ignition temperatures are determined by counterflowing a vitiated air jet against a premixed fuel/air jet. Computationally, detailed modeling of the experiments is performed, using a recently developed H_2/CO reaction model. Numerical simulations show generally good agreement with experimental data.

Keywords: CO/H_2 Oxidation Kinetics, Shock Tube Ignition, Flame Ignition, Flame Propagation

1. Introduction

The use of synthesis gas (syngas) in Integrated Gasification Combined Cycle (IGCC) applications offers a highly efficient, low-emission alternative to the direct combustion of coal in power generation. Syngas is usually produced from steam reforming of coal or other condense-phase hydrocarbon fuels. They contain mainly carbon monoxide and hydrogen. Depending on the coal used and the post processing technique, syngases can have wide ranges of composition variations. While some of them contain CO and H_2 only, large amounts of CO_2 and H_2O may be present in others. These composition variations pose some problems in combustor design and emission controls. Because the flame properties of a particular syngas can be strongly sensitive to the variation in the CO_2 dilution [1], the batch-to-batch composition variations can lead to a range of problems, including local flame extinction and incomplete combustion, which usually cannot be predicted *a priori*. Reliable kinetic models, that can accurately predict the ignition and flame properties of an arbitrary syngas, are can therefore be valuable in combustor design and operation.

Early shock-tube investigations of CO-H_2 oxidation sought to determine the oxidation rates of CO-O_2 with minimal H_2 addition [2-5]. Subsequent studies have extended the mixture and shock conditions to even wider ranges [6-9]. The flame properties of mixtures of CO and H_2 with air have been extensively studied, experimentally and numerically. Previous flame studies have concentrated on laminar flame speeds and extinction strain rates (e.g., [1,10,11]). On more than one occasions, the auto-ignition of CO-H_2 mixtures has also been studied in Rapid Compression Machines at high pressures [12,13]. Detailed kinetic models have been proposed and validated generally based on flow reactor and laminar flame speed experiments of CO-H_2-O_2 mixtures [14-16]. These mixtures are designed to provide better insight into the oxidation kinetics of CO-H_2 mixtures. They usually do not cover the range of composition variations found in syngases. In particular, the roles of CO_2 and H_2O on the combustion properties of H_2-CO mixtures remain poorly understood.

The goal of the current investigation was to initiate the development of a comprehensive shock-tube and flame experiment database for syngas combustion, and to systematically test a previously optimized H_2-CO-O_2 reaction mechanism [15] on a wide range of shock tube-and flame data. Undiluted fuel-air mixtures containing CO-H_2 fuel blends with hydrogen content from 5 to 80% were studied behind reflected shock waves at conditions of immediate interest to syngas applications: elevated pressures (1 – 20 atm) and fuel-lean

stoichiometry [17,18]. The flame properties considered include flame ignition and propagation. It should be noted that while laminar flame speed is a useful property, as it is free of parameters or mechanisms external to the mixture, ignition, as well as extinction, limits are more sensitive to reaction kinetics compared to laminar flame speed [19,20]. Experimental and modeling results of flame ignition limits and laminar flame speeds are presented for H_2-CO-CO_2 mixtures, which are typical to dry syngases.

2. Experimental approaches

2.1 Shock tube experiments

They were conducted using the facility described elsewhere [21]. Briefly, the shock tube, made of stainless steel, has a driver section 3.5 meters in length and 7.62 cm in diameter and a driven section 10.7 meters in length with a 16.2-cm inner diameter. All experiments were performed behind the reflected shock wave. The reaction progress was followed by emission from OH* chemiluminescence from the $A^2\Sigma^+ \rightarrow X^2\Pi$ transition. A CaF_2 optical port on the endwall of the shock tube allowed for optical access. The ultraviolet emission was collected from a CaF_2 optical port on the endwall of the shock tube with a Hamamatsu 1P21 photomultiplier tube (PMT) fitted with a narrow-band filter centered at 310±5 nm. A PCB 134A pressure transducer, located at the endwall, and five fast-response (<1 μs) PCB 113A pressure transducers and four Fluke model PM6666 time-interval counters monitored the incident-shock speed at various locations along the shock tube.

The principal objective of the current shock experiments was to examine the effect of pressure behind reflected shock waves p_5 on the ignition delay times of five CO-H_2-air mixtures (equivalence ratio ϕ = 0.5). The p_5 values, investigated herein, ranged from 1 to 20 atm for three of these mixtures. The ignition delay time was determined as the onset of OH* chemiluminescence. Fig. 1 shows typical pressure and emission traces as measured from the endwall of the shock tube. Further details and the complete set of shock-tube experiments are beyond the scope of this paper and are presented in Kalitan et al. [18].

2.1 Flame experiments

They were conducted in the following manner. First, for fuel-lean flames the total reaction of a dry syngas with oxygen is defined as follows:

$$\phi\left[\alpha H_2 + (1-\alpha)CO + \gamma CO_2\right] + \frac{1}{2}O_2 \leftrightarrow \phi\left[\alpha H_2O + (1-\alpha+\gamma)CO_2\right] + \frac{1-\phi}{2}O_2,$$

where α characterizes the H_2-to-CO ratio, and γ is the level of CO_2 dilution. The coefficients for H_2 and CO are constrained such that they sum to unity. A particular dry syngas can be entirely characterized by three independent parameters ϕ, α, and γ. Since the parameter space of ϕ, α, and γ is rather wide, special considerations are made so that the experimental mixtures are designed to offer a maximum amount of experimental information for a given set of experiments.

Dry syngases typically have $\alpha/(1-\alpha)$ = 0.4 to 1.0 with a nominal value equal to 0.7. For CO_2-containing mixtures, $\gamma/(1-\alpha)$ typically ranges from 0 to 0.67 with a nominal value of 0.25. We employ a 2^2 factorial design plus the nominal point to give a total of 5 different mixtures [22]. This approach effectively covers the entire composition space of dry syngases. The current paper reports the results for 4 of such mixtures as shown in Table 1.

Flame ignition temperatures and laminar flame speeds were determined in the counterflow configuration at ambient pressure. Flame ignition was achieved by counterflowing a fuel-air mixture against a hot jet of vitiated air, resulting from an ultra-lean H_2-air mixture catalytically oxidized on a platinum screen. This experimental approach and its validity have been discussed in a previous publication [23]. The platinum screen was supported on a ceramic disk 1 mm above the bottom burner. The ceramic disk is made of 99.9% aluminum oxide, chosen here because it is non-porous, can withstand fast temperature loading (thermal shock), and has a low thermal conductivity (to minimize heat loss in the radial direction). The separation distance between the platinum screen and the top burner is 1 cm, equal to the diameter of burner nozzles. A pilot flame provided the initial energy required to activate the H_2-air mixture on the platinum screen. By varying ϕ of the H_2-air mixture the temperature of the platinum screen can range from 400-900 °C, which spans the entire range required for the current experiment. The platinum screen locks the flame at the exit of the burner and the oxidation on its surface results in vitiated air composed largely of hot O_2, N_2, minor

amounts of H_2O, and negligible amounts of radicals to have an effect on the ignition kernel [24]. The temperatures were determined using a K-type thermocouple placed at the center of the flow. The ignition temperature, T_{ign}, was defined as the highest temperature in the flowfield at the state of ignition, and it is essentially the temperature measured just downstream of the platinum screen. All temperatures were corrected for radiation in a manner described in [24].

There are two sources of uncertainty associated with the reported T_{ign}'s. The first is the ± 20 K that is inherent and constant for all fine-wire thermocouples. The second is that caused by the location of the thermocouple with respect to the platinum screen. Efforts were made to bring the thermocouple junction as close as possible to the screen in order to record the maximum temperature of the catalyzed oxidation of H_2. At the same time care was taken to avoid contact between the junction and the screen that could alter the nature of both. As a result, measurements taken at different times are susceptible to some variability of the thermocouple location and the attendant measured temperature, which is estimated to be of the order of 10 to 15 K.

The laminar flame speeds S_u^o were determined using the stagnation flame method [10,25]. Using the Digital Particle Image Velocimetry (DPIV) [26], a reference flame speed, S_{ref}, was determined at a given strain rate, K, defined as the maximum absolute value of the axial velocity gradient along the centerline. Subsequently, the variation of S_{ref} with K was graphically recorded, and S_u^o determined through linear extrapolation to zero stretch.

3. Numerical Approach

The detailed kinetic model used for the simulations was taken from Davis *et al* [15]. The model contains 12 species and 30 elementary reactions, and was optimized against a large number of fundamental H_2 and H_2-CO combustion data. In a recent high-pressure shock tube study [9], it was found that capturing the peculiar temperature dependence for the reaction

$$OH + HO_2 \leftrightarrow H_2O + OH, \qquad \text{(R15)}$$

as described by Hippler et al. [27], was critical to model the data over the pressure range of 25 to 450 atm. This temperature dependence causes k_{15} to drop suddenly as the temperature is increased to above 1100 K. For $T > 1300$ K, k_{15} rises sharply again. Consequently the bi-modified Arrenhius expression of k_{15} in [15] was revised to

$$k_{15}\ (\mathrm{cm^3mol^{-1}s^{-1}}) = 1.41\times10^{18}\ T^{-1.76}\ e^{-30/T} + 1.12\times10^{85}\ T^{-22.3}\ e^{-13538/T} + 5.37\times10^{70}\ T^{-16.72}\ e^{-16558/T}$$
$$+ 1.0\times10^{136}\ T^{-40}\ e^{-17514/T} + 2.51\times10^{12}\ T^{2}\ e^{-20131/T},$$

to account for the peculiar temperature dependence, using kinetic data from a large number of studies [27-35] and over the temperature range of 298 to 1600 K. This revision led to no change in model applicability with respect to all optimization and validation targets considered in [15].

Laminar flame speeds were calculated using the PREMIX one-dimensional flame code [36]. The opposed-jet configuration was simulated along the stagnation streamline by solving the quasi-one-dimensional conservation equations of mass, momentum, energy, and species concentration (e.g., [37]). In previous studies [15,19], the transport data of H_2 and H were revised on the basis of more recent quantum chemistry calculations and direct numerical integration of the collision integrals. The Sandia Transport subroutines [38] were revised accordingly to account for the newly updated diffusion coefficients. These revised database and subroutines are used here along with the multi-component transport formulation and thermal diffusion of all species considered.

The ignition state was numerically determined by starting with a non-reacting solution and by successively solving the governing equations with increasing values of the vitiated air temperature. The composition of the vitiated air is determined by an equilibrium calculation. In order to capture the turning-point behavior at ignition, the code was modified to impose a one-point continuation with respect to the H-

atom profile (e.g., [39,40]). A predetermined increment in the H-atom concentration was imposed at the point of its maximum gradient on the side closest to the hot jet. This new boundary condition replaces the burner-exit temperature of the hot jet. Progressive steady-state solutions were obtained until a turning point is observed on the response curve of maximum H mass fraction, Y_H, versus the temperature of the hot jet. T_{ign} is defined to be the temperature at this turning point.

4. Results and Discussion

The following section contains two types of analysis. The first compares the ignition delay time data with those predicted by the detailed kinetic model of H_2-CO oxidation. The second describes the comparisons for laminar flame speeds and flame ignition data.

As described earlier shock-tube experimental data were collected for a range of reflected-shock temperatures (900 K < T_5 < 1330 K) with pressures near one atmosphere and at elevated pressures of, approximately, 2 and 15 atm. Figures 2 through 4 depict the comparisons of experimental and computed ignition delay times. In most cases, the kinetic model is in excellent agreement with the experimental data. The only exceptions are that the model tends to predict much longer ignition delay times at 2 atm and lower temperatures.

Experimental S_u°'s of the current study are compared to literature data. Figure 5(a) depicts that the S_u°'s of the current study are in close agreement with the data reported by McLean et al. [11] for 50%H_2-50%CO-air mixtures (mixture B with $\alpha = 0.5$ and $\gamma = 0$). At $\phi = 0.62$, for example, the current study yielded S_u° = 53 cm/s, whereas McLean et al. reported a value of 50 cm/s. Figure 5 also shows the variation of S_u° with the equivalence ratio for 50%H_2-50%CO-air mixtures with different levels of CO_2-dilution. As expected, the flame speed is influenced by CO_2 dilution and the thermal effect resulting from its large specific heat. As the level of CO_2 dilution (γ = 0.5) increases, S_u° of the same H_2-CO mixture decreases by 50 to 70%, depending on ϕ. In general, the reaction model is in good agreement with the experimental data.

The variation of S_u° with ϕ for mixtures E and F is shown in Fig. 6. Again the effect of CO_2 dilution is evident. Compared to the results shown in Fig. 5, the smaller difference in S_u° is the result of a smaller

difference in the level of CO_2 dilution. The agreement between the experiment and model is similar to that of Fig. 5.

Results of the sensitivity analysis show that the flame speeds are the most sensitive to the rate coefficients of

$$CO + OH \leftrightarrow CO_2 + H$$

$$H + O_2 (+M) \leftrightarrow HO_2 (+M)$$

and

$$HO_2 + H \leftrightarrow OH + OH.$$

A recent study [41] showed that above 600 K the bi-exponential rate expression of Davis et al. [15] is fully supported by available experimental kinetic data and the results of a RRKM/master equation analysis carried out in that study. Therefore the discrepancy between model and experiments seen in Figs. 5 and 6 cannot be resolved by uncertainties in the rate coefficient of $CO + OH \leftrightarrow CO_2 + H$.

The dilution and thermal effects of CO_2 do not lead to appreciable changes in T_{ign}, as seen in Fig. 7, comparing mixtures A and B and in Fig. 8 for mixtures E and F. The reported uncertainty bars represent the standard one of ± 20 K. The uncertainty associated with the thermocouple location is reflected by the slight data scatter for each set of conditions.

Despite the fact that the dilution leads to a lower concentration of H_2 and CO in the fuel jet, and the thermal effect causes slower conductive heating of the fuel mixture, the T_{ign}'s with and without CO_2 dilution remain within experimental uncertainty. However, on the average the presence of CO_2 results in somewhat lower T_{ign}'s, as expected. The numerical simulations also predict the minor effect of CO_2 dilution on T_{ign}. At a lower level of CO_2 dilution (*cf*, mixtures E and F in Fig. 8), the measured T_{ign}'s do not differ notably, as expected. The computed T_{ign}'s also differ minimally. In addition, T_{ign} neither exhibits a strong dependence on the equivalence ratio, nor does it depend on the CO-to-H_2 ratio in the unburned mixture, as all data cluster around 1050 K.

The lack of sensitivity of T_{ign} with respect to the mixture composition indicates that, for the conditions reported in Figs. 7 and 8, the ignition process is rather immune to both reactant diffusion towards and the kinetics within the ignition kernel. This is anticipated, as H_2 is characterized by both fast kinetics and high

diffusivity. The ignition kernel resides right next to the hot boundary, as dictated by the Arrhenius kinetics. Thus, and "fuel" has to cross the stagnation plane and reach the kernel through diffusion against the convection of the vitiated air. Under such conditions, the H_2 diffusive transport towards the kernel overwhelms that of CO for all conditions considered. Thus, for all cases ignition will take place at nearly the same conditions, as the transport of H_2 is not a rate-limiting process. As a result, similar T_{ign}'s are realized. Analogous results have been reported in non-premixed H_2-air ignition studies [23,42], in which the effect of H_2 diffusion has been shown to be important only under extreme conditions of ultra-low H_2 concentration in the inert-diluted fuel stream.

Sensitivity analysis shows that T_{ign} is sensitive only to reactions of H_2, i.e.,

$$H + O_2 \leftrightarrow O + OH$$

$$HO_2 + H \leftrightarrow OH + OH$$

$$OH + H_2 \leftrightarrow H + H_2O$$

$$O + H_2 \leftrightarrow H + OH$$

$$HO_2 + OH \leftrightarrow H_2O + H.$$

The lack of sensitivity to the chain terminating reaction $H + O_2 (+M) \leftrightarrow HO_2 (+M)$ suggests that the role of CO_2 cannot be kinetic, since kinetically the presence of CO_2 can only increase the rate of chain terminating reactions due to its relatively large Chaperon efficiency.

5. Concluding Remarks

We carried out an experimental and computational study of ignition delay times of H_2-CO oxidation in air behind reflected shock waves and H_2-CO-CO_2-air flames. Shock-tube ignition delay times were obtained for five CO-H_2-air mixtures (equivalence ratio $\phi = 0.5$) over the pressure range of 1 to 20 atm and temperatures from 950 to 1330 K. Laminar flame speeds and flame ignition temperatures were measured for dry syngas like mixtures over an equivalence ratio range of 0.5 to 1.0. The variations of mixture composition are designed with a statistical factorial method and represent the composition variations of actual syngases. These experimental data were compared with the results of detailed numerical simulations using a recently optimized kinetic model of H_2 and H_2-CO combustion.

The kinetic model was found to result in reasonably good agreement with the experimental data. The model captures the pressure dependence of the ignition delay times. It also reproduces the anticipated sensitivity of laminar flame speed with respect to CO_2 dilution. The flame ignition temperature was found to be relatively insensitive to CO_2 dilution, H_2-to-CO ratio, and equivalence ratio.

Acknowledgements

This work was supported by AFOSR (Grant FA9550-04-1-0006 and FA9550-05-1-0010) under the technical supervision of Dr. Julian M. Tishkoff. Additional support (UCF) came from DOE via a University Turbine Systems Research grant from the South Carolina Institute for Energy Studies (Contract Number 04-01-SR114).

References

[1] J. Natarajan, S. Nandula, T. Lieuwen, J. Seitzman, Proceedings, ASME Turbo Expo 2005.

[2] K. G. P. Sulzmann, B. F. Myers, E. R. Bartle, J. Chem. Phys. 42 (1965) 3969-3979.

[3] B. F. Myers, K. G. P. Sulzmann, E. R. Bartle, J. Chem. Phys. 43 (1965) 1220-1228.

[4] T. A. Brabbs, F. E. Belles, R. S. Brokaw, Proc. Combust. Inst. 13 (1970) 129-136.

[5] W. C. Gardiner, M. McFarland, K. Morinaga, T. Takeyama, B. F. Walker, J. Phys. Chem. 75 (1971) 1504-1509.

[6] W.C. Gardiner, W. G. Mallard, M. McFarland, K. Morinaga, J. H. Owen, W. T. Rawlins, T. Takeyama, B. F. Walker, Proc. Combust. Inst. 14 (1972) 61-75.

[7] A. M. Dean, D. C. Steiner, E. E. Wang, Combust. Flame 32 (1978) 73-83.

[8] M. Slack, A Grillo, Combust. Flame 59 (1985) 189-196.

[9] R. Sivaramakrishnan, A. Comandini, R. S. Tranter, K. Brezinsky, S. G. Davis, H. Wang, "Combustion of CO/H_2 mixtures at elevated pressures," Proc. Combust. Inst., submitted, 2005.

[10] C.M. Vagelopoulos, F.N. Egolfopoulos, Proc. Combust. Inst. 25 (1994) 1317-1323.

[11] I. C. McLean, D. B. Smith, S. C. Taylor, Proc. Combust. Inst. 25 (1994) 749-757.

[12] D. Lee, S. Hochgreb, Int. J. Chem. Kinet. 30 (1997) 385-406

[13] G. Mittal, C.-J. Sung, R. A. Yetter "Autoignition of H_2/CO at elevated pressures in rapid compression machine," Int. J. Chem. Kinet., submitted, 2005.

[14] M.A. Mueller, R.A. Yetter, F.L. Dryer, Int. J. Chem. Kinet. 31 (1999) 705-724.

[15] S. G. Davis, A. V. Joshi, H. Wang, F. Egolfopoulos, Proc. Combust. Inst. 30 (2005) 1283-1292.

[16] Saxena, P., Williams F. A. "Testing a small detailed chemical-kinetic mechanism for the combustion of hydrogen and carbon monoxide." Combust. Flame, in press, 2005.

[17] D.M. Kalitan, M. W. Crofton, E.L. Petersen, J. Prop. Power, in preparation (2006).

[18] D.M. Kalitan, M.W. Crofton, E.L. Petersen, J.D. Mertens, ASME Paper GT2006-90488 (2006).

[19] Y. Dong, A.T. Holley, M.G. Andac, F.N. Egolfopoulos, S.G. Davis, P. Middha, H. Wang, Combust. Flame, 142 (2005) 374-387

[20] A.T. Holley, Y. Dong, Y. Fan, M.G. Andac, F.N. Egolfopoulos, "Extinction of Premixed Flames of Practical Liquid Fuels: Experiments and Simulations," in press, Combust. Flame (2005).

[21] E. L. Petersen, M. J. A. Rickard, M. W. Crofton, E. D. Abbey, M. J. Traum, D. M. Kalitan, Measurement Sci. Technol. 16 (2005) 1716-1729.

[22] D.A. Sheen, R. Kinslow, M. Call, A.T. Holley, X. You, M.G. Andac, H. Wang, F.N. Egolfopoulos, "A detailed atudy of $CO/H_2/O_2$ kinetics in dry aynthesis-gas/air flames," 2005 Fall Meeting of the Western States Section of the Combustion Institute, Stanford, CA, October 16-18, 2005.

[23] J.A. Langille, Y. Dong, M.G. Andac, F.N. Egolfopoulos, T.T. Tsotsis, "Non-Premixed Ignition by Vitiated Air in Counterflow Configurations," in press, Combust. Sci. Tech. (2005).

[24] W. Qin, Ph.D. Dissertation Thesis, University of Southern California, Department of Chemical Engineering

[25] C.K. Law, Proc. Combust. Inst. 22: 1381-1402 (1988).

[26] Y. Dong, C.M. Vagelopoulos, G. Spedding, F.N. Egolfopoulos, Proc. Combust. Inst. 29 (2002) 1419-1426.

[27] H. Hippler, H. Neunaber, J. Troe. *J. Chem. Phys.* 103 (1995) 3510-3516.

[28] H. Kijewski, J. Troe, *Int. J. Chem. Kinet.* 3 (1971) 223-235.

[29] J. Peeters, G. Mahnen, Proc. Combust Inst. 14 (1973) 133-141.

[30] R.-R. Lii, R. A. Gorse, M. C. Sauer, S. Gordon, *J. Phys. Chem.* 84 (1980) 819-821.

[31] J. P. Burrows, R. A. Cox, R. G. Derwent, *J. Photochem.* 16 (1981) 147-168.

[32] W. B. DeMore, *J. Phys. Chem.* 86 (1982) 121-126.

[33] L. F. Keyser, *J. Phys. Chem.* 92 (1988) 1193-1200.

[34] H. Hippler, J. Troe, *Chem Phys. Lett.* 192 (1992) 333-337.

[35] Ch. Kappel, K. Luther, J. Troe, Phys. Chem. Chem. Phys. 4 (2002) 4392-4398.

[36] R.J. Kee, J.F. Grcar, M.D. Smooke, J.A. Miller, Sandia Report SAND85-8240, 1985.

[37] F.N. Egolfopoulos, C.S. Campbell, J. Fluid Mech. 318 (1996) 1-29

[38] R. J. Kee, G. Dixon-Lewis, J. Warnatz, M. W. Coltrin, J. A. Miller, Sandia Report SAND86-8246, 1986.

[39] M. Nikiosha, C.K. Law, T. Takeno, Combust. Flame 104 (1996) 328-342

[40] F.N. Egolfopoulos, P. Dimotakis, Proc. Combust. Inst. 27 (1998) 641-648.

[41] A. V. Joshi, H. Wang, "Master Equation Modeling of Wide-Range Temperature and Pressure Dependence of CO + OH → Products," Int. J. Chem. Kinet., in press, (2005).

[42] C.G. Fotache, T.G. Kreutz, D.L. Zhu, C.K. Law, Combust. Sci. Tech. 109 (1995) 373-393.

Table 1. Mixture compositions of flame experiments

Mixture	$\alpha/(1-\alpha)$	$\gamma/(1-\alpha)$	α	γ
A	1	0.67	0.5	0.33
B	1	0	0.5	0
E	0.7	0.25	0.41	0.146
F	0.7	0.25	0.41	0

Figure Captions

Figure 1. Pressure and OH^* emission traces measured at the end wall of the shock tube for a 7%H_2-10.4%CO-air mixture (T_5 = 1148 K, p_5 = 1.05 atm)).

Figure 2. Experimental (symbols) and computed (lines) ignition delay times of H_2-CO-air mixtures behind reflected shock waves.

Figure 3. Experimental (symbols) and computed (lines) ignition delay times of H_2-CO-air mixtures behind reflected shock waves.

Figure 4. Experimental (symbols) and computed (lines) ignition delay times of H_2-CO-air mixtures behind reflected shock waves.

Figure 5. Variation of laminar flame speed with equivalence ratio for 50% H_2-50%CO fuel mixtures (α = 0.5, a: γ = 0; b: γ = 0.1 and 0.2, c: γ = 0.33). Symbols are experimental data; lines are results of numerical simulations.

Figure 6. Variation of laminar flame speed with equivalence ratio for H_2-CO fuel mixtures (α = 0.41) with γ = 0 and 0.146. Experiments (symbols) are from this work.

Figure 7. Variations of flame ignition temperature in the counterflow configuration with equivalence ratio. Symbols: experimental data; lines: numerical simulations (solid line: γ = 0; dashed line: γ = 0.33).

Figure 8. Variations of ignition temperature in the counterflow configuration with equivalence ratio. Symbols: experimental data; lines: numerical simulations (solid line: γ = 0; dashed line: γ = 0.146. The two lines are indistinguishable from each other).

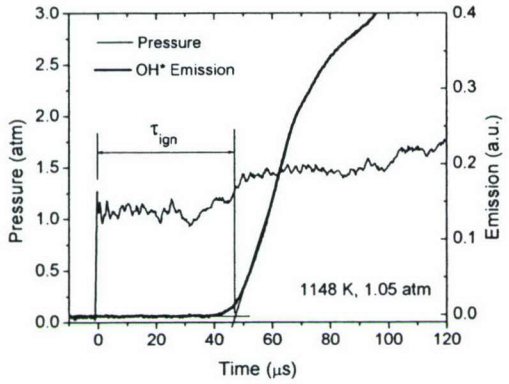

Figure 1. Pressure and OH* emission traces measured at the end wall of the shock tube for a 7%H_2-10.4%CO-air mixture (T_5 = 1148 K, p_5 = 1.05 atm).

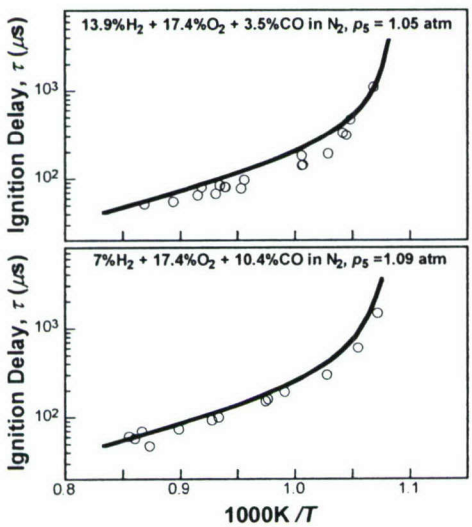

Figure 2. Experimental (symbols) and computed (lines) ignition delay times of H_2-CO-air mixtures behind reflected shock waves.

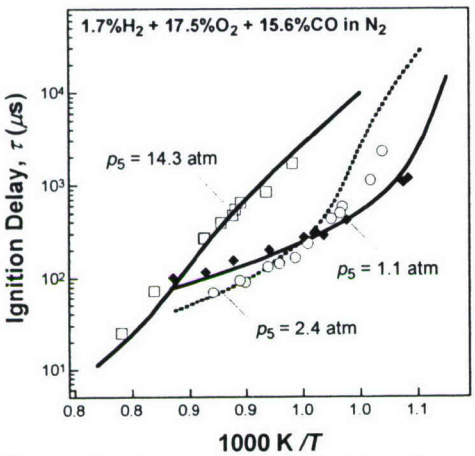

Figure 3. Experimental (symbols) and computed (lines) ignition delay times of H_2-CO-air mixtures behind reflected shock waves.

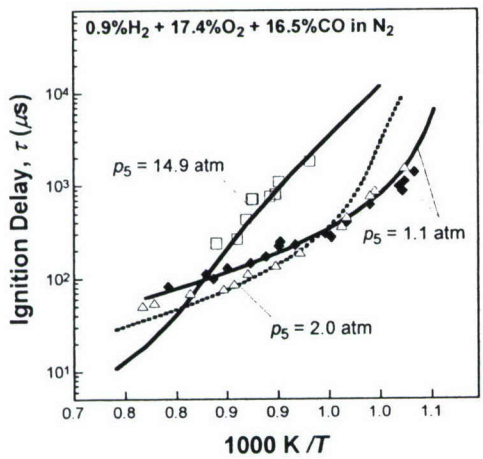

Figure 4. Experimental (symbols) and computed (lines) ignition delay times of H_2-CO-air mixtures behind reflected shock waves.

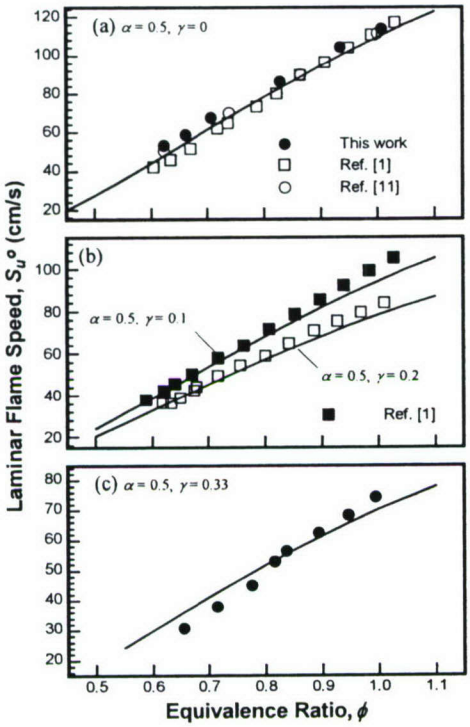

Figure 5. Variation of laminar flame speed with equivalence ratio for 50% H_2-50%CO fuel mixtures (α = 0.5, a: γ = 0; b: γ = 0.1 and 0.2, c: γ = 0.33). Symbols are experimental data; lines are results of numerical simulations.

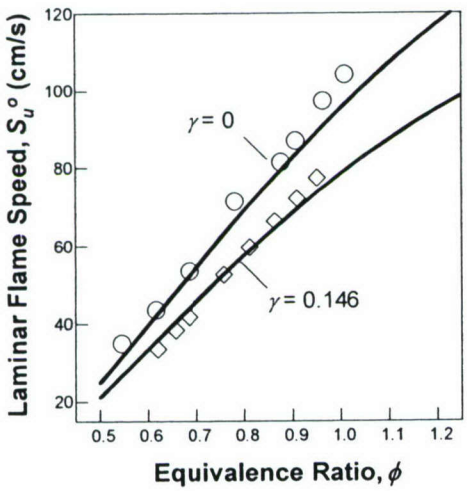

Figure 6. Variation of laminar flame speed with equivalence ratio for H_2-CO fuel mixtures (α = 0.41) with γ = 0 and 0.146. Experiments (symbols) are from this work.

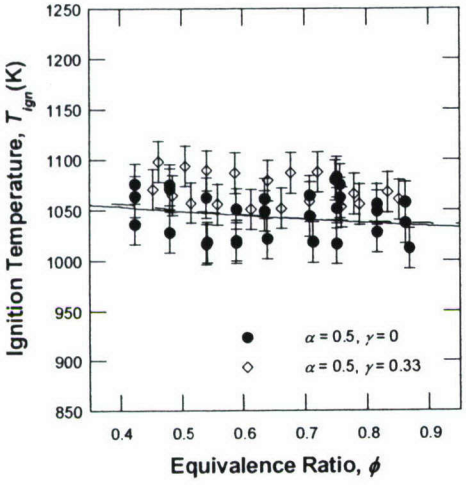

Figure 7. Variations of flame ignition temperature in the counterflow configuration with equivalence ratio. Symbols: experimental data; lines: numerical simulations (solid line: $\gamma = 0$; dashed line: $\gamma = 0.33$).

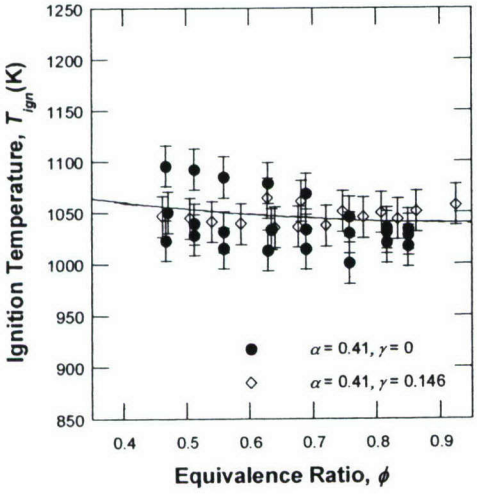

Figure 8. Variations of ignition temperature in the counterflow configuration with equivalence ratio. Symbols: experimental data; lines: numerical simulations (solid line: $\gamma = 0$; dashed line: $\gamma = 0.146$. The two lines are indistinguishable from each other).

Available online at www.sciencedirect.com
SCIENCE DIRECT
Combustion and Flame 144 (2006) 448–460
Combustion and Flame
www.elsevier.com/locate/combustflame

Extinction of premixed flames of practical liquid fuels: Experiments and simulations

A.T. Holley, Y. Dong, M.G. Andac, F.N. Egolfopoulos *

Department of Aerospace and Mechanical Engineering, University of Southern California, Los Angeles, CA 90089-1453, USA

Received 17 April 2005; received in revised form 8 July 2005; accepted 8 August 2005

Available online 3 October 2005

Abstract

Compared to those for gaseous fuels, fundamental flame studies for liquid fuels are less extensive. The reasons are the experimental difficulty in handling the liquid phase and the complexity of kinetics stemming from the structure of liquid fuel molecules. However, such fuels are important in power generation, transportation, and propulsion. In this investigation, a systematic study has been conducted on the extinction of mixtures of methanol, ethanol, *n*-heptane, and iso-octane with air. The experiments were performed in the counterflow configuration and the extinction strain rates were determined through the use of digital particle image velocimetry. The introduction of the liquid fuel into the air was achieved through a liquid fuel feeder. The liquid flow rates were determined through the use of a high-precision pump. The experiments were conducted at ambient pressure and temperature and the maximum achievable equivalence ratios were limited by the attendant vapor pressure of each liquid fuel. The experiments were numerically simulated using detailed descriptions of chemical kinetic and molecular transport. A number of kinetic mechanisms were tested against the experimentally determined extinction strain rates. The mechanisms were also tested against literature data of laminar flame speeds. It was found that while most mechanisms satisfactorily predict laminar flame speeds, the experimental and predicted extinction strain rates can differ by factors of as much as 2 to 3. Under certain conditions, distinct differences were identified in the kinetic pathways that control the phenomena of propagation and extinction. Additionally, it was found that the sensitivity of laminar flame speeds and extinction strain rates to diffusion could be of the same order as that to kinetics.

Keywords: Practical liquid fuels; Flame extinction; Premixed flames; Mechanism validation

1. Introduction

The use of the stagnation flow configuration has been essential for the determination of fundamental flame properties such as laminar flame speeds, S_u^o, extinction strain rates, K_{ext}, and thermal and concentration structures [1–3]. The accurate determination of these properties is very important, as they can be used for the partial validation of chemical kinetics.

This approach has been extensively used for gaseous fuels. S_u^o has been the most commonly determined property for a number of reasons. First, it is in its own right a very important property of a combustible mixture and it is free of any influences caused by mechanisms that are external to the mixture. Sec-

* Corresponding author.
E-mail address: egolfopo@usc.edu (F.N. Egolfopoulos).

0010-2180/$ – see front matter
doi:10.1016/j.combustflame.2005.08.001

ond, it is conveniently used in kinetic mechanism optimization [4]. These extensive studies on the determination of S_u^o's for gaseous fuels have contributed the development of chemical kinetics mechanisms that predict with an increased degree of confidence the oxidation characteristics of H_2, CO, and gaseous C_1–C_4 hydrocarbons [4–6].

Compared to gaseous fuels, significantly fewer studies have appeared on the determination of fundamental flame properties of practical liquid fuels. This is a result of the complexities that the liquid phase introduces into the experimentation and also the fact that the chemical kinetics of liquid fuels are far more complex and less understood than those of gaseous fuels. Furthermore, the kinetics of these lower-molecular-weight gaseous fuels constitute important subsets of the kinetics of the heavier liquid fuels. Consequently, the kinetics of the former must be validated first. Using the counterflow configuration, S_u^o's of mixtures of methanol and ethanol with air have been determined by Egolfopoulos, Law, and co-workers in the early 1990s [7,8], while S_u^o's of mixtures of C_7–C_8 hydrocarbons with air have been recently determined by Davis and Law [9].

This work is the first step of an ongoing effort initiated by the authors' group to quantify fundamental flame properties of practical liquid fuels. The approach includes the determination of K_{cxt}'s for methanol/air, ethanol/air, *n*-heptane/air, and isooctane/air mixtures and the use of such information to validate chemical kinetics mechanisms.

K_{cxt} was chosen to be studied over S_u^o for two reasons. First, while K_{cxt} can be determined directly, S_u^o in most cases cannot. This is because in order for a flame to be stabilized and measured, a stabilization mechanism is required. The stabilization mechanism introduces an influence that is external to the mixture, such as the strain rate in the stagnation flow method [2]. Typically, extrapolations or extensive data processing are required to determine S_u^o, which is the propagation speed of a steady, one-dimensional, planar, adiabatic, laminar flame.

Second, it is expected that since both propagation and extinction are high-temperature phenomena, they must be controlled by similar kinetics. This has been shown to be the case by sensitivity analysis performed in a recent study of ethylene/air flames [10]. Furthermore, it has been shown [11,12] that C_1/C_2 kinetic mechanisms that closely predict S_u^o of methane/air flames also satisfactorily predict experimentally determined K_{cxt} for such flames.

In view of these considerations, the main goal of this investigation was to provide archival experimental K_{cxt} data for practical alcohol and liquid hydrocarbon fuels and to compare them with predictions derived from detailed numerical simulations. Through these comparisons, various published chemical kinetics mechanisms were tested against extinction data for the first time. Additionally, the thesis that flame propagation and extinction are controlled by similar kinetics was further assessed. This is an important point, as in large-scale simulations of practical combustors the semidetailed or reduced kinetics models that are used have been typically validated against S_u^o data only. However, if the extinction response of the flamelets, which are typically induced by fluid mechanics and/or heat loss influences, is not predicted accurately, the fidelity of such simulations is compromised.

2. Experimental approach

The experiments involve the use of the counterflow technique, which allows for the establishment of a single planar flame. A single flame results by counterflowing a fuel/air jet against an opposing air or nitrogen jet, with both jets injected at ambient temperature. For fuel-lean mixtures air was used, while for near-stoichiometric and fuel-rich mixtures nitrogen was used to avoid the formation of an additional nonpremixed flame downstream of the premixed flame. This single-flame configuration was preferred over the symmetric twin-flame one [1], because for the same equivalence ratio, ϕ, this configuration results in lower K_{cxt} compared to the twin-flame one. As a result, lower Reynolds numbers are required, thus minimizing the effect of intrinsic instabilities that are present in the flow system, and that can potentially affect the flame topology and response.

The measurements were taken using digital particle image velocimetry (DPIV) for the determination of the axial velocity profile along the stagnation streamline of the counterflow [13]. The flow was seeded by 0.3-μm-diameter silicon oil droplets that were produced by a nebulizer similarly to Hirasawa et al. [14]. The absolute value of the maximum preflame velocity gradient is defined as the imposed (local) strain rate, K. K_{cxt} cannot be directly measured if one considers the fact that measurements are not possible in the extinction state and, therefore, extrapolations may be needed. This problem was circumvented, however, by establishing flames in states very close to extinction, determining the prevailing K, and subsequently achieving extinction through a minor reduction (increment) of the fuel flow rate for fuel-lean (fuel-rich) flames. It has been shown both experimentally and numerically that the value of the (local) strain rate is minimally affected through this slight reduction (increment) of the fuel flow rate. Thus, the measured value of K for a slightly richer (leaner) ϕ compared to that at the state of extinction for fuel-

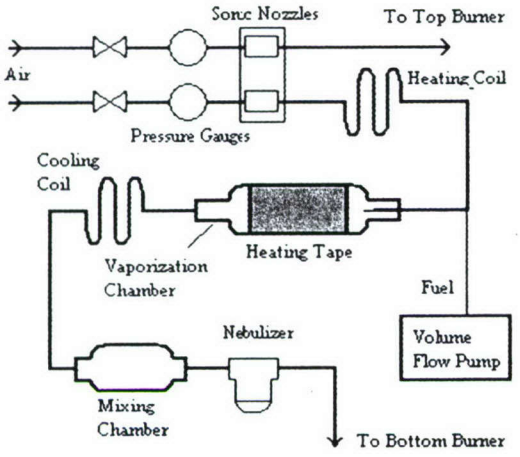

Fig. 1. Schematic of the liquid fuel system.

lean (fuel-rich) flames is a very close representation of that at the extinction state, i.e., of K_{ext}. This approach provides a "direct" measurement of K_{ext} that can be used with confidence in validating chemical kinetics mechanisms.

Another important point in these experiments was the introduction of the liquid fuel into the airflow and maintaining it in the gaseous phase. An approach similar to that of Davis and Law [9] was adopted and the schematic is shown in Fig. 1. A precision-volume flow pump is used to accurately control the flow rate of the liquid fuel, which is then sprayed into a heated vaporization chamber with a heated air coflow. The liquid fuel vaporizes into the airflow and mixes within the chamber. The mixture is then cooled to ambient temperature and delivered to the burners. Condensation does not occur in the system, as the partial pressure of the fuel is maintained below the vapor pressure at the prevailing temperature. Heating of the air and the vaporization chamber is required to ensure rapid and effective vaporization, to prevent any possible condensation at cold spots, and to decrease the response time of the system. This system allows fuels that are normally liquid at room temperature to be maintained and tested in the gaseous phase. The maximum achievable ϕ is limited by the vapor pressure of each fuel.

Four liquid fuels were tested, namely methanol, ethanol, n-heptane, and iso-octane. At atmospheric pressure and an ambient temperature of 300 K, n-heptane and iso-octane are limited to a maximum ϕ of about 2.7, while methanol and ethanol are limited to a maximum ϕ of about 0.95. K_{ext}'s of mixtures of all four fuels with air were determined for the entire achievable ϕ-range for each fuel. S_u^o values were taken from recent literature and were compared with numerical predictions. More specifically, the S_u^o's for methanol/air and ethanol/air mixtures were taken from Refs. [7,8], respectively, while those for n-heptane/air and iso-octane/air mixtures were taken from Ref. [9].

3. Numerical approach

The numerical simulation of the counterflow configuration was conducted by solving the conservation equations of mass, momentum, species concentrations and energy along the stagnation streamline. The code is based on the original formulation of Kee and co-workers [15] for a twin-flame configuration and has been subsequently modified to allow for asymmetric flame configurations by accounting for independent boundary conditions at the exits of the two opposing burners [11,16]. Additional modifications have also been made to account for the effect of thermal radiation from CH_4, H_2O, CO_2, and CO at the optically thin limit [11]. The code is integrated with the CHEMKIN [17] and Sandia Transport [18] subroutine libraries.

The extinction condition is achieved by first establishing a vigorously burning flame for a given ϕ at a relatively low K and by subsequently increasing the flow velocities at the burner exits that increase the strain rate to the point of extinction. At the extinction state the response of any flame property to the strain rate is characterized by a turning-point behavior that introduces a singularity if the strain rate is considered as the independent variable. The code has been also modified to allow capturing this singular behavior and allow, thus, the accurate determination of K_{ext} [19]. More specifically, a two-point continuation approach was implemented by imposing a predetermined temperature or species mass fraction, at two points in the flow field, so that the strain rate is solved for, rather than imposed as a boundary condition. Locations where the temperature or species concentrations have maximum slopes are chosen as the two points, following the recommendations of Nishioka et al. [20].

It should be noted that while the experiments involved the determination of ϕ at extinction for a range of K's, the simulations involved the determination of K at extinction, i.e., K_{ext}, for a range of ϕ's. However, the two approaches are equivalent, as K_{ext} is a singled-value function of ϕ for the conditions studied herein. Additionally, plug flow boundary conditions were considered at the burner exits in accordance with what was determined experimentally for near-extinction conditions.

The experimental results were simulated using a number of kinetic mechanisms summarized in Table 1. The mechanisms of Fischer et al. [21] (hereafter referred to as "FDC00"), Held and Dryer [22] (here-

Table 1
Kinetic mechanisms used to simulate present and literature experimental data

Mechanism	Tested fuels	Species	Reactions	Validation against data obtained in
FDC00 [21]	CH_3OH C_2H_5OH	81	359	Flow reactors, shock tubes, stirred reactors
HD98 [22]	CH_3OH	21	93	Static reactors, flow reactors, shock tubes, laminar flame speeds
LHD03 [23,24]	CH_3OH	21	93	Laminar flame speeds
MRN99 [25]	C_2H_5OH	57	383	Ignition delays, flow reactors, laminar flame speeds
DL98 [9]	n-C_7H_{16} iso-C_8H_{18}	68	399	flow reactors, laminar flame speeds
DL98 (rev)	n-C_7H_{16} iso-C_8H_{18}	69	421	N/A
PPS96 [28]	iso-C_8H_{18}	26	40	Laminar flame speeds

Table 2
CH_2CHO reactions involved in DL98 (revised) mechanism

Reaction	A ($cm^{3(n-1)}\,mol^{-(n-1)}\,s^{-n}$)	a	E (cal/mol)
$C_2H_3 + O_2 = CH_2CHO + O$	3.000E+11	0.290	11.00
$C_2H_3 + HO_2 = CH_2CHO + OH$	1.000E+13	0.000	0.00
$CH_2CHO + H = CH_3CO + H$	5.000E+12	0.000	0.00
$CH_2CHO + H = CH_3 + HCO$	9.000E+13	0.000	0.00
$CH_2CHO + H = CH_2CO + H_2$	2.000E+13	0.000	4000.00
$CH_2CHO + O = CH_2CO + OH$	2.000E+13	0.000	4000.00
$CH_2CHO + OH = CH_2CO + H_2O$	1.000E+13	0.000	2000.00
$CH_2CHO + O_2 = CH_2CO + HO_2$	1.400E+11	0.000	0.00
$CH_2CHO + O_2 = CH_2O + CO + OH$	1.800E+10	0.000	0.00
$CH_2CHO = CH_3 + CO$	7.800E+41	−9.147	46,900.00[a]
$CH_2CHO + H + M = CH_3HCO + M$	1.000E+14	0.000	0.00
Low	5.200E+39	−7.297	4700.00
Troe	0.558900	4350.000	7244.00
Enhanced third body efficiencies: H_2/2.0 H_2O/6.0 CH_4/2.0 CO/1.5 CO_2/2.0 C_2H_6/3.0 C_2H_2/3.0 C_2H_4/3.0			

Note. n is the reaction order.

[a] Pressure-dependent reaction with multiple reaction rates for different pressure regimes; the rate constants for atmospheric pressure are shown.

after referred to as "HD98"), and Li et al. [23,24] (hereafter referred to as "LHD03") were used to model methanol/air mixtures; LHD03 is a modified version of the HD98 mechanism, optimized to better predict S_u^o's of methanol/air flames. The Marinov [25] (hereafter referred to as "MRN99") and the FDC00 mechanisms were used to model ethanol/air flames. To model n-heptane/air and iso-octane/air flames the Davis and Law [9] mechanism (hereafter referred to as "DL98") and its revised version, DL98 (revised), were used. The DL98 (revised) was derived from the original DL98 with the addition of CH_2CHO and its kinetics. The added, to the DL98, kinetics of CH_2CHO were taken from Wang et al. [26,27] and are listed in Table 2. Iso-octane/air flames were also modeled using the Pitsch et al. [28] (hereafter referred to as "PPS96") mechanism. PPS96 is a greatly reduced mechanism that was compiled to predict S_u^o of iso-octane/air mixtures.

Laminar flame speeds were numerically determined using the Premix code [29] to simulate freely propagating flames (FPF).

To compare the controlling mechanisms for FPFs and near-extinction flames (NEF), integrated reaction path and sensitivity analyses were performed. While the standard CHEMKIN-based codes [29] do allow automated sensitivity analysis of S_u^o and all temperature and species concentrations to all reaction rate constants, this is not the case for K_{ext}. This, however, could be achieved by realizing, as described earlier, that K_{ext} becomes a dependent variable when the aforementioned two-point continuation approach is invoked. As a result it is possible to perform rigorous sensitivity analysis with respect to rate constants for K_{ext} at the exact location that is determined experimentally, i.e., where it reaches its maximum value in the hydrodynamic zone. This approach to performing sensitivity analysis on K_{ext} was introduced for the

first time by the authors, in a recent study on the extinction of H_2/air flames [30].

In summary, assessing the ability of all mechanisms to predict K_{ext}'s, after having been optimized to closely predict experimental values of S_u^o, was one of the main goals of this investigation.

4. Results and discussion

4.1. Experimental results on extinction strain rates

K_{ext}'s of mixtures of methanol, ethanol, *n*-heptane, and iso-octane with air are shown in Fig. 2 as functions of ϕ. As mentioned earlier, at unburned mixture temperature 300 K, only lean methanol/air and ethanol/air flames could be established and measured due to their low vapor pressure, while for *n*-heptane/air and iso-octane/air flames the measurements were extended well into the fuel-rich domain. For all data reported in this investigation, the experimental uncertainty was determined to be less than 2% in ϕ and less than 4% in K_{ext}. It should be also noted that the experiments were performed for ϕ's that are neither ultralean nor ultrarich. Thus, the effect of radiation on the flame response is negligible, as has been shown to be the case for mixtures that are not near to their flammability limits [11]. Additionally, soot was not formed in the reported experiments.

Comparing the K_{ext}'s of all four fuels, the alcohols appear to be more resistant to extinction than the hydrocarbons for the same ϕ. Also, the methanol/air and the ethanol/air mixtures exhibit rather similar extinction characteristics for the range of ϕ's tested. The K_{ext}'s of *n*-heptane/air mixtures exceed those of iso-octane/air mixtures for all ϕ's tested, except for the more fuel-lean concentrations. These findings have implications for flame stability; K_{ext} is a measure of flame stability, because flames that are more resistant to extinction result in more stable combustion, given that local extinction is less likely to occur. Thus, mixing alcohols with hydrocarbons to formulate alternative fuels for spark ignition engines (SIE) could improve the overall engine performance.

4.2. Numerical predictions of extinction strain rates

Fig. 3 depicts the experimental and predicted K_{ext}'s for methanol/air mixtures. FDC00 underpredicts the experimental K_{ext} by a factor of 3! The kinetics described by FDC00 becomes so slow at the state of extinction as ϕ decreases that solutions for $\phi < 0.7$ were not possible. However, flames with $\phi < 0.6$ were experimentally established. The K_{ext} data are slightly underpredicted by HD98 for $\phi < 0.75$ and the agreement is much closer for $\phi > 0.75$. LHD03 underpredicts K_{ext} by factors that are slightly smaller that those of FDC00. LHD03 is a modified version of HD98 and has been optimized to predict S_u^o's of methanol/air mixtures. The two mechanisms are, in general, very similar. Three reaction rates were modified (R10, R15, R16), one reaction was removed (R18), one duplicate reaction was added (R5), and one third-body collision efficiency was modified (R11). The R index refers to the reactions shown in Table 3; details of the modifications to HD98 that resulted in LHD03 are shown in Table 4. The present results reveal that modifications in the original mechanism (HD98) that could be casually considered as "minor" caused a large change in the predicted K_{ext}.

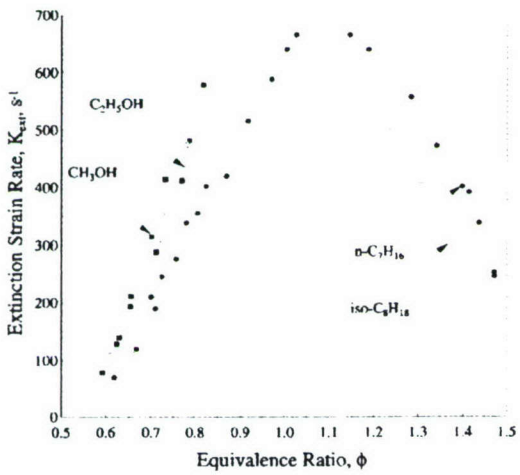

Fig. 2. Variation of the experimentally determined K_{ext}'s with ϕ, for mixtures of air with all liquid fuels considered in this study.

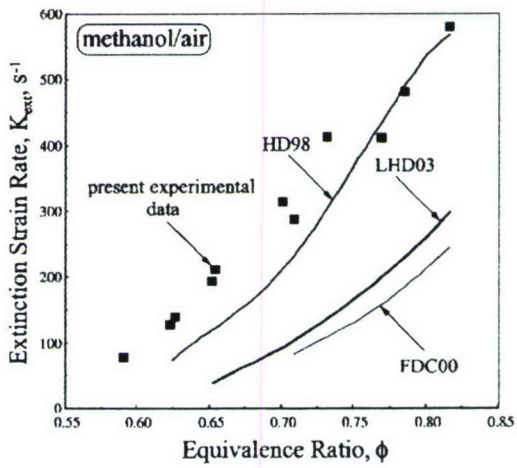

Fig. 3. Variation of experimental and computed K_{ext}'s with ϕ for methanol/air flames using the FDC00, HD98, and LHD03 mechanisms.

Table 3
List of reactions discussed in the text

Reaction #	Reaction	Mechanisms containing reaction
	H_2 and CO reactions	
R1	$H + O_2 = O + OH$	All
R2	$O + H_2 = H + OH$	All
R3	$H + OH + M = H_2O + M$	All
R4	$H_2 + OH = H_2O + H$	All
R5	$HO_2 + OH = H_2O + O_2$	All
R6	$HO_2 + H = OH + OH$	All
R7	$HO_2 + H = H_2 + O_2$	All but PPS96
R8	$HO_2 + HO_2 = H_2O_2 + O_2$	All but PPS96
R9	$CO + OH = CO_2 + H$	All
R10	$CO + O + M = CO_2 + M$	All but PPS96
R11	$HCO + M = H + CO + M$	All
R12	$HCO + O_2 = CO + HO_2$	All but PPS96
R13	$HCO + H = CO + H_2$	All
R14	$CH_2 + O_2 = CO + H_2O$	DL98, DL98 (rev), MRN99, FDC00
	Alcohol reactions	
R15	$CH_2O + OH = HCO + H_2O$	All but PPS96
R16	$CH_2O + HO_2 = HCO + H_2O_2$	DL98, DL98 (rev), FDC00, HD98, LHD03
R17	$CH_2OH + O_2 = CH_2O + HO_2$	MRN99, FDC00, HD98, LHD03
R18	$CH_3O + H = CH_3 + OH$	MRN99, HD98
R19	$CH_3O + M = CH_2O + H + M$	All but PPS96
R20	$CH_3O + O_2 = CH_2O + HO_2$	All but PPS96
R21	$CH_3OH + H = CH_2OH + H_2$	MRN99, FDC00, HD98, LHD03
R22	$CH_3OH + OH = CH_3O + H_2O$	MRN99, HD98, LHD03
R23	$CH_3OH + OH = CH_2OH + H_2O$	MRN99, FDC00, HD98, LHD03
	n-C_7H_{16}/iso-C_8H_{18} reactions	
R24	$CH_2CHO + H = CH_3 + HCO$	DL98 (rev), MRN99
R25	$CH_2CHO = CH_3 + CO$	DL98 (rev), MRN99
R26	$C_2H_3 + O_2 = CH_2CHO + O$	DL98 (rev), MRN99, FDC00
R27	$C_2H_3 + M = C_2H_2 + H + M$	DL98, DL98 (rev), MRN99, FDC00
R28	$C_3H_6 + OH = C_3H_5 + H_2O$	DL98, DL98 (rev), MRN99
R29	iso-$C_4H_8 + O$ = iso-$C_4H_7 + OH$	DL98, DL98 (rev), PPS96
	C_3H_5/C_3H_4 loop reactions	
R30	$C_3H_5 + H = C_3H_4 + H_2$	DL98, DL98 (rev), PPS96, MRN99
R31	$C_3H_5 + OH = C_3H_4 + H_2O$	DL98, DL98 (rev), MRN99
R32	$C_3H_5 + O = C_2H_3HCO + H$	DL98, DL98 (rev), MRN99
R33	$C_3H_5 + O_2 = C_3H_4 + HO_2$	DL98, DL98 (rev), PPS96, MRN99
R34	$C_3H_4 + H = C_3H_5$	DL98, DL98 (rev), PPS96, MRN99
R35	$C_3H_4 + O = CH_2O + C_2H_2$	DL98, DL98 (rev)
R36	$C_3H_4 + O = CO + C_2H_4$	DL98, DL98 (rev), MRN99
R37	$C_3H_4 + OH = CHO + C_2H_4$	PPS96

Fig. 4 depicts the experimental and predicted K_{cxt}'s for ethanol/air mixtures. Both FDC00 and MRN99 underpredict the experimental K_{cxt} by nearly a factor of 2, with the predictions of FDC00 being slightly higher than those of MRN99. Similarly to methanol/air flames, solutions for very fuel-lean concentrations were not possible.

The experimentally determined and numerically predicted K_{cxt}'s for n-heptane/air mixtures are depicted in Fig. 5. The DL98 and DL98 (revised) mechanisms were used in the numerical simulations. For conditions that are not very fuel-rich, DL98 underpredicts the experimental data by almost a factor of 2 at worst, and by a factor of approximately 1.7 for near-stoichiometric flames. DL98 (revised) at worst underpredicts the experiments by a factor of less than 1.5 and on average predicts the experiments more closely by about 15%, compared to DL98. This improvement resulted from the addition of 1 species and 11 reactions, only 3 of which have a notable effect on the burning response of n-heptane/air mixtures, i.e., reactions R24, R25, and R26. Both DL98 and DL98 (revised) predict the maximum K_{cxt} to be at $\phi = 1.22$, while the experimental K_{cxt} peaks at about $\phi = 1.08$.

Table 4
List of reactions included in LHD03 that differ from HD98

	A ($cm^{3(n-1)}\,mol^{-(n-1)}\,s^{-n}$)	a	E (cal/mol)
	Modified reaction rates		
$CH_2O + OH = HCO + H_2O$	3.430E+09	1.18	−447.00
$CH_2O + HO_2 = HCO + H_2O_2$	2.000E+12	0.00	11,660.00
$CO + O + M = CO_2 + M$	1.800E+10	0.00	2384.00
Low	1.550E+24	−2.79	4191.00
H_2/2.5 H_2O/12 CO/1.9 CO_2/3.8			
	Modified third body efficiencies of H_2O and CO_2		
$HCO + M = H + CO + M$	0.186E+18	−1.00	17,000.00
H_2/2.5 H_2O/3.0 CO/1.9 CO_2/3.0			
	Additional reaction		
$HO_2 + OH = H_2O + O_2$	5.000E+16	0.00	22,000.00[a]
	Removed reaction		
$CH_3O + H = CH_3 + OH$	3.200E+13	0.00	0.00

Note. n is the reaction order.
[a] Duplicate reaction.

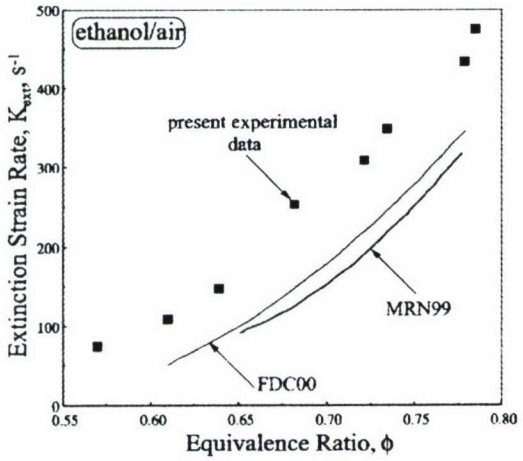

Fig. 4. Variation of experimental and computed K_{ext}'s with ϕ for ethanol/air flames using the FDC00 and MRN99 mechanisms.

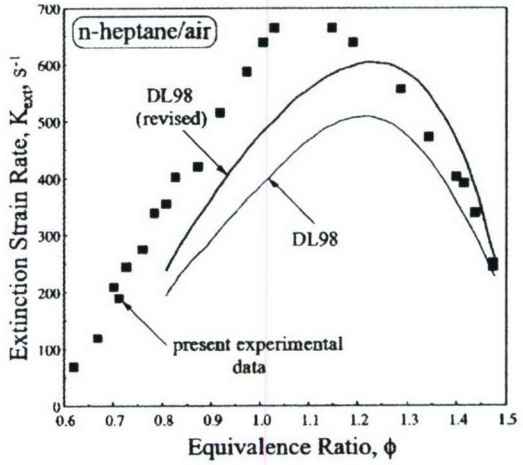

Fig. 5. Variation of experimental and computed K_{ext}'s with ϕ for n-heptane/air flames using the DL98 and the DL98 (revised) mechanisms.

Fig. 6 depicts the experimentally determined K_{ext} values for iso-octane/air mixtures, along with the numerical predictions. The PPS96, DL98, and DL98 (revised) mechanisms were used. All three mechanisms fail to predict the experimental data, especially for lean mixtures, for which they underpredict the experimental data by a factor of 2 or more, with the DL98 (revised) exhibiting relatively better agreement with the experiments. All mechanisms predict the experimental data more closely under fuel-rich conditions. All mechanisms tested also predicted that K_{ext} peaks at a notably greater ϕ than in the experiments. The experimental K_{ext} peaks around $\phi = 1.15$, while DL98 and DL98 (revised) predict a peak at approximately $\phi = 1.25$, and PPS96 at about $\phi = 1.30$. Overall DL98 (revised) exhibits a 10% improvement over the range of ϕ tested compared to DL98.

Of all seven mechanisms tested, only one of them, the HD98 mechanism, came close to reproducing the experimental K_{ext} data. With few exceptions, all mechanisms were found to underpredict the experimental K_{ext} by factors as large as 2 to 3. Furthermore, they all predicted excessively weak burning under fuel-lean conditions, to the point where convergence was not possible even though flames could be experimentally established. It is of interest to note that the HD98 mechanism was subsequently optimized to predict S_u^o's of methanol/air flames, which led to

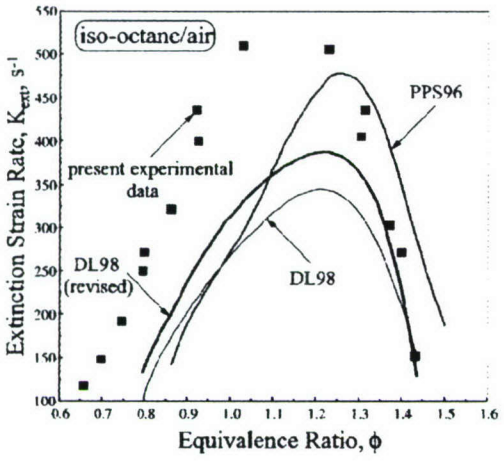

Fig. 6. Variation of experimental and computed K_{ext}'s with ϕ for iso-octane/air flames using the PPS96, DL98, and DL98 (revised) mechanisms.

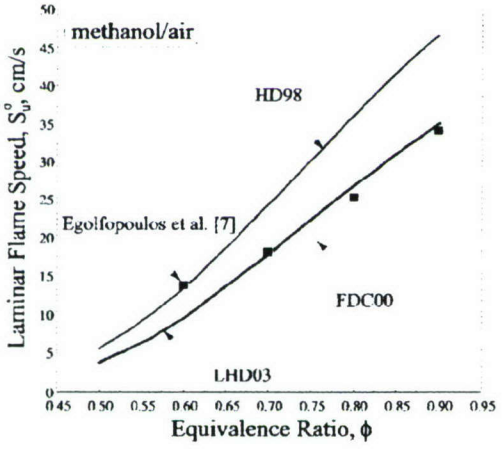

Fig. 7. Variation of experimental and computed S_u^o's with ϕ for methanol/air flames using the FDC00, HD98, and LHD03 mechanisms. The experimental data were taken from Ref. [7].

the LHD03 mechanism. However, this optimization to predict S_u^o more closely caused a rather notable underprediction of the experimental K_{ext} by LHD03, as reported in Fig. 3. Based on this observation and the fact that most of the mechanisms have been tested only against S_u^o, the ability of all mechanisms to simultaneously predict S_u^o's and K_{ext}'s was further assessed and is discussed next.

4.3. Comparisons of phenomena of laminar flame propagation and extinction

Fig. 7 depicts numerical predictions and Ref. [7] S_u^o data for methanol/air mixtures. While HD98 notably overpredicts the experimental data, LHD03

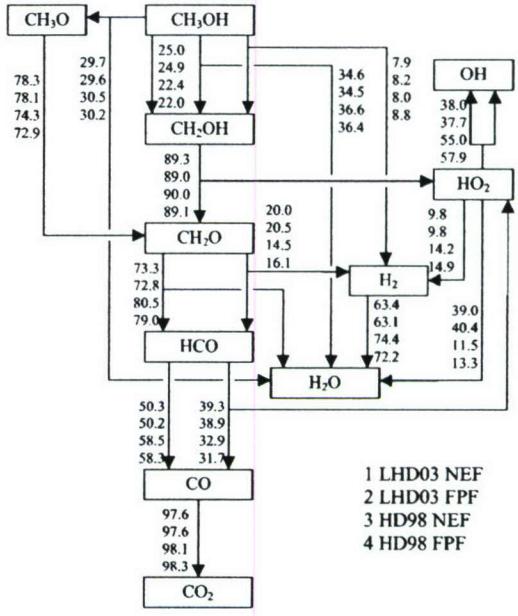

Fig. 8. Integrated species consumption paths for a $\phi = 0.769$ NEF and FPF methanol/air flame, computed using the HD98 and LHD03 mechanisms.

closely predicts them except for fuel-lean conditions, and FDC00 slightly underpredicts them.

Integrated reaction path analyses revealed that all three mechanisms have similar combustion paths for methanol; the percentage consumption paths for the HD98 and LHD03 mechanisms, both NEFs and FPFs, are shown in Fig. 8 for a $\phi = 0.769$ methanol/air flame. The reaction path analysis showed that the combustion pathways for NEFs and FPFs are nearly identical and that each mechanism favored slightly different paths. For example, the FDC00 mechanism (not shown in Fig. 8) was found to favor the H_2 production directly from methanol via R21, compared to the other two mechanisms. R21 accounts for over 50% of the methanol consumption for FDC00, but under 10% for HD98 and LHD03.

Comparison of the reaction path analysis results obtained for LHD03, which closely predicts S_u^o, and for HD98, which closely predicts K_{ext}, revealed that relatively minor changes in a mechanism can lead to significant changes in the prediction of global flame properties. The main difference between the two mechanisms is in the HO_2 chemistry. The LHD03 mechanism places greater importance on the HO_2 chemistry by decreasing the third-body efficiencies of H_2O and CO_2 for reaction R11. The reduction of the R11 rate favors the consumption of HCO through R12, which produces more HO_2. The HO_2 chemistry has also been modified by adding reaction R5, which shifts almost 30% of the consumption of HO_2 toward

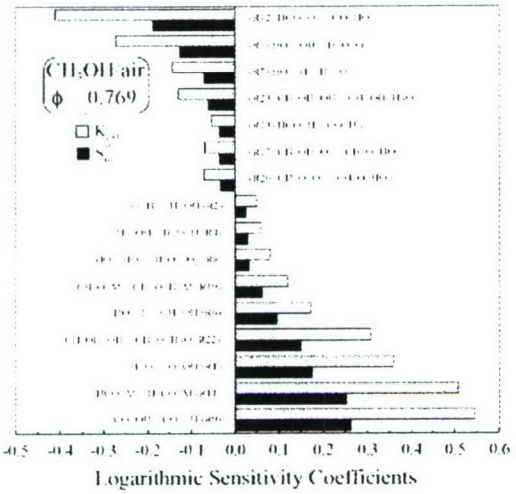

Fig. 9. Logarithmic sensitivity coefficients of S_u^o and K_{ext} to reaction rate constants for a $\phi = 0.769$ methanol/air flame computed using LHD03.

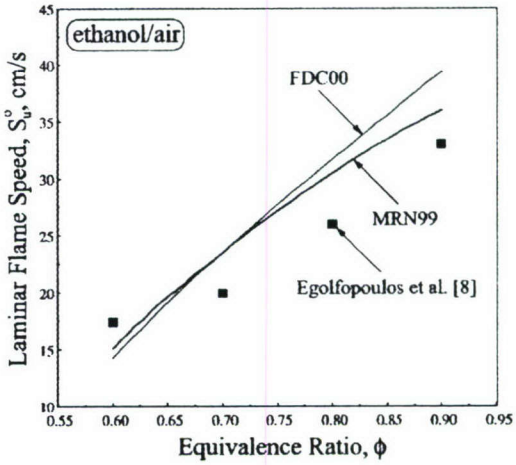

Fig. 10. Variation of experimental and computed S_u^o's with ϕ for ethanol/air flames using the FDC00 and the MRN99 mechanisms. The experimental data were taken from Ref. [8].

the production of H_2O. This has a negative effect on the overall reactivity of the flame because it slows down the rate of R6, which produces two OH radicals that are important to the overall branching. Thus, LHD03 predicts weaker burning characteristics than HD98. This weakening allows LHD03 to predict S_u^o more closely than HD98. However, LHD03 fails to predict K_{ext}. This indicates that validations against S_u^o's are not sufficient for a mechanism and its reduced versions to be used in large-scale simulations, because other high-temperature flame phenomena are not necessarily predicted.

The logarithmic sensitivity coefficients of S_u^o and K_{ext} to reaction-rate constants for a $\phi = 0.769$ methanol/air flame computed using the LHD03 mechanism are shown in Fig. 9. (The authors chose the term "logarithmic sensitivity coefficient" over the term "normalized sensitivity coefficient," which is properly defined in Ref. [29]. A similar discussion can be also found in Ref. [30].) It can be seen that while the reactions that largely affect S_u^o and K_{ext}'s are the same, the sensitivities of K_{ext} are approximately twice as great as for S_u^o. The latter indicates the greater influence of kinetics on the phenomenon of extinction as compared to propagation. It is apparent that the observed qualitative similarities of the sensitivities of S_u^o and K_{ext} do not point to a rate or rates that could be responsible for the failure of the kinetics to predict both phenomena. On the other hand, the quantitative differences of the sensitivity coefficients, which are uniformly described by a factor or 2, could be considered as a potential source of the observed discrepancies between the two phenomena. However, such improvements of rate constants could only be achieved via rigorous global mechanism optimization [4,26], rather than individual rate-constant modifications.

The relative performance of the mechanisms between the two different flame phenomena is summarized as follows: FDC00 underpredicts S_u^o by about 25% and it underpredicts K_{ext} by almost 300% for the range tested. Note that the flame-temperature difference between NEF and FPF at $\phi = 0.769$ is only 138 K. Comparing LHD03 and HD98, it can be seen that modifying a mechanism to decrease S_u^o by 30% reduces the predicted K_{ext} by 60%, i.e., by a factor of 2, which is consistent with the sensitivity results shown in Fig. 9.

Fig. 10 depicts numerical predictions using FDC00 and MRN99 and Ref. [8] S_u^o data for ethanol/air mixtures. It can be seen that both FDC00 and MRN99 predict rather closely the experimental S_u^o's, and that there is on average less than 10% difference between the predicted values and the experimental data for both mechanisms. Similarly to methanol/air flames, integrated reaction path analysis revealed that there are only minor differences between the pathways for NEFs and FPFs as predicted by the two mechanisms. Similarly to methanol/air flames, the sensitivity analysis revealed that the two phenomena share similar sensitivity values, with the sensitivities of K_{ext} being greater than those of S_u^o by approximately a factor of 2.

From the analysis performed for methanol/air and ethanol/air FPFs and NEFs, it is apparent that the kinetic mechanisms that were tested exhibit similar reaction paths and sensitivities for both the phenomena of propagation and extinction, and that no reaction was identified as responsible for the observed discrepancies.

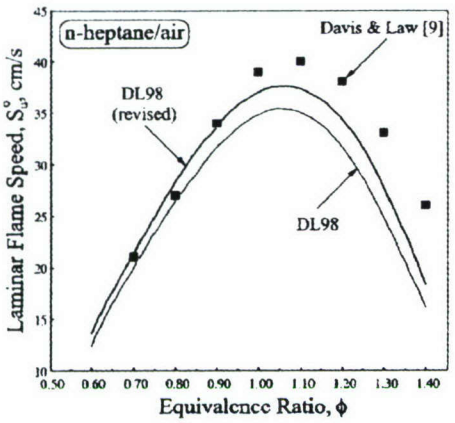

Fig. 11. Variation of experimental and computed S_u^o's with ϕ for n-heptane/air flames using the DL98 and DL98 (revised) mechanisms. The experimental data were taken from Ref. [9].

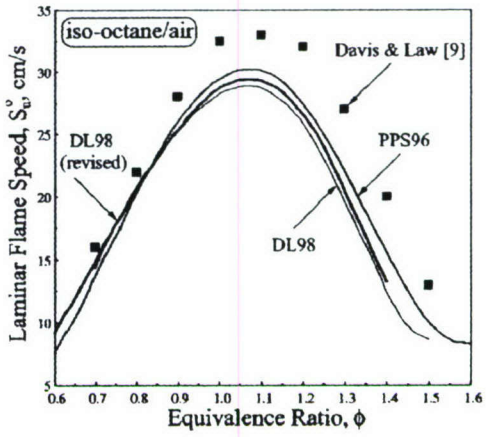

Fig. 12. Variation of experimental and computed S_u^o's with ϕ for iso-octane/air flames using the PPS96, DL98, and DL98 (revised) mechanisms. The experimental data were taken from Ref. [9].

There are several points to be made here. First, the analysis was performed based on mechanisms that were developed based on S_u^o predictions. Thus, if species are missing and/or rate constants have not been optimized to account for phenomena other than laminar flame propagation, it is possible that the reaction path and/or sensitivity analyses performed were falsified and they could not accurately identify the causes responsible for the poor prediction of K_{ext}. While the authors were reluctant to attempt rate constant modifications, the effect of adding species to a mechanism that has been compiled based on S_u^o predictions was assessed and is discussed next.

Fig. 11 depicts numerical predictions using DL98 and DL98 (revised) and Ref. [9] S_u^o data for n-heptane/air mixtures. While both mechanisms accurately predict S_u^o for $\phi < 1.0$, they slightly underpredict S_u^o for $\phi \geqslant 1.0$. The DL98 (revised) was an improvement for predicting S_u^o of n-heptane/air mixtures as well as K_{ext}, as shown earlier in Fig. 5. For example, the addition of CH_2CHO and its kinetics improved the predictions of S_u^o by 9% for $\phi = 1.0$ compared to DL98. However, Fig. 5 depicts that the prediction of K_{ext} was improved by nearly 25% for $\phi = 1.0$, i.e., a factor or 3 improvement over that for S_u^o. Reducing a mechanism to speed up the processing time is necessary for these complex fuels. However, the reduction of a mechanism could result in errors with respect to phenomena that have not been investigated and that are important to the modeling of practical combustors. In this particular case, the introduction of one species and 11 reactions was able to notably improve the performance of the mechanism. Integrated reaction path and sensitivity analyses were performed and will be discussed in reference to iso-octane/air flames.

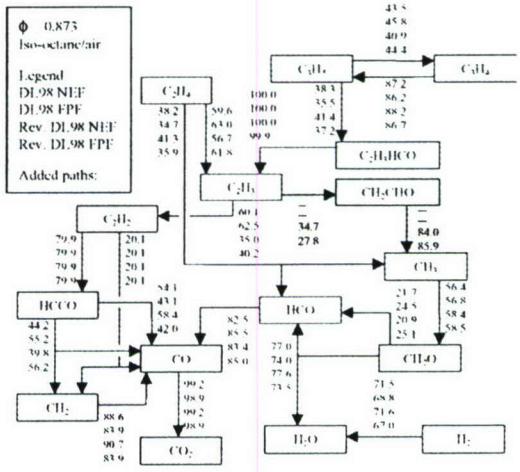

Fig. 13. Integrated species consumption paths for a $\phi = 0.873$ NEF and FPF iso-octane/air flame, computed using the DL98 and DL98 (revised) mechanisms.

Fig. 12 depicts numerical predictions using PPS96, DL98, and DL98 (revised) and Ref. [9] S_u^o data for iso-octane/air mixtures. While all three mechanisms closely predict the experiments for $\phi < 1.0$, they notably underpredict them for $\phi \geqslant 1.0$. The DL98 (revised) is an improvement over the DL98, but only by 4% on average. The modification improved the prediction of K_{ext} by 10% on average, as discussed earlier.

Integrated reaction path analysis revealed, again, relatively minor differences between NEFs and FPFs for iso-octane/air mixtures. This is shown in Fig. 13, in which only the "lower section" of the hydrocarbon oxidation chain is shown, due to its considerable size and the fact that all of the fuel con-

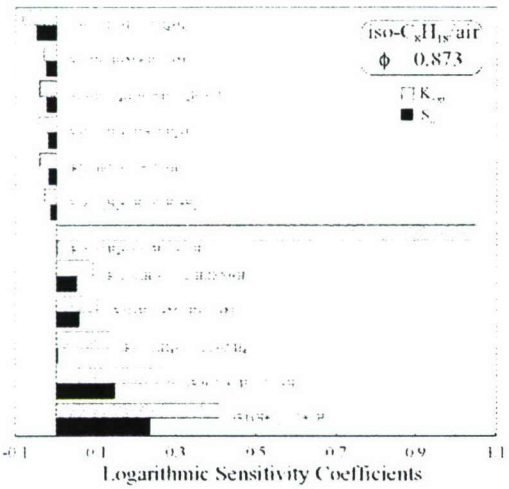

Fig. 14. Logarithmic sensitivity coefficients of S_u^o and K_{ext} to reaction rate constants for a $\phi = 0.873$ iso-octane/air flame computed using the DL98 mechanism.

sumption paths largely converge through these molecules: C_2H_4, C_3H_4, and C_3H_5. The added CH_2CHO species and chemistry are also highlighted in Fig. 13. The extra C_2H_3 consumption pathway (R26) leading to CH_2CHO and then to CH_3 via R24 and R25 strengthens the overall burning intensity. The CH_3 path is favored over the main C_2H_2 path (R27), since it adds more radicals to the radical pool. The C_2H_2 path (R27) is still important, since it leads to CO production through HCCO and CH_2, which in turn accelerates the heat-release rate via the CO oxidation. R26 constitutes between 25 and 35% of the consumption of C_2H_3 and affects NEFs more notably than FPFs.

Fig. 14 depicts the logarithmic sensitivity coefficients of S_u^o and K_{ext} to reaction rate constants for $\phi = 0.873$ iso-octane/air mixtures calculated using DL98. Similar to the other fuels, the sensitivity coefficients of K_{ext} are greater than for S_u^o. The sensitivities are again qualitatively similar for the two phenomena, with the exception of reactions between $C_3H_4 + O$ (i.e., R35 and R36), which do not result in C_3H_5 (i.e., R34). It was found that the sensitivity of K_{ext} to R35 and R36 for DL98 and R37 for PPS96 are dominant. In Fig. 14 the sensitivities to R35 and R36 are shown and their effects are apparent. On the other hand, the sensitivities of S_u^o to R35, R36, and R37 were determined to be minor. As expected, the main branching (R1) and the main CO-oxidation (R9) reactions appear to notably affect K_{ext}, but far less than the $C_3H_4 + O$ channels.

The high sensitivities found for K_{ext} as compared to S_u^o, magnify the significance of a special set of reactions of C_3H_5 and C_3H_4 that are key to the oxidation of both n-heptane/air and iso-octane/air flames. A loop exists between C_3H_5 and C_3H_4 that is basically described by reactions R30, R31, R33, R34, R35, R36, and R37, which cause the bulk of C_3H_5 to be converted to C_3H_4 and then nearly 90% of C_3H_4 to form back C_3H_5. This loop can be seen in the path diagram of Fig. 13. The analysis revealed that while R35 and R36 are responsible for a rather small portion of the C_3H_4 consumption, they constitute "exit" channels from this loop that "traps" mass and lower the overall reaction intensity. Thus, the sensitivity of K_{ext} to the response of this loop is rather large. This point is further supported by the fact that R30 exhibits the largest negative sensitivity, which is physically reasonable given that R30 constitutes the main loop-initiating step. Additionally, R32 exhibits notable positive sensitivity, as it is a consumption path of C_3H_5 that bypasses the $C_3H_5 \Leftrightarrow C_3H_4$ loop. The presence of this loop slows down the rate of conversion of the main fuel to CO_2 and H_2O, thus increasing the time between fuel consumption and heat release. This effect is more profound for NEFs for which residence time considerations at the state of extinction are crucial. This is not the case for FPFs, for which the flame is allowed to fully consume all intermediate species.

4.4. Diffusion effects

While typical analyses of computed flames are usually limited to chemical kinetics effects, it is also of interest to assess diffusion effects, which have been shown to be very important for highly diffusive fuel molecules such as H_2 [30]. In the present investigation, the fuel molecules are large and the effect of their diffusivities could also be important. To test this thesis, the mass diffusivities of all fuels was perturbed in the numerical simulations of both S_u^o and K_{ext}. Similarly to the approach taken in Ref. [29], the logarithmic sensitivities of S_u^o and K_{ext} to the mass diffusivities were calculated using the following equations, in which the superscripts 1 and 2 correspond to the unperturbed and perturbed values, respectively, for both the independent (i.e., fuel diffusivities) and the dependent (i.e., S_u^o and K_{ext}) variables:

$$\frac{({}^2S_u^o - {}^1S_u^o)/{}^1S_u^o}{({}^2D - {}^1D)/{}^1D}, \qquad \frac{({}^2K_{ext} - {}^1K_{ext})/{}^1K_{ext}}{({}^2D - {}^1D)/{}^1D}.$$

The sensitivities of S_u^o and K_{ext} to the fuel diffusivities were then compared to the ones attendant on the main branching reaction R1 and the results are shown in Table 5.

For both lean iso-octane/air and n-heptane/air flames, S_u^o exhibits a small negative sensitivity to diffusion, with values that are an order of magnitude less than the sensitivity to R1. On the other hand, the effect of diffusion on K_{ext} appears to be notably greater and of the same order compared to that of R1.

Table 5
Logarithmic sensitivity coefficients of S_u^o and K_{ext} to the rate of the main branching reaction R1 and to the fuel diffusivity for methanol/air, ethanol/air, *n*-heptane/air, and iso-octane/air mixtures

Fuel	Mechanism		ϕ	Sensitivity to R1	Sensitivity to fuel diffusion
Iso-octane	DL98	S_u^o	0.873	0.320	−0.017
		K_{ext}	0.873	0.409	0.186
n-Heptane	DL98	S_u^o	0.800	0.308	−0.056
		K_{ext}	0.808	0.397	0.185
Ethanol	FDC00	S_u^o	0.682	0.455	−0.137
		K_{ext}	0.682	0.794	0.422
Methanol	FDC00	S_u^o	0.769	0.347	−0.316
		K_{ext}	0.769	0.581	0.032

Similar results are shown for lean ethanol/air flames, with the exception that the sensitivity of S_u^o to diffusion is rather similar in magnitude to that to R1. For lean methanol/air flames it can be seen that the magnitudes of the sensitivities of S_u^o to diffusion and R1 are very close, while that of K_{ext} to R1 is an order of magnitude greater than for diffusion.

Negative sensitivities of S_u^o to diffusion coefficients have been also reported in Ref. [29]. In the absence of stretch, as is the case of FPFs, it can be shown [30] that if the fuel diffusivity, say, increases by a certain amount, the diffusive layer of the fuel increases at a greater rate, thus reducing the fuel diffusive flux into the reaction zone. As a result, the burning intensity of these fuel-lean flames is reduced. This is not the case, though, for stretched flames at their extinction states, for which an increase of the diffusivity of the heavier fuels effectively reduces the mixture's Le number. This in turn augments the gain of fuel flux relative to the heat loss out of the flame zone. For the case of methanol/air flames whose Le number is close to one, this effect is less profound.

The results presented in Table 5 clearly suggest that the effect of uncertainties of diffusion coefficients cannot be overlooked, as this could compromise the value of kinetic rates that are validated against experimental data on flame propagation and extinction.

5. Concluding remarks

A systematic study was conducted on the experimental and numerical determination of K_{ext}'s of mixtures of methanol, ethanol, *n*-heptane, and iso-octane with air under atmospheric temperature and pressure. The experiments involved the use of the counterflow configuration, a high-precision liquid fuel feeder, and a digital particle image velocimetry system for the accurate measurement of flow velocities. The numerical simulations of the experiments involved the use of seven recent kinetic mechanisms that have been validated against data obtained in flow, static, and stirred reactors, shock tubes, and S_u^o's.

Results showed that for the same equivalence ratio, the alcohol flames are more resistant to extinction than *n*-heptane and iso-octane flames under fuel-lean conditions. Comparisons between experimentally determined and computed K_{ext}'s revealed that mechanisms that closely predict S_u^o's fail to predict K_{ext}'s by factors as large as 2–3, suggesting that while propagation and extinction are both high-temperature phenomena, the controlling kinetics may notably differ. This finding also reveals that validating a mechanism in flames against S_u^o's only is not sufficient for describing the global flame response.

Through the aid of detailed sensitivity and reaction path analyses, further insight was provided into the mechanisms controlling NEFs and FPFs. The reaction path analysis revealed that the species consumption is rather similar for NEFs and FPFs. However, it was found that the sensitivities to kinetics are notably higher for NEFs than for FPFs. Furthermore, for *n*-heptane/air and iso-octane/air flames a set of reactions were identified that had dominant sensitivities for NEFs but not for FPFs.

The effect of diffusion was also assessed and sensitivity coefficients of S_u^o and K_{ext} to the fuel diffusivity were determined for all fuels and compared to the ones obtained for the main branching reaction, $H + O = OH + O$. Results showed that under certain conditions, the sensitivities to diffusion could be of the same order as those to kinetics. Thus, validation of kinetics against fundamental flame phenomena without considering the effects of the uncertainties of diffusion coefficients could compromise the fidelity of the rate constants that are derived from flame studies.

Acknowledgments

This work was supported by AFOSR (Grant FA9550-04-1-0006) under the technical supervision of Dr. Julian M. Tishkoff. The discussions on the ki-

netics aspects of this work with Professor Hai Wang are greatly appreciated.

References

[1] C.K. Law, D.L. Zhu, G. Yu, Proc. Combust. Inst. 21 (1986) 1419–1426.
[2] C.K. Law, Proc. Combust. Inst. 22 (1988) 1381–1402.
[3] C.M. Vagelopoulos, F.N. Egolfopoulos, Proc. Combust. Inst. 27 (1998) 513–519.
[4] G.P. Smith, D.M. Golden, M. Frenklach, N.W. Moriarty, B. Eiteneer, M. Goldenberg, C.T. Bowman, R.K. Hanson, S. Song, W.C. Gardiner Jr., V. Lissianski, Z. Qin, GRI-Mech 3.0, 2000, available at: http://www.me.berkeley.edu/gri_mech/.
[5] C.J. Sun, C.J. Sung, H. Wang, C.K. Law, Combust. Flame 107 (1996) 321–335.
[6] S.G. Davis, C.K. Law, H. Wang, Proc. Combust. Inst. 27 (1998) 305–312.
[7] F.N. Egolfopoulos, D.X. Du, C.K. Law, Combust. Sci. Technol. 83 (1992) 33–75.
[8] F.N. Egolfopoulos, D.X. Du, C.K. Law, Proc. Combust. Inst. 24 (1992) 833–841.
[9] S.G. Davis, C.K. Law, Proc. Combust. Inst. 27 (1998) 521–527.
[10] F.N. Egolfopoulos, P.D. Dimotakis, Combust. Sci. Technol. 162 (2001) 19–36.
[11] F.N. Egolfopoulos, Proc. Combust. Inst. 25 (1994) 1375–1381.
[12] F.N. Egolfopoulos, H. Zhang, Z. Zhang, Combust. Flame 109 (1997) 237–252.
[13] Y. Dong, C.M. Vagelopoulos, G. Spedding, F.N. Egolfopoulos, Proc. Combust. Inst. 29 (2002) 1419–1426.
[14] T. Hirasawa, C.J. Sung, H. Wang, C.K. Law, Proc. Combust. Inst. 29 (2002) 1427–1434.
[15] R.J. Kee, J.A. Miller, G.H. Evans, G. Dixon-Lewis, Proc. Combust. Inst. 22 (1988) 1479–1494.
[16] F.N. Egolfopoulos, C.S. Campbell, J. Fluid Mech. 318 (1996) 1–29.
[17] R.J. Kee, F.M. Rupley, J.A. Miller, Chemkin-II: A Fortran Chemical Kinetics Package for the Analysis of Gas-Phase Chemical Kinetics, Report SAND89-8009, Sandia National Laboratories, 1989.
[18] R.J. Kee, J. Warnatz, J.A. Miller, A FORTRAN Computer Code Package for the Evaluation of Gas-Phase Viscosities, Conductivities, and Diffusion Coefficients, Report SAND83-8209, Sandia National Laboratories, 1983.
[19] F.N. Egolfopoulos, P.E. Dimotakis, Proc. Combust. Inst. 27 (1998) 641–648.
[20] M. Nishioka, C.K. Law, T. Takeno, Combust. Flame 104 (1996) 328–342.
[21] S.L. Fischer, F.L. Dryer, H.J. Curran, Int. J. Chem. Kinet. 32 (12) (2000) 713–740.
[22] T.I. Held, F.L. Dryer, Int. J. Chem. Kinet. 30 (11) (1998) 805–830.
[23] J. Li, Z. Zhao, A. Kazakov, F.L. Dryer, in: Chemical and Physical Processes in Combustion, 2003 Technical Meeting of the Eastern States Section of the Combustion Institute, University Park, PA, 2003, pp. 169–171.
[24] J. Li, F.L. Dryer, personal communication, 2004.
[25] N.M. Marinov, Int. J. Chem. Kinet. 31 (3) (1999) 183–220.
[26] H. Wang, A. Laskin, Z.M. Djurisic, C.K. Law, S.G. Davis, D.L. Zhu in: Chemical and Physical Processes in Combustion, the 1999 Fall Technical Meeting of the Eastern States Section of the Combustion Institute, Raleigh, NC, 1999, pp. 129–132.
[27] H. Wang, personal communication, 2004.
[28] H. Pitsch, N. Peters, K. Seshadri, Proc. Combust. Inst. 26 (1996) 763–771.
[29] R.J. Kee, J.F. Grcar, M.D. Smooke, J.A. Miller, PREMIX: A Fortran Program for Modeling Steady Laminar One-Dimensional Premixed Flames, Report SAND85-8240, Sandia National Laboratories, 1985.
[30] Y. Dong, A.T. Holley, M.G. Andac, F.N. Egolfopoulos, S.G. Davis, P. Middha, H. Wang, Combust. Flame (2005), in press.

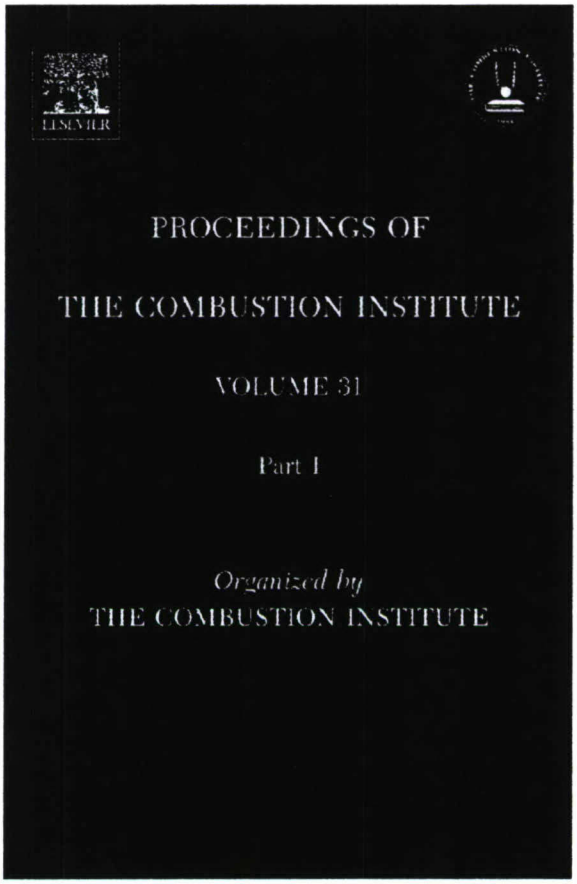

Available online at www.sciencedirect.com

ScienceDirect

Proceedings of the Combustion Institute 31 (2007) 1165–1172

Proceedings of the Combustion Institute

www.elsevier.com/locate/proci

Diffusion and kinetics effects on the ignition of premixed and non-premixed flames

M.G. Andac *, F.N. Egolfopoulos

Department of Aerospace and Mechanical Engineering, University of Southern California, Los Angeles, CA 90089-1453, USA

Abstract

The relative importance of molecular transport and chemical kinetics on flame ignition was investigated through detailed numerical simulations. The study was conducted in stagnation-type flows for atmospheric, laminar premixed and non-premixed *iso*-C_8H_{18}, *n*-C_7H_{16}, and H_2 flames. Ignition of premixed flames was studied by: (1) increasing the temperature of a N_2 jet counterflowing against a fuel/air jet, (2) increasing the temperature of a solid wall against which a fuel/air jet was injected. Ignition of non-premixed flames was studied by increasing the temperature of an air jet counterflowing against a fuel-containing jet. The simulations were performed along the stagnation streamline, and included detailed descriptions of chemical kinetics, molecular transport, and radiative heat transfer. Sensitivity analyses of the ignition temperatures to the diffusion coefficients of the reactants as well as to the kinetics were performed. Results revealed that premixed flame ignition is rather sensitive to the fuel diffusivity in the opposed-jet configuration, and notably less in the jet-wall. This is due to the diffusive transport that is required to convey the reactants towards the ignition kernel in the opposed-jet. It was found that the two approaches result in similar ignition temperatures only for fuel-rich cases and that the ignition temperatures tend to be lower as the equivalence ratio increases in the opposed-jet configuration. However, the ignition temperatures were found to depend mildly on the equivalence ratio in the jet-wall configuration. The sensitivity of ignition to diffusion in non-premixed systems was found to also be notable, especially for cases in which the fuel is highly diluted by an inert. For both premixed and non-premixed flames, the sensitivity of ignition to diffusion coefficients was found to be of the same order or larger than that to kinetics. This is important when flame ignition data are used to validate kinetics, as rate constants could be potentially falsified.

Keywords: Ignitio; Laminar flames; Diffusion effects; Kinetics effects

1. Introduction

The effects of molecular transport and chemical kinetics on flames have been recognized decades ago (e.g., [1]). However, the combustion community has been rather inclined to use flame data to validate chemical kinetics, by implicitly assuming that the transport coefficients are accurately represented by existing theories, such as for example that of Chapman–Enskog. However, such theories are based on several assumptions that may introduce uncertainties in the calculation of transport coefficients. For example, the assumption of spherical geometry

* Corresponding author. Fax: +1 213 740 8071.
E-mail address: andac@usc.edu (M.G. Andac).

1540-7489/$ - see front matter © 2006 The Combustion Institute. Published by Elsevier Inc. All rights reserved.
doi:10.1016/j.proci.2006.07.254

although mathematically convenient, could be challenged for large and highly linear molecules such as, for example, the important primary reference fuels n-C_7H_{16} and iso-C_8H_{18}. On the other hand, uncertainties associated with transport properties in highly diffusive systems such as for example H_2/air mixtures, could also have a first order effect on the predicted flame response. The effect of the molecular diffusion model has also been shown to be important in turbulent combustion [2] and comparable to that of switching between two different kinetic mechanisms. Thus, ignoring without justification the effects of diffusion when kinetics are validated against flame data, could result in the falsification of rate constants.

Past studies have assessed the effects of preferential diffusion (Lewis number effects) (e.g., [3]) and thermal diffusion (thermally driven, non-Fickian, Ludwig–Soret drift) (e.g., [4]) on the flame response. The effect of molecular diffusion on flame structure, propagation, and extinction (e.g., [5–12]) has also been investigated. Some recent studies on the effects of molecular diffusion on the extinction of CH_4/air [10] and H_2/air [11] flames revealed discrepancies in predicted flame properties anywhere between 20% and 40% depending on the transport model selected. The effects of kinetics and diffusion on ignition have also been addressed (e.g., [13–15]) either directly or indirectly (through the effect of strain rate), but not as systematically compared to flame propagation and extinction.

Based on these considerations, the main goal of this study was to numerically investigate the relative importance of chemical kinetics and molecular transport on the ignition of laminar, atmospheric, premixed and non-premixed iso-C_8H_{18}, n-C_7H_{16}, and H_2 flames in two stagnation-type flows, namely the opposed-jet and jet-wall configurations. They both have been widely used in the past (e.g., [16–20]) to study various flame phenomena. The stagnation flow configurations considered in this study are well-controlled environments in which the effect of molecular transport can be systematically augmented or minimized, as it will be discussed. The fuels chosen are of practical importance and have diffusivities that are notably different compared to O_2 and N_2.

2. Numerical approach

The simulations were conducted by solving the quasi-one-dimensional conservation equations of mass, momentum, species concentrations, and energy along the stagnation streamline (e.g., [21–23]). The effect of thermal radiation from CH_4, H_2O, CO_2, and CO was also included at the optically thin limit (e.g., [22]). The code was integrated with the CHEMKIN [24] and Sandia Transport [25] subroutine libraries.

Four kinetics models were used in the simulations:

1. Davis and Law [26] mechanism for iso-C_8H_{18} (hereafter referred to as "DL98");
2. Pitsch et al. [27] mechanism for iso-C_8H_{18} (hereafter referred to as "PPS96"); PPS96 is a greatly reduced mechanism compiled to predict laminar flame speeds of iso-C_8H_{18}/air mixtures;
3. Liu et al. [16] mechanism for n-C_7H_{16} (hereafter referred to as "LHCP04");
4. Davis et al. [28] mechanism for H_2 (hereafter referred to as "DJWE05").

Three configurations were considered (**Fig. 1**):

(i) *A fuel/air jet counterflowing against a N_2 jet.* A premixed flame was ignited by increasing the injection temperature at the N_2-jet boundary, T_{inj,N_2}. The value of T_{inj,N_2} resulting in flame ignition was defined as the ignition temperature, T_{ign}. The momenta of both jets were kept constant by adjusting the velocity boundary conditions while T_{inj,N_2} is increased, to keep the stagnation plane (SP) at the center of the domain. A separation distance of 20 mm between the nozzles was used.

(ii) *A fuel/air jet impinging on an inert stagnation-wall.* Increasing the wall temperature, T_{wall}, a premixed flame was ignited. The original opposed-jet code had been modified allowing for the no-slip velocity boundary conditions at the wall [17]. The value of T_{wall} resulting in flame ignition was defined as T_{ign}. A separation distance of 10 mm between the nozzle and the wall was used.

(iii) *A fuel or fuel/N_2 jet counterflowing against an air jet.* A non-premixed flame was ignited by increasing the temperature of the air-jet boundary, $T_{inj,air}$. The value of $T_{inj,air}$ resulting in flame ignition was defined as T_{ign}. Similarly to (i), the velocity boundary conditions were adjusted while $T_{inj,air}$ was increased to

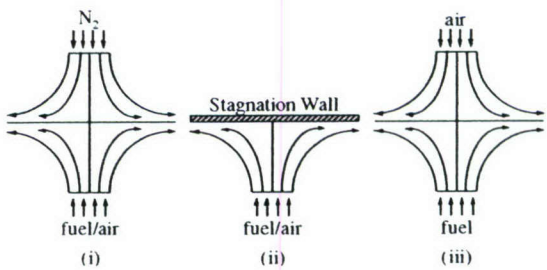

Fig. 1. Schematics of the stagnation flow configurations.

keep the SP at the center of the domain. A separation distance of 20 mm between the nozzles was used.

For the studies of premixed flame ignition in configurations (i) and (ii), the fuel/air mixture was injected at 300 K since all fuels considered, including *iso*-C_8H_{18} and *n*-C_7H_{16}, could exist in the gaseous phase [19] at 300 K including fuel-rich flammable mixtures. However, for the studies of non-premixed flame ignition of *iso*-C_8H_{18} and *n*-C_7H_{16} in configuration (iii), the fuel/N_2 jet was injected at 450 K that would maintain the fuels in the gaseous phase under all conditions considered; the H_2/N_2 jet was injected at 300 K similarly to the premixed case.

For the ignition of premixed flames, the imposed global strain rate, K_{glb}, was in the range of $20 \leqslant K_{glb} \leqslant 50\ s^{-1}$ for *iso*-C_8H_{18}/air and *n*-C_7H_{16}/air, and $55 \leqslant K_{glb} \leqslant 330\ s^{-1}$ for H_2/air, and was varied with equivalence ratio, ϕ. Those values of K_{glb} were determined by imposing velocities at the nozzle exit that were slightly higher than the attendant laminar flame speeds. Thus, steady flames could be established upon ignition while maintaining the lowest possible strain rate for each ϕ. More specifically, the Karlovitz numbers, *Ka*, were determined to be $Ka \sim O(10^{-3}\text{–}10^{-2})$. Under such conditions it has been demonstrated that the premixed flame structure is relatively immune to the variations of the strain rate [29]. This was also confirmed in the present simulations by imposing small but finite strain-rate variations and the effect on T_{ign} was found to be minor. For the non-premixed flame ignition the imposed strain rates were chosen to be one to two orders of magnitude less than the attendant extinction values, assuring again small sensitivity of T_{ign} on the strain rate.

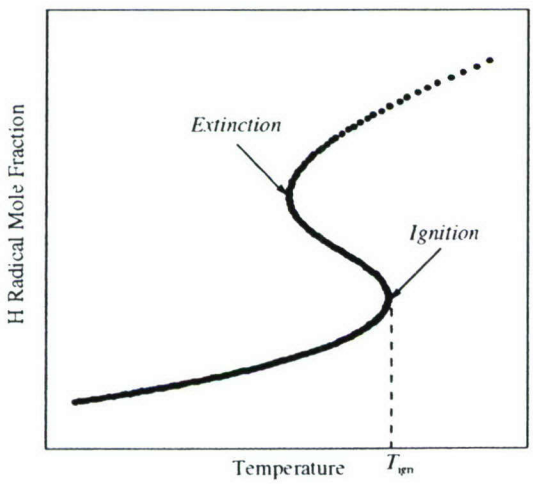

Fig. 2. Ignition and extinction turning-point response for a convective–diffusive–reactive system.

The ignition response exhibits a turning-point behavior as T_{inj} or T_{wall} increases. Introducing a one-point continuation [30,31] into the original code captured this singular behavior, as shown in Fig. 2. Starting the simulations from a non-ignited state, a pre-determined species concentration increment was imposed at the location where the species concentration exhibits a maximum slope. This serves as a new boundary condition replacing T_{inj} for the opposed-jet or T_{wall} for the jet-wall configuration, upon which the "*S*-curves" are single-valued. It should be mentioned that *n*-C_7H_{16} may in certain circumstances exhibit a two-stage ignition [16] however, for the cases studied and for the kinetic mechanism used this was not the case and one-stage high-temperature ignition was observed.

Sensitivity analysis was performed to assess the effects of diffusion coefficients and chemical kinetics on T_{ign}. A "brute force" approach was implemented for the determination of the sensitivities to diffusion. The mass diffusivity of each species i to the mixture, $D_{i,m}$, was perturbed by small amounts and then T_{ign} was determined. Subsequently, a logarithmic sensitivity coefficient (LSC) was formulated as $LSC \equiv d(\ln T_{ign})/d(\ln D_{i,m})$. LSC's of T_{ign} to diffusivities were determined through ±10% perturbation of the fuel diffusivity to the mixture for all ϕ's and of the mass diffusivity of O_2 to the mixture for fuel-rich mixtures only. One should note that perturbation of the mass diffusivity of a reactant also affects the thermal diffusivity of that particular reactant, as thermal diffusivity is dependent upon mass diffusivity.

LSC's of T_{ign} to kinetics were determined rigorously by the code, given that T_{ign} is a dependent variable when the aforementioned one-point continuation approach is invoked. As a result it is possible to perform rigorous sensitivity analysis with respect to rate constants for T_{ign}, similarly to previous studies on flame extinction [11,19].

3. Results and discussion

Figure 3 depicts the LSC's of T_{ign} to the reactant diffusivities for premixed *iso*-C_8H_{18}/air (DL98 and PPS96) and *n*-C_7H_{16}/air (LHCP04) mixtures in both the opposed-jet (i) and jet-wall (ii) configurations. The variation of ϕ was in the range $0.65 \leqslant \phi \leqslant 1.35$ and that of K_{glb} was $20 \leqslant K_{glb} \leqslant 50\ s^{-1}$.

Results indicate that ignition is substantially more sensitive to the fuel transport in the opposed-jet configuration compared to the jet-wall for both fuels. This is due to the fact that in the opposed-jet configuration, ignition occurs close to the hot (N_2) boundary, as the Arrhenius kinetics dictate. Thus, the fuel diffusion against

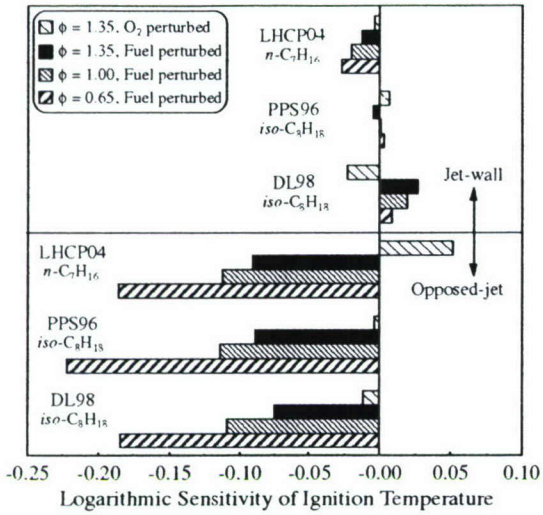

Fig. 3. Logarithmic sensitivity coefficients of ignition temperature of *iso*-C_8H_{18}/air and *n*-C_7H_{16}/air flames on the diffusion coefficients of the fuel and O_2 determined at various ϕ's in the opposed-jet and jet-wall configurations.

the opposing convection after it crosses the SP becomes the controlling factor. This is not the case in the jet-wall configuration as both reactants are transported primarily by convection to the ignition kernel that is located at the immediate vicinity of the wall. For the hydrocarbons considered, the fuel is the largest molecule in the flowfield and its diffusion across the SP becomes the rate-controlling process in the opposed-jet configuration for low ϕ's. At higher ϕ's, the LSC's are lower because the fuel concentration gradient

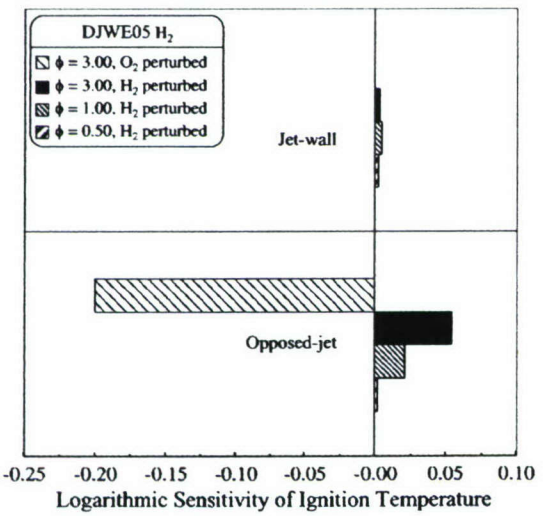

Fig. 4. Logarithmic sensitivity coefficients of ignition temperature of H_2/air flames on the diffusion coefficients of the fuel and O_2 determined at various ϕ's in the opposed-jet and jet-wall configurations.

increases and, thus, its diffusive transport is not anymore the rate-controlling process.

Figure 4 depicts LSC's of T_{ign} to the reactant diffusivities for H_2/air (DJWE05) mixtures in both the opposed-jet (i) and jet-wall (ii) configurations. The variation of ϕ was in the range $0.50 \leqslant \phi \leqslant 3.00$ and that of K_{glb} was $55 \leqslant K_{glb} \leqslant 330\ s^{-1}$. For H_2/air mixtures, O_2 is the largest molecule in the flowfield and the ignition process is limited by its transport to the kernel. Hence, comparing the results of Figs. 3 and 4, which have the same scales, reveals that the sensitivity of T_{ign} to the O_2 diffusivity is substantially larger for H_2/air mixtures.

It is also of interest to note that while the LSC's to the fuel diffusivity are negative for hydrocarbon/air they are positive for H_2/air mixtures in the opposed-jet configuration. This indicates that as the H_2 diffusivity increases T_{ign} increases, i.e., ignition is inhibited. This is physically sound given that the process of ignition largely depends on the *relative* magnitude of the diffusive transport of fuel and O_2 towards the ignition kernel, which is located close to the hot (N_2) boundary. For the case of *n*-C_7H_{16} and *iso*-C_8H_{18}, the fuel diffusivity is smaller than O_2 and the fuel transport is the rate-limiting process. Thus, increasing the fuel diffusivity promotes ignition, i.e., T_{ign} decreases. For the case of H_2, the diffusive transport of O_2 is instead the rate-limiting process, given its notably lower diffusivity compared to H_2. Thus, increasing the H_2 diffusivity is equivalent of further reducing the rate of transport of O_2 relative to H_2, which in turn inhibits ignition, i.e., T_{ign} increases.

The results shown in Fig. 3 also reveal that for *iso*-C_8H_{18}/air flames the LSC's to the fuel diffusivity calculated using the DL98 mechanism, assume small but positive values in the jet-wall configuration. It was found that as the fuel diffusivity increases its concentration increases within the ignition kernel, enhancing thus termination reactions between the fuel and radicals that tend to inhibit ignition. Comparing the opposed-jet and the jet-wall configurations, it is apparent that when the later is used to investigate premixed flame ignition, the effect of reactant diffusion is minimized so that the kinetics can be validated with greater degree of confidence as compared to the opposed-jet.

It is also of interest to note that the values of the LSC's reported in Figs. 3 and 4 are as high as 0.22. While such values can be considered as rather small for flame propagation and extinction, this is not the case when *ignition temperatures* are considered. For example, for T_{ign} in the range 900–1700 K, which is of relevance to the present study, a 10% perturbation of the diffusivity of *n*-C_7H_{16} results in a change of T_{ign} of about 50 K for a $\phi = 0.65$ flame. A 50 K difference in T_{ign} is

rather large given the exponential dependence of reaction rates on temperature. Thus, the uncertainties associated with the diffusivities need to be considered in ignition studies. This will be further discussed in a latter section.

Figure 5 depicts the values of T_{ign} for the *iso*-C_8H_{18}/air mixtures that were referenced in Fig. 3. It is apparent that the ignition occurs more readily for the jet-wall configuration as T_{ign}'s are lower compared to the opposed-jet by as much as 250 K under fuel-lean conditions. However, under fuel-rich conditions the T_{ign}'s determined in the two configurations are approaching each other as ϕ increases, and nearly coincide at $\phi = 1.35$. For fuel-lean conditions in the opposed-jet configuration, the fuel diffusion to the ignition kernel, which is close to the hot (N_2) boundary, is the controlling factor. As ϕ increases, the fuel's transport to the kernel becomes more effective due to the larger concentration gradient, and as a result the effect of the fuel diffusivity on ignition diminishes. Thus, the ignition becomes kinetically controlled and the choice of the reacting configuration has a second order effect. The LSC's reported in Fig. 3 also support this argument, as their values decrease as ϕ increases for both *n*-C_7H_{16} and *iso*-C_8H_{18} flames.

The results of Fig. 5 also reveal that T_{ign} decreases as ϕ increases in the opposed-jet but stays relatively constant in the jet-wall configuration. This is reasonable given that for the opposed-jet configuration, ignition occurs more readily at higher ϕ's, as discussed in the previous paragraph, and thus T_{ign} is lower. For the jet-wall configuration, the effect of ϕ on T_{ign} is largely kinetic and not diffusive. Furthermore, the T_{ign} values calculated by two kinetic mechanisms differ as much as 100 K for the same configuration, with DL98 resulting in lower values.

The effect of the reactant diffusivities on T_{ign} for non-premixed flames [configuration (iii)] was also assessed, by considering a fuel/N_2 jet impinging on a heated air jet. The cases of 100% and 5% fuel mole fraction in the fuel stream were considered and the results are shown in Fig. 6. Comparing to the ignition of premixed flames in the opposed-jet configuration, the LSC's to the fuel diffusivity are lower. Comparing the undiluted (100% fuel) and highly diluted (5% fuel) cases it can be seen that the LSC's increase with the N_2-dilution. This is expected; ignition is largely controlled by kinetics for low N_2-dilution and fuel diffusion for high N_2-dilution of the fuel stream. Note that the reported LSC's for the hydrocarbons are finite even for the undiluted case. However, this is not the case for undiluted H_2 flames for which the LSC's on both H_2 and O_2 are excessively small. Under such conditions H_2 is supplied at the maximum possible concentration and diffuses at large rates towards the ignition kernel. Thus, ignition is controlled by the H_2 oxidation kinetics that are rather fast compared to hydrocarbons, and as a result the effect of diffusion is minor. For the diluted (5% fuel) case, the effect of reactant diffusion on ignition becomes notable.

Figure 7 depicts the LSC's of T_{ign} to kinetics for lean, stoichiometric, and rich premixed *iso*-C_8H_{18}/air flames by utilizing DL98, in both the opposed-jet and the jet-wall configurations. The sensitivity of T_{ign} to the main chain-branching reaction $H + O_2 \rightarrow OH + O$ (R1) is apparent, especially in the opposed-jet configuration. However, the analysis reveals that other reactions are as important. In the opposed-jet configuration

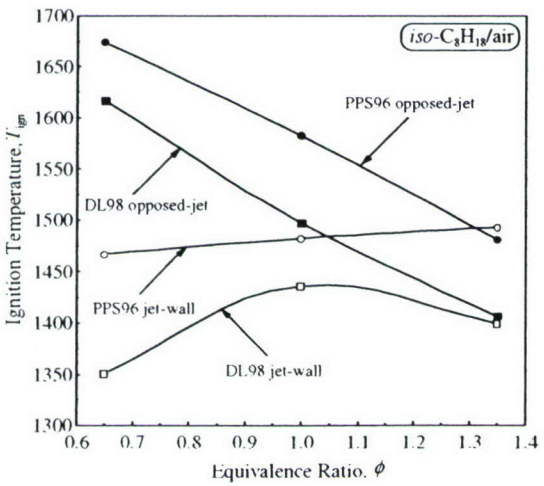

Fig. 5. Ignition temperatures of *iso*-C_8H_{18}/air premixed flames determined for various ϕ's in both the opposed-jet and jet-wall configurations.

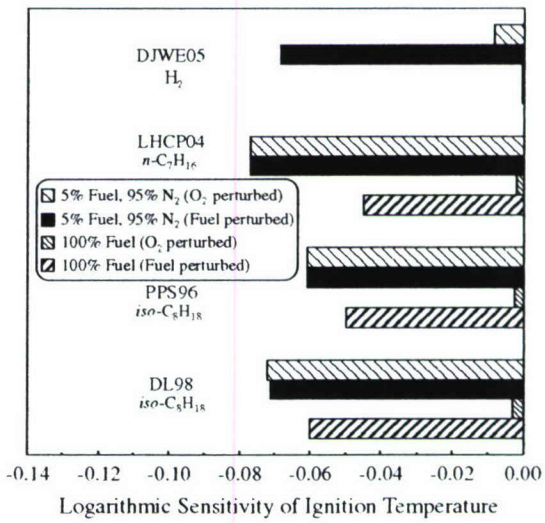

Fig. 6. Logarithmic sensitivity coefficients of ignition temperature of diluted and undiluted non-premixed flames on the diffusion coefficients of the fuel and O_2.

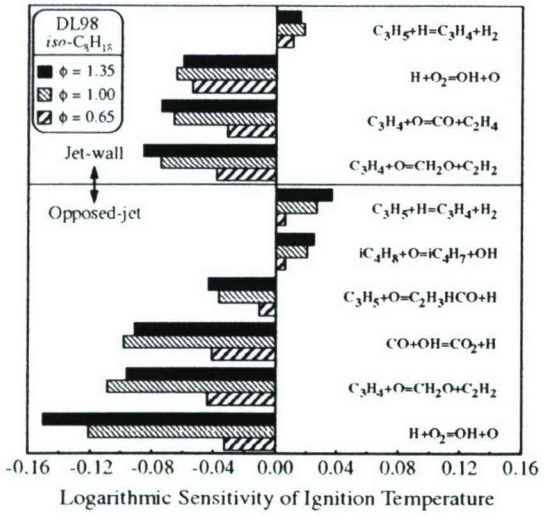

Fig. 7. Logarithmic sensitivity coefficients of ignition temperature of *iso*-C_8H_{18}/air flames on kinetics, determined for various ϕ's in the opposed-jet configuration, by using the DL98 mechanism.

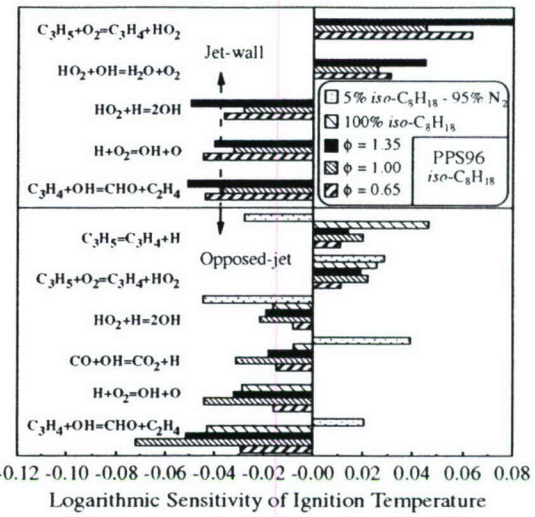

Fig. 8. Logarithmic sensitivity of ignition temperature of premixed and non-premixed *iso*-C_8H_{18} flames on kinetics, determined for various ϕ's in the opposed-jet configuration, by using the PPS96 mechanism.

these are $C_3H_4 + O \rightarrow CH_2O + C_2H_2$ (R2) and $CO + OH \rightarrow CO_2 + H$ (R3). In fact, reaction R2 exhibits higher sensitivity than R1 for fuel-lean cases. As ϕ increases, ignition becomes more sensitive to R1. As expected, R1 and R2 exhibit negative LSC's, i.e., increasing their rates results in lower T_{ign}, i.e., ignition is promoted. A similar analysis was also performed for the non-premixed cases, undiluted and inert-diluted, and only R1 was found to have considerable LSC (~0.05). Thus, these cases were not included in Fig. 7.

Comparisons of the results shown in Figs. 3 and 4 and those in Fig. 7 reveal that the LSC's of ignition to the reactant diffusivities could be comparable and even larger than those to kinetics. For example the LSC's to the diffusivity of *iso*-C_8H_{18} are indeed larger than those to the kinetics for fuel-lean mixtures.

To assess the effect of the kinetic mechanism, a similar analysis was conducted by using PPS96 and the results are shown in Fig. 8. Based on this mechanism, reaction $C_3H_4 + OH \rightarrow CHO + C_2H_4$ (R4) exhibits the highest LSC that is similar to R1 in the opposed-jet. The sensitivity of T_{ign} to the main chain-termination reaction $H + O_2 + M \rightarrow HO_2 + M$ (R5) was found to be positive, as expected. Comparing the results shown in Figs. 3 and 8 reveals that, the LSC's to the *iso*-C_8H_{18} diffusivity are larger than those to kinetics, similarly to what was found using DL98. This suggests that the finding regarding the relative magnitude of LSC's to diffusion and kinetics holds regardless of the kinetic mechanism used.

Figure 9 depicts the LSC's of T_{ign} to kinetics for premixed and non-premixed *n*-C_7H_{16}/air flames. For premixed flames both the opposed-jet and jet-

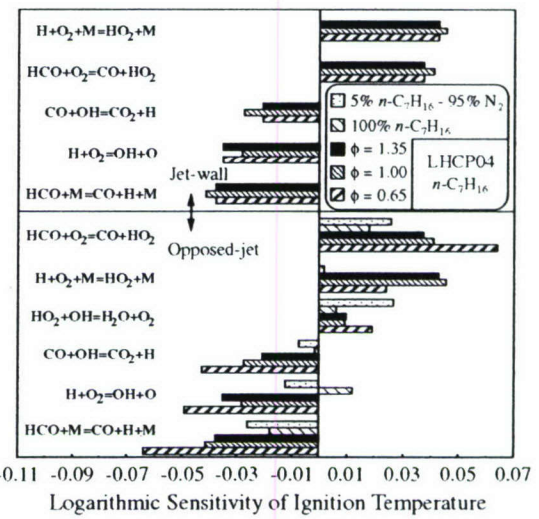

Fig. 9. Logarithmic sensitivity of ignition temperature of premixed and non-premixed *n*-C_7H_{16} flames on kinetics, determined for various ϕ's in the opposed-jet configuration, by using the LHCP04 mechanism.

wall configurations were considered. Two reactions involving HCO, namely $HCO + M \rightarrow CO + H + M$ (R6) and $HCO + O_2 \rightarrow CO + HO_2$ (R7) exhibit the largest negative and positive LSC, respectively. LSC's for non-premixed flames are consistently lower than those for premixed flames.

Figure 10 depicts LSC's for premixed and non-premixed H_2 flames. As expected, in both configurations R1 and R5 exhibit the largest negative and positive sensitivities, respectively. Sensitivities

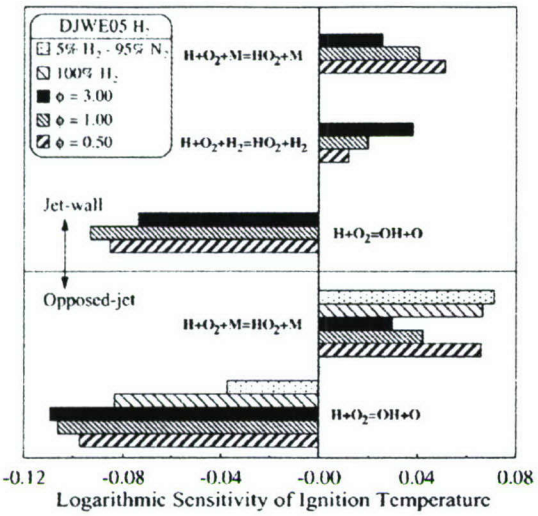

Fig. 10. Logarithmic sensitivity of ignition temperature of premixed and non-premixed H_2 flames on kinetics, determined for various ϕ's in the opposed-jet configuration, by using the DJWE05 mechanism.

for non-premixed flames were found to be comparable to the premixed flames. Similarly to hydrocarbons, comparing the results of Figs. 4 and 10 reveals that the LSC's to reactant diffusivities can be of the same order or larger compared to those to kinetics.

It is important to acknowledge that the kinetic mechanisms used to model flame ignition for both n-C_7H_{16} and iso-C_8H_{18} have not been developed based on or tested against flame ignition data. Additionally, they are rather simplified to accurately predict the details of ignition of these complex fuels. Kinetic mechanisms that could provide a more accurate prediction of ignition would contain hundreds of species and thousands of reactions. Such simulations would be excessively costly, but they would not alter the basic conclusions of the present study. This can be justified by the fact that similar results were obtained by using three hydrocarbon mechanisms that are rather different and some of them notably more simplified than others. For both fuels and by using all three mechanisms it was shown that ignition could be as sensitive to diffusion as it is on kinetics.

4. Concluding remarks

The effects of molecular diffusion and chemical kinetics on the ignition of premixed and non-premixed iso-C_8H_{18}, n-C_7H_{16}, and H_2 flames were numerically determined by using three different reacting configurations and four kinetic mechanisms. All fuels tested have distinctly different diffusivities compared to O_2 and N_2.

Results revealed that the ignition of premixed flames could be notably more sensitive to the fuel diffusivity in the opposed-jet and much less in the jet-wall configuration. This was attributed to the reduced role of diffusion in the jet-wall configuration in which the reactants are transported into the ignition kernel largely by convection. It was found that the two configurations result in similar ignition temperatures only for fuel-rich cases. Furthermore, the ignition temperatures were found to decrease as the equivalence ratio increases in the opposed-jet but remain nearly constant in the jet-wall configuration. The sensitivity of the ignition temperature to the fuel diffusivity was determined to be negative for hydrocarbons and positive for H_2, indicating that ignition is promoted or inhibited as the fuel diffusive flux increases for hydrocarbons and decreases for H_2, respectively. The sensitivity of ignition to diffusion was also found to be important in non-premixed systems, even for undiluted cases for which ignition is largely controlled by kinetics.

Comparisons of the sensitivity coefficients to kinetics and diffusion revealed that the effect of diffusion on ignition could be of the same order or greater compared to kinetics. This is important given that experimental results on flame ignition are utilized to compile and/or optimize kinetic mechanisms. Unless the effect of diffusion is either accounted for or minimized, the derived kinetics information could be falsified.

Acknowledgments

This work was supported by AFOSR (Grant FA9550-04-1-0006) under the technical supervision of Dr. Julian M. Tishkoff. The discussions with Prof. Hai Wang on various issues pertaining to diffusion coefficients calculations are mostly appreciated.

References

[1] J. Adler, M.B. Zaturska, *Combust. Flame* 10 (3) (1966) 273–278.
[2] R. Hilbert, F. Tap, H. El-Rabii, D. Thevenin, *Prog. Energy Combust. Sci.* 30 (1) (2004) 61–117.
[3] B. Cuenot, T. Poinsot, *Combust. Flame* 104 (2) (1996) 111–137.
[4] P.L. García-Ybarra, C. Treviño, *Combust. Flame* 96 (3) (1994) 293–303.
[5] P.A. Libby, K.N.C. Bray, J.B. Moss, *Combust. Flame* 34 (1979) 285–301.
[6] M.K. Mishra, R.A. Yetter, Y. Reuven, H. Rabitz, M.D. Smooke, *Int. J. Chem. Kinet.* 26 (4) (1994) 437–453.
[7] P.H. Paul, J. Warnatz, *Proc. Combust. Inst.* 27 (1998) 495–504.
[8] A. Ern, V. Giovangigli, *Combust. Theor. Model.* 2 (1998) 349–372.

[9] A. Ern, V. Giovangigli, *Combust. Sci. Technol.* 149 (1999) 157–181.
[10] B.A. Williams, *Combust. Flame* 124 (2) (2001) 330–333.
[11] Y. Dong, A.T. Holley, M.G. Andac, et al., *Combust. Flame* 142 (4) (2005) 374–387.
[12] Z. Zhao, J. Li, A. Kazakov, F.L. Dryer, *Combust. Sci. Technol.* 177 (1) (2005) 89–106.
[13] R. Knikker, A. Dauptain, B. Cuenot, T. Poinsot, *Combust. Sci. Technol.* 175 (10) (2003) 1783–1806.
[14] R. Seiser, H. Pitsch, K. Seshadri, W. Pitz, H.J. Curran, *Proc. Combust. Inst.* 28 (2000) 2029–2037.
[15] V. Gopalakrishnan, J. Abraham, *Combust. Flame* 136 (4) (2004) 557–566.
[16] S. Liu, J.C. Hewson, J.H. Chen, H. Pitsch, *Combust. Flame* 137 (3) (2004) 320–339.
[17] F.N. Egolfopoulos, H. Zhang, Z. Zhang, *Combust. Flame* 109 (2) (1997) 237–252.
[18] T. Sano, A. Yamashita, *Fluids Therm. Eng.* 37 (1) (1994) 180–186.
[19] A.T. Holley, Y. Dong, M.G. Andac, F.N. Egolfopoulos, *Combust. Flame* 144 (3) (2006) 448–460.
[20] C.G. Fotache, H. Wang, C.K. Law, *Combust. Flame* 117 (4) (1999) 777–794.
[21] R.J. Kee, J.A. Miller, G.H. Evans, G. Dixon-Lewis, *Proc. Combust. Inst.* 22 (1988) 1479–1494.
[22] F.N. Egolfopoulos, *Proc. Combust. Inst.* 25 (1994) 1375–1381.
[23] F.N. Egolfopoulos, C.S. Campbell, *J. Fluid Mech.* 318 (1996) 1–29.
[24] R.J. Kee, F.M. Rupley, J.A. Miller, Report No. SAND89-8009, Sandia National Laboratories, 1989.
[25] R.J. Kee, G. Dixon-Lewis, J. Warnatz, M.E. Coltrin, J.A. Miller, Sandia Report SAND86-8246, 1986.
[26] S.G. Davis, C.K. Law, *Proc. Combust. Inst.* 27 (1998) 521–527.
[27] H. Pitsch, N. Peters, K. Seshadri, *Proc. Combust. Inst.* 26 (1996) 763–771.
[28] S.G. Davis, A.V. Joshi, H. Wang, F.N. Egolfopoulos, *Proc. Combust. Inst.* 30 (2005) 1283–1292.
[29] C.K. Law, C.J. Sung, G. Yu, R.L. Axelbaum, *Combust. Flame* 98 (2) (1994) 139–154.
[30] M. Nishioka, C.K. Law, T. Takeno, *Combust. Flame* 104 (3) (1996) 328–342.
[31] F.N. Egolfopoulos, P.E. Dimotakis, *Proc. Combust. Inst.* 27 (1998) 641–648.

Available online at www.sciencedirect.com

ScienceDirect

Proceedings of the Combustion Institute xxx (2006) xxx–xxx

Proceedings of the Combustion Institute

www.elsevier.com/locate/proci

An assessment of the lean flammability limits of CH_4/air and C_3H_8/air mixtures at engine-like conditions

F.N. Egolfopoulos [a,*], A.T. Holley [a], C.K. Law [b]

[a] *Department of Aerospace and Mechanical Engineering, University of Southern California, Los Angeles, CA 90089-1453, USA*

[b] *Department of Mechanical and Aerospace Engineering, Princeton University, Princeton, NJ 08540-5263, USA*

Abstract

The lean flammability limits of CH_4/air and C_3H_8/air mixtures were numerically determined for a wide range of pressures and unburned mixture temperatures in order to assess the near-limit flame behavior under conditions of relevance to internal combustion engines. The study included the simulation of freely propagating flames with the inclusion of detailed descriptions of chemical kinetics and molecular transport, radiative loss, and a one-point continuation method to solve around singular points as the flammability limit is approached. Results revealed that both pressure and unburned mixture temperature have significant effects on the lean flammability limit as well as the attendant limit flame temperature. Specifically, the lean limit was found to first increase and then decrease with pressure, while the limit temperature decreases with pressure in general, and can be reduced to values as low as 900 K under engine-like conditions. Through sensitivity and species consumption path analyses it was further shown that the chain mechanisms that control the near-limit flame response critically depend on the thermodynamic state of the mixture. Thus, mechanisms that are identified as important at near-atmospheric conditions may not be relevant at higher pressures and unburned mixture temperatures. In particular, the response of near-limit flames was found to resemble the homogeneous explosion limits of hydrogen/oxygen mixtures in that while at low pressures the main branching and termination reactions are respectively $H + O_2 \rightarrow OH + O$ and $H + O_2 + M \rightarrow HO_2 + M$, at the elevated pressures relevant to internal combustion engines the system branching is controlled by the HO_2–H_2O_2 kinetics. Potential avenues for extending the lean operation limits of internal combustion engines are suggested based on the understanding gained herein.

Keywords: Flammability; Flame extinction; Premixed flames

1. Introduction

The term "flammability limit" has been loosely used to describe the concentration limits beyond which flame propagation is not possible. A more formal definition [1] involves the failure of propagation of the ideal one-dimensional, steady, laminar, planar, nearly adiabatic flame, hereafter referred to as the Ideal One-Dimensional Flame (IODF).

Spalding [2] first assessed the influence of thermal radiation on flames by incorporating volumetric heat loss in the IODF model, with the

* Corresponding author. Fax: +1 213 740 8071.
E-mail address: egolfopo@usc.edu (F.N. Egolfopoulos).

1540-7489/$ - see front matter © 2006 Published by Elsevier Inc. on behalf of The Combustion Institute.
doi:10.1016/j.proci.2006.08.018

use of one-step chemistry. A turning-point behavior was identified as the heat loss parameter was increased. This formulation and finding, while conceptually powerful, could not be confirmed over the years, for two reasons: the IODF model cannot be established in the laboratory and the simplified nature of the formulation, involving constant properties and one-step chemistry, cannot be substantiated quantitatively.

Experimentally, "flammability limits" have been determined through the use of the standard flame tube (e.g., [3,4]) and/or the spherical bomb (e.g., [5]). Both approaches, however, include parameters such as heat and radical losses, unsteadiness, strain rate, and ignition energy "memory effect" that are external to the mixture. Law et al. [6] proposed the use of stagnation-type flames to experimentally determine the "true" flammability limit, ϕ_{limit}. The technique involves determining the extinction strain rate, K_{ext}, by systematically varying the mixture's equivalence ratio, ϕ, and the subsequent determination of ϕ_{limit} through linear extrapolation to $K_{\text{ext}} = 0$.

In subsequent studies (e.g., [7–15]) further insight was acquired into the concept of flammability limits through experiments at normal and reduced gravity as well as detailed numerical simulations. In particular, by simulating the IODF using detailed descriptions of chemical kinetics and thermal radiation, failure of flame propagation was identified at low fuel concentrations in [8], while Spalding's turning point behavior was reproduced in [9] and as such allows for the quantitative determination of ϕ_{limit}. Indeed, the numerical values were shown to agree well with the empirical ones within experimental and modeling uncertainties. Law and Egolfopoulos [9] also attempted to unify the separate concepts of flame extinction through heat loss and kinetic limitation by noting that near-limit flames are particularly sensitive to chain mechanisms. Thus, by adopting the concept of the flammability exponent α, advanced in [7] and defined as the logarithmic sensitivity coefficient of the rate of the main termination reaction, w_T, on the rate of the main branching reaction, w_B, at the location of the maximum rate of the branching reaction through the relation $w_T \sim w_B^{\alpha}$, it was found that α assumed a value close to unity as the turning-point limit is approached, in agreement with the postulate of [7]. The usefulness of this concept was also highlighted in the plenary paper on chemical kinetics by Miller [16] at the 26th Symposium.

We further note that while this chain-thermal concept is general in nature, independent of the thermodynamic state of the mixture, the studies of [7,9] were conducted for atmospheric and near-atmospheric conditions because prior interests were mostly motivated by safety considerations. It was particularly innovative that recently this concept has been insightfully applied in [17] to assess the flammability limits in the high-temperature and pressure environments of internal combustion engines. Specifically, by equating the maximum reaction rates of the important $H–O_2$ branching and termination reactions, which are respectively

$$H + O_2 \rightarrow OH + O \qquad (R1)$$

$$H + O_2 + M \rightarrow HO_2 + M, \qquad (R2)$$

it was found that, for CH_4/air and C_3H_8/air flames in a 650 K and 50 bar environment, the rate of R2 would exceed that of R1 when $\phi \approx 0.6$ with an adiabatic flame temperature around 1900 K. Testing with both spark ignition and Diesel engines [17] also revealed that flame extinction and high unburned-hydrocarbon emissions result when the in-cylinder combustion temperature fall below a "critical" value of about 1900 K. It was therefore suggested that these results impose a fundamental lean limit for the operation of internal combustion engines and a corresponding lower limit for which NO_x can be reduced through lean burning.

The present study was motivated by the practically important study of [17] to further examine the role of the flammability limit in the operation of internal combustion engines. In particular, we note that the limit condition identified in [17] was based on kinetic assessment instead of the more rigorous turning-point consideration allowing for radiative loss [8,9]. Furthermore, this assessment was obtained by equating the maximum rates of R1 and R2, and as such is different from the original criterion of [7] based on the flammability exponent being unity. Third, since the important branching and termination pathways at pressures as high as 50 bars could be substantially more involved than R1 and R2, a point also recognized in [17], a more comprehensive evaluation of the kinetic competition between branching and termination reactions may be needed. Indeed, through a more detailed study of the flammability states at high pressures and initial temperatures, it will be shown that the turning-point criterion results in a substantially wider range of lean operation, and that additional branching-termination channels involving the $HO_2–H_2O_2$ chemistry emerge under such high-pressure conditions, yielding useful insights into the constraints limiting the operational ranges of internal combustion engines.

The numerical specification, results, and discussions of the present study are sequentially presented in the following

2. Numerical approach

Freely propagating flames were computed using the Premix code [18] that was properly

Please cite this article as: F.N. Egolfopoulos et al., An assessment of the lean flammability limits of CH_4/air ..., Proceedings of the Combustion Institute (2006), doi:10.1016/j.proci.2006.08.018.

modified. The effect of thermal radiation from CO_2, H_2O, CO, and CH_4 at the optically thin limit was incorporated, similarly to previous studies, e.g., [8,9,11]. The code was also modified to allow for capturing the singular behavior around the turning point and allowing, thus, the accurate determination of ϕ_{limit}. Similar to previous studies of stagnation-type flames, e.g., [19,20], a one-point continuation approach was implemented by imposing a predetermined temperature or mass fraction of a specific species, at one point in the flow field. Thus, the fuel concentration in the unburned mixture is solved for, rather than imposed as a boundary condition.

The code was integrated with the CHEMKIN [21] and Sandia Transport [22] subroutine libraries. The GRI 3.0 mechanism [23] was used to describe the oxidation of CH_4/air flames. For the modeling of C_3H_8/air flames, a C_3 mechanism compiled by Wang and co-workers [24, H. Wang, personal communications, 2003] was used. Both mechanisms predict closely various flame properties of CH_4/air and C_3H_8/air mixtures.

The mixture's equivalence ratio was varied from $\phi = 1.0$ to ultra-lean fuel concentrations at which the turning point behavior could be computed. Additionally, the unburned mixture's temperature, T_u, was varied between 300 and 700 K and the thermodynamic pressure, p, between 1 and 50 atm; it is noted that the T_u used in the radiation term as the far-field temperature [8,9,11] would vary accordingly from 300 and 700 K and was *not* set arbitrarily to 300 K for all cases.

Insight into the processes that control the near-limit flame behavior was obtained through the use of detailed sensitivity and integrated species consumption path analyses.

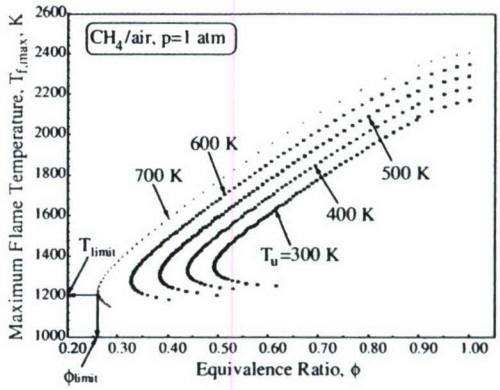

Fig. 1. Variation of $T_{f,max}$ with ϕ and T_u, for CH_4/air flames at $p = 1$ atm, and the determination of ϕ_{limit} and T_{limit}.

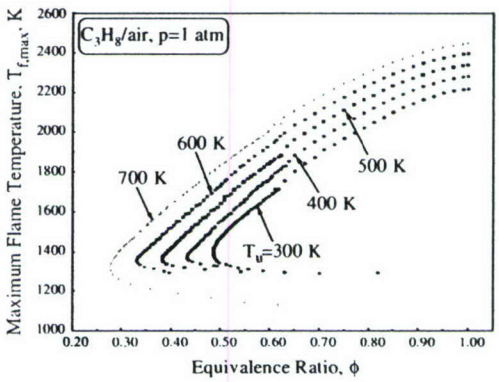

Fig. 2. Variation of $T_{f,max}$ with ϕ and T_u, for C_3H_8/air flames at $p = 1$ atm.

3. Results and discussion

Previous investigations (e.g., [8,9,11–15]) have shown that the inclusion of thermal radiation in the energy equation results in a non-monotonic temperature profile throughout the flame. It first increases from the unburned value and reaches a maximum, $T_{f,max}$, just downstream of the reaction zone. As a result of the radiative loss, it then slowly decreases towards T_u. It has also been shown that, by comparing adiabatic and non-adiabatic flames, the effect of thermal radiation on the flame structure and global response becomes significant only for weakly burning flames at near-limit ϕ's, for example around $\phi \approx 0.6$ for CH_4/air mixtures at $p = 1$ atm and $T_u = 300$ K.

At ultra-lean fuel concentrations, the presence of radiative loss eventually results in a turning-point behavior. This is shown in Figs. 1 and 2 for $p = 1$ atm CH_4/air and C_3H_8/air mixtures, respectively, with $T_u = 300$, 400, 500, 600, and 700 K; similar behavior was found at all other pressures considered, namely $p = 5$, 10, 20, and 50 atm. The turning-point then defines the flammability limit, ϕ_{limit}, and the attendant $T_{f,max}$ as the limit temperature, T_{limit}, as schematically shown in Fig. 1. Figures 1 and 2 depict that ϕ_{limit} decreases as T_u increases, hence extends the flammable range. This is physically sound given that with increasing T_u, extra enthalpy is added to the total energy of the mixture and becomes flammable at lower fuel concentrations. Additionally, it is seen that as T_u increases, T_{limit} decreases to as low as 1200 K at $p = 1$ atm and $T_u = 700$ K. Note that the ϕ_{limit}'s obtained at $p = 1$ atm and $T_u = 300$ K for both CH_4/air and C_3H_8/air mixtures are in close agreement with the experimentally determined lean flammability limits (e.g., [6,12,15]).

Figures 3 and 4 depict the ϕ_{limit} and T_{limit}, respectively, for the CH_4/air mixtures as functions of p and T_u, while Figs. 5 and 6 show similar results for the C_3H_8/air mixtures. The results for ϕ_{limit} reveal that, for a given p, ϕ_{limit} decreases

Please cite this article as: F.N. Egolfopoulos et al., An assessment of the lean flammability limits of CH_4/air ..., Proceedings of the Combustion Institute (2006), doi:10.1016/j.proci.2006.08.018.

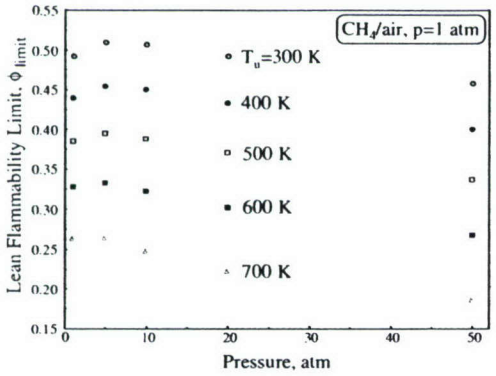

Fig. 3. Variation of ϕ_{limit} with p and T_u, for CH_4/air flames.

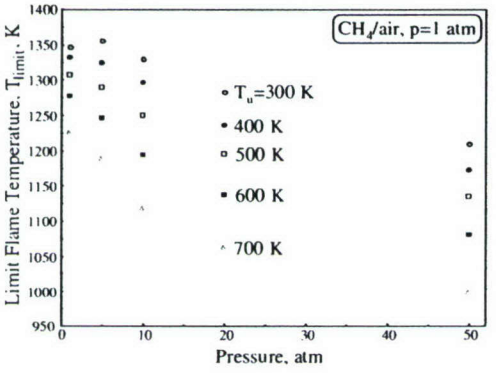

Fig. 4. Variation of T_{limit} with p and T_u, for CH_4/air flames.

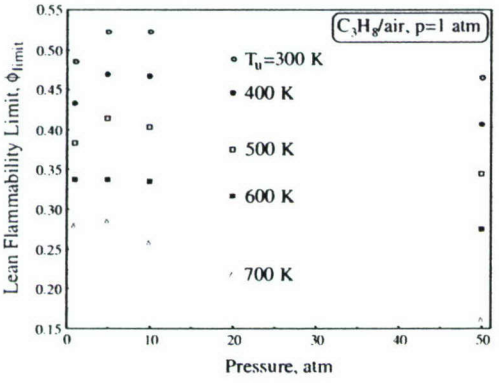

Fig. 5. Variation of ϕ_{limit} with p and T_u, for C_3H_8/air flames.

as T_u increases, as noted earlier. On the other hand, for a given T_u, ϕ_{limit} first increases and then decreases as p increases for all T_u's and for both fuels. Figures 4 and 6 show that T_{limit} decreases as T_u increases for a given p. This is expected, given that as T_u increases ϕ_{limit} decreases, thus resulting in lower flame temperatures at the limit. It is also seen that for a given T_u, T_{limit} decreases with p for the higher T_u's. For the lower T_u's, T_{limit} increases first between $p = 1$ and 5 atm, and subsequently decreases as p increases. This behavior can be explained based on the combined effects of ϕ_{limit} and p on T_{limit}. While increasing (decreasing) ϕ_{limit} increases (decreases) T_{limit}, increasing p decreases T_{limit} as a result of the attendant increase of the rate of the radiative loss; effects of p on product dissociation are negligible for the low flame temperatures of near-limit mixtures. At low T_u's and p's, ϕ_{limit} increases with p and its effect dominates that of p on T_{limit}. Thus, T_{limit} increases with p. For higher T_u's and low p's, the effect of p in reducing T_{limit} dominates that of ϕ_{limit}. This is because higher T_u's result in lower T_{limit}'s, and radiation effects are more profound for these lower flame temperatures (e.g., [9,11–15]). As a result, T_{limit} decreases with p. For $p > 5$ atm, ϕ_{limit} decreases with p and the two effects are synergistic in monotonically reducing T_{limit}.

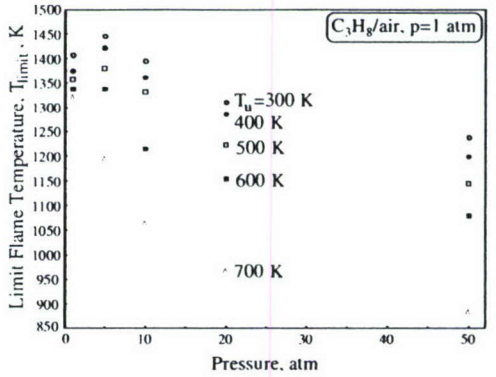

Fig. 6. Variation of T_{limit} with p and T_u, for C_3H_8/air flames.

The most striking results shown in Figs. 4 and 6 are the very low T_{limit}'s that are realized at high T_u's. In particular for $p = 50$ atm and $T_u = 700$ K, the computed values of T_{limit} are as low as 900 K for C_3H_8/air mixtures. This is to be contrasted with the reported experimental $T_{limit} \approx 1900$ K [17] for similar conditions. This finding suggests that using the flammability limit argument to explain experimentally observed engine behavior may not be sufficient and additional factors must be considered.

The original argument of [7,9], regarding the effect of the competition between R1 and R2, could be used to explain the near-limit behavior for low pressures, say $1 \leqslant p \leqslant 5$ atm. This competition for H radicals is analogous to the second explosion limit of homogeneous H_2/O_2 mixtures, and causes ϕ_{limit} to increase with p. However, at higher p's the excessive production of HO_2 may

Please cite this article as: F.N. Egolfopoulos et al., An assessment of the lean flammability limits of CH_4/air ..., Proceedings of the Combustion Institute (2006), doi:10.1016/j.proci.2006.08.018.

result in additional branching channels similar to those of the third explosion limit, and causes ϕ_{limit} to decrease with p. To examine such a possibility the kinetic effects at the ϕ_{limit}'s were assessed in detail via sensitivity and integrated species consumption path analyses for $p = 1$, 5, 10, and 50 atm and $T_u = 300$ and 700 K, to be discussed next.

Figures 7 and 8 depict the logarithmic sensitivity coefficients of the mass-burning rate on the kinetics for limit CH_4/air mixtures at $p = 1$ atm and 50 atm, respectively, while Figs. 9 and 10 show similar results for C_3H_8/air mixtures.

The sensitivity results for $p = 1$ atm, CH_4/air (Fig. 7) and C_3H_8/air (Fig. 9) mixtures confirm the previously reported results [7,9] that R1 and R2 exhibit the highest positive and negative sensitivities respectively, at least for $T_u = 300$ K. Significant negative sensitivity is also exhibited by:

$$HO_2 + OH \rightarrow O_2 + H_2O \qquad (R3)$$

as it results in OH consumption that is important for the fuel and CO oxidation. At $T_u = 700$ K it is seen that R3 has the highest negative sensitivity for C_3H_8/air mixtures and is rather notable for CH_4/air mixtures. Consequently, the current simulation suggests that, even for $p = 1$ atm, the chain mechanism effects on near-limit flames cannot be solely attributed to the R1-vs-R2 competition. The calculations reported in Refs. [7] and [9]

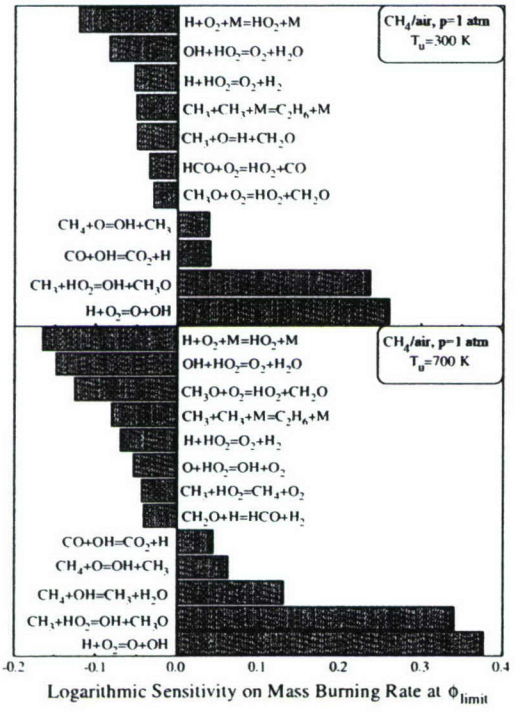

Fig. 7. Sensitivity of the mass-burning rate on kinetics for limit CH_4/air flames, at $p = 1$ atm and $T_u = 300$ and 700 K.

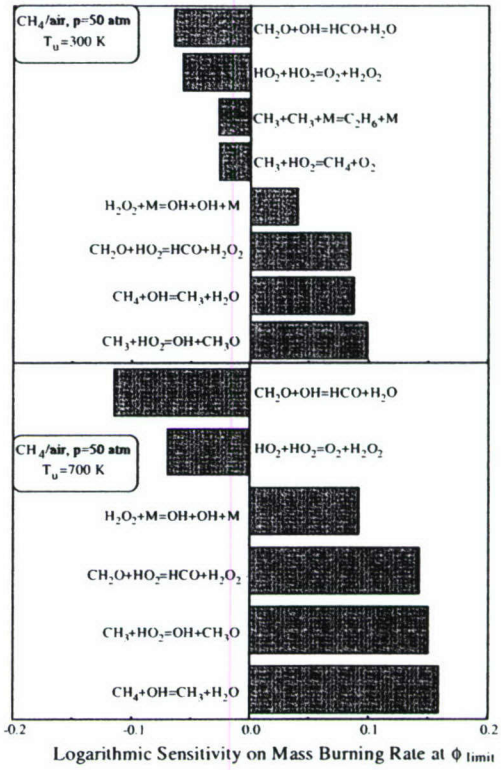

Fig. 8. Sensitivity of the mass-burning rate on kinetics for limit CH_4/air flames, at $p = 50$ atm and $T_u = 300$ and 700 K.

were performed using different kinetic mechanisms that apparently predicted a more profound effect of the R1-vs-R2 competition on the flammability limits. This was also shown in the present simulation, by formulating the flammability exponent based only on the rates of R1 and R2, and their values were computed at the numerically determined ϕ_{limit}'s. It was found that while for $T_u = 300$ K the flammability exponents at the ϕ_{limit}'s are in the range of 0.9–1.0, at higher T_u's these values were in the range of 0.75–1.0. This is reasonable as considering that R1-vs-R2 competition alone cannot adequately describe the kinetic effects on the flammability limit.

The sensitivity results for the $p = 5$ atm CH_4/air and C_3H_8/air mixtures revealed that while the effect of R2 is notable for CH_4/air, its effect is not direct on C_3H_8/air flames but is instead indirect via R3 that utilizes HO_2 produced by R2 to consume OH. It was also found that the importance of R1 is reduced especially for C_3H_8/air flames, and that reactions between the carbon-containing species and HO_2 become important.

The sensitivity results for $p = 10$ atm CH_4/air and C_3H_8/air mixtures revealed the initiation of reaction pathways that resemble those controlling the third explosion limit of homogeneous H_2/O_2

Please cite this article as: F.N. Egolfopoulos et al., An assessment of the lean flammability limits of CH_4/air ..., Proceedings of the Combustion Institute (2006), doi:10.1016/j.proci.2006.08.018.

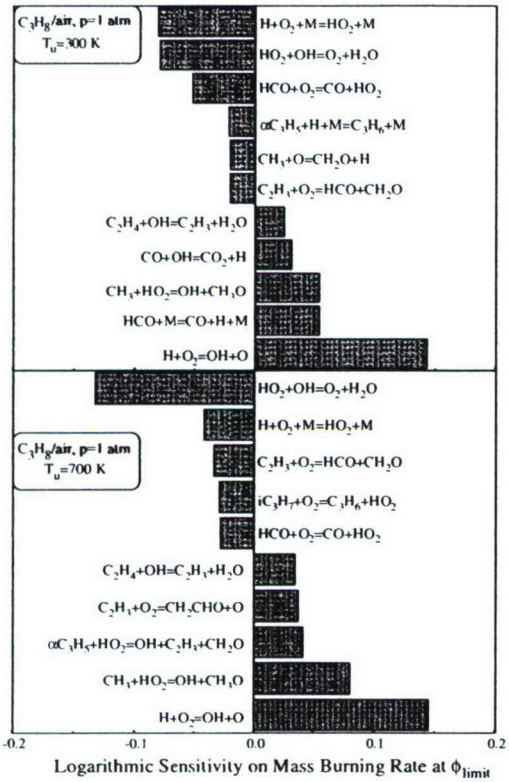

Fig. 9. Sensitivity of the mass-burning rate on kinetics for limit C_3H_8/air flames, at $p = 1$ atm and $T_u = 300$ and 700 K.

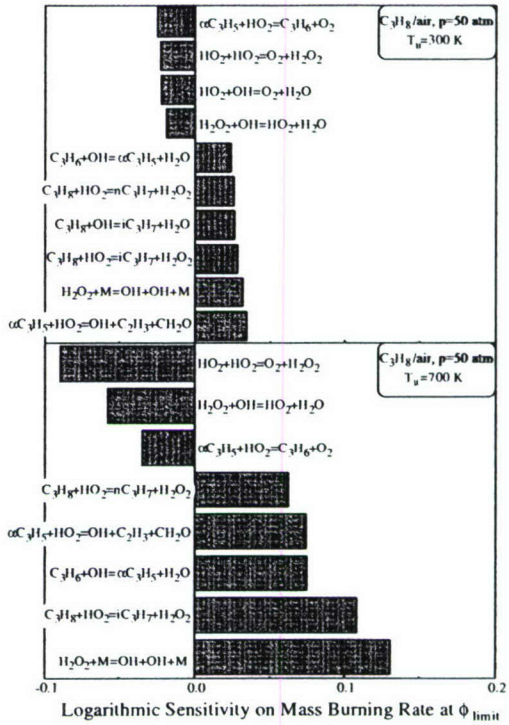

Fig. 10. Sensitivity of the mass-burning rate on kinetics for limit C_3H_8/air flames, at $p = 50$ atm and $T_u = 300$ and 700 K.

mixtures. More specifically, the excessive production of HO_2 via R2 leads eventually to H_2O_2 production, whose decomposition

$$H_2O_2 + M \rightarrow OH + OH + M \quad \text{(R4)}$$

is an effective branching step as it produces two OH radicals that are crucial to the overall oxidation process. The sensitivities of reactions that involve consumption of carbon-containing species via HO_2 were also found to be significantly larger compared to those at the lower p's.

The third-limit like behavior becomes more prominent at $p = 50$ atm, as shown in Figs. 8 and 10 for CH_4/air and C_3H_8/air mixtures respectively. Under such high pressures, R4 has a dominant contribution to the system branching, so that the $H/O_2 \Rightarrow HO_2 \Rightarrow H_2O_2 \Rightarrow OH$ pathway becomes the main OH-production channel. As a result, the lean flammability limits are extended to leaner fuel concentrations with lower T_{limit}'s.

Calculations similar to those in [17] were also performed and the maximum rates of R1 and R2 were calculated for a wide range of conditions. As expected, their relative values do not correlate with the existence of the flammability limits. For example, for the $p = 1$ atm CH_4/air mixtures the maximum rate of R1 exceeds that of R2 at ϕ_{limit} by a factor of 5 for both $T_u = 300$ and 700 K. However, at $p = 50$ atm similar calculations revealed that the maximum rate of R2 exceeds that of R1 by *two orders* of magnitude at ϕ_{limit}.

Integrated species consumption analysis provided further insight into the pathways that result in radical production. To illustrate this, the kinetic pathways resulting in the production of OH radicals were chosen. The analysis showed that for the CH_4/air limit flames at $p = 1$ atm, OH is mainly produced by R1 and to a lesser extent by

$$H_2O + O \rightarrow OH + OH \quad \text{(R5)}$$

$$HO_2 + CH_3 \rightarrow OH + CH_3O \quad \text{(R6)}$$

As pressure increases, the importance of R1 in OH production diminishes, and that OH is largely produced by R6 and to a lesser extent by R4 and

$$HO_2 + CO \rightarrow OH + CO_2 \quad \text{(R7)}$$

Similar results were determined for the C_3H_8/air limit flames.

From the sensitivity and integrated species consumption results, the analogy between the near-limit flame behavior and the explosion limits of homogeneous H_2/O_2 mixtures is apparent. As pressure increases first the competition between

Please cite this article as: F.N. Egolfopoulos et al., An assessment of the lean flammability limits of CH_4/air ..., Proceedings of the Combustion Institute (2006), doi:10.1016/j.proci.2006.08.018.

R1 and R2 determines the limit flame response, but subsequently the HO_2–H_2O_2 kinetics become the controlling mechanism of the radical production.

4. Concluding remarks

A detailed numerical investigation was conducted for near-limit laminar premixed CH_4/air and C_3H_8/air flames, over a wide range of pressures and unburned mixture temperatures that are of relevance to internal combustion engines. The simulations included the use of the Premix code modified to allow for radiative losses, together with the one-point continuation to compute the turning-point behavior observed at near-limit concentrations. Such turning points define the numerically determined flammability limits, as they conform to their fundamental definition.

Results revealed that the lean flammability limits of both CH_4/air and C_3H_8/air mixtures as well as the attendant limit flame temperatures vary significantly with both pressure and unburned mixture temperature. For a given pressure, it was found that the lean flammability limit decreases as the unburned mixture temperature increases. On the other hand, for a given unburned mixture temperature, the lean flammability limit first increases and subsequently decreases as pressure increases. The limit flame temperature was found to decrease with pressure in general; for the extreme conditions of 50 atm pressure and 700 K unburned mixture temperature, limit flame temperatures as low as 900 K were determined. Through the use of sensitivity and integrated species consumption analyses, the importance of the HO_2–H_2O_2 chemistry at such high pressures was demonstrated.

From practical considerations, the present study suggests that, upon ignition, sustainable burning in internal combustion engines is more robust than previously recognized. On the other hand, steady engine operation has not been achieved with the ultra-lean concentrations identified herein. Several possibilities can be suggested for such a disagreement, offering potential avenues for further investigation and optimization. The first cause for the observed narrower limit is the facilitation of extinction due to the unavoidable turbulence and bulk aerodynamic stretching. Second, the fuel/air charge may not be well mixed, resulting in diffusion-controlled burning which is more susceptible to stretch-induced extinction. Third, the successful firing of an engine could be more critically controlled by the ignitability of the unburned mixture instead of the extinguishability of established flames. This is consistent with the hysteresis nature of combustion phenomena in that, for the same thermodynamic and aerodynamic state, ignition is more difficult to achieve than extinction. Consequently rational strategies towards extending the lean limit of engine operations should be focused on promoting mixture homogeneity as well as on enhancing ignition because flames will propagate once they are established, allowing of course the omnipresence of stretch.

Acknowledgments

This work at the University of Southern California was supported by NASA (Grant NCC3-678) under the technical supervision of Dr. Fletcher Miller, and by AFOSR (Grants FA9550-04-1-0006 and FA9550-04-1-0003) under the technical supervision of Dr. Julian M. Tishkoff. The work at Princeton University was also supported by the AFOSR under the technical management of Dr. Julian M. Tishkoff.

References

[1] F.A. Williams, *Combustion Theory*, second ed., Benjamin Cummins, Menlo Park, 1985.
[2] D.B. Spalding, *Proc. R. Soc. London A* 240 (1957) 83–100.
[3] H.F. Coward, G.W. Jones, *Bureau Mines Bull.* 503 (1952).
[4] R.A. Strehlow, K.A. Noe, B.L. Wherley, *Proc. Combust. Inst.* 21 (1986) 1899–1908.
[5] P.D. Ronney, H.Y. Wachman, *Combust. Flame* 62 (1985) 107–119.
[6] C.K. Law, D.L. Zhu, G. Yu, *Proc. Combust. Inst.* 21 (1986) 1419–1426.
[7] C.K. Law, F.N. Egolfopoulos, *Proc. Combust. Inst.* 23 (1990) 413–421.
[8] K.N. Lakshmisha, P.J. Paul, H.S. Mukunda, *Proc. Combust. Inst.* 23 (1990) 433–440.
[9] C.K. Law, F.N. Egolfopoulos, *Proc. Combust. Inst.* 24 (1992) 137–144.
[10] G. Dixon-Lewis, *Proc. Combust. Inst.* 25 (1994) 1325–1332.
[11] F.N. Egolfopoulos, *Proc. Combust. Inst.* 25 (1994) 1375–1381.
[12] K. Maruta, M. Yoshida, Y. Ju, T. Niioka, *Proc. Combust. Inst.* 26 (1996) 1283–1289.
[13] C.J. Sung, C.K. Law, *Proc. Combust. Inst.* 26 (1996) 865–873.
[14] H. Guo, Y. Ju, K. Maruta, T. Niioka, F. Liu, *Combust. Flame* 109 (1997) 639–651.
[15] H. Zhang, F.N. Egolfopoulos, *Proc. Combust. Inst.* 28 (2000) 1875–1882.
[16] J.A. Miller, *Proc. Combust. Inst.* 26 (1996) 461–480.
[17] P.F. Flynn, G.L. Hunter, L. Farrell, et al., *Proc. Combust. Inst.* 28 (2000) 1211–1218.
[18] R.J. Kee, J.F. Grcar, M.D. Smooke, J.A. Miller, *Sandia Report* Sand 85-8240, 1985.
[19] F.N. Egolfopoulos, P.E. Dimotakis, *Proc. Combust. Inst.* 27 (1998) 641–648.
[20] M. Nishioka, C.K. Law, T. Takeno, *Combust. Flame* 104 (1996) 328–342.

Please cite this article as: F.N. Egolfopoulos et al., An assessment of the lean flammability limits of CH_4/air ..., Proceedings of the Combustion Institute (2006), doi:10.1016/j.proci.2006.08.018.

[21] R.J. Kee, F.M., Rupley, J.A. Miller, *Sandia Report* SAND89-8009, 1989.
[22] R.J. Kee, J. Warnatz, J.A. Miller, *Sandia Report* SAND83-8209, 1983.
[23] G.P. Smith, D.M. Golden, M. Frenklach, et al., GRI-Mech 3.0, 2000. Available from: http://www.me.berkeley.edu/gri_mech/.
[24] H. Wang, A. Laskin, Z.M. Djurisic, C.K. Law, S.G. Davis, D.L. Zhu, A comprehensive mechanism of C_2H_y and C_3H_y fuel combustion, in: *Chemical and Physical Processes in Combustion*, the 1999 Fall Technical Meeting of the Eastern States Section of the Combustion Institute, Raleigh, NC, October, 1999, pp. 129–132.

Please cite this article as: F.N. Egolfopoulos et al., An assessment of the lean flammability limits of CH_4/air ..., Proceedings of the Combustion Institute (2006), doi:10.1016/j.proci.2006.08.018.